A Study Of A Moving Contact Algorithm

by

Jiann-Yuarn Wu

Thesis submitted to the Faculty of the

Virginia Polytechnic Institute and State University

in partial fulfillment of the requirements for the degree of

Master of Science

in

Civil Engineering

APPROVED:

Richard M. Barker (Chairman)

Raymond H. Plaut

Siegfried M. Holzer

February, 1987

Blacksburg, Virginia

A Study Of A Moving Contact Algorithm

by

Jiann-Yuarn Wu

Richard M. Barker (Chairman)

Civil Engineering

(ABSTRACT)

A nonlinear moving contact algorithm has been implemented to model the sticking-sliding inelastic behavior in the interlocks of steel sheet pile sections subjected to axial tension. Previously, numerical instabilities were encountered during the solution process while conducting a series of verification problems for the algorithm by the Newton-Raphson method. In an attempt to identify the cause of these instabilities, an in-depth study of the effect of fineness of the finite element mesh on the convergence of the solution has been undertaken.

The solution process credited to Riks and Wempner has been used to find the postbuckling equilibrium path of shallow reticulated domes. This algorithm, with some modifications, is used to move from one load step to another step in this study.

As in most nonlinear problems, the size of the load step influences the rate of convergence. In addition, in the moving contact problem nodes can move along the sides of an element on the contact surface. Thus, the mesh refinement also affects the rate of convergence.

To study the effects of both of these parameters, a series of test problems was run with variable load steps and mesh refinements. The modified Riks-Wempner algorithm, which automatically adjusts the load step size as the solution process advances, successfully solved all the inelastic and large displacement problems attempted. From the mesh refinement studies two conclusions were reached : for curved boundaries use curved elements and avoid the use of irregularly shaped elements.

Finally, the improved solution algorithm is applied to sheet pile interlocks loaded in axial tension. Results for progressively increasing load show the spread of yielding in

the thumbs and fingers of the interlocks and the sliding of one past another as the deformations increase.

Acknowledgements

The author expresses his sincere appreciation to Dr. Richard M. Barker for his guidance, suggestions, encouragement, and good sense of humor.

Appreciation is also expressed to Dr. Raymond H. Plaut for his review of this thesis, and his serving on the committee.

Special thanks go to Dr. Siegfried M. Holzer for his many helpful discussions, and his serving on the committee.

Discussions with fellow graduate students, especially William Sage, are also greatly appreciated.

Finally, the author would like to thank his beloved family and friends. Without their love, support, and constant encouragement given during the years of education, this work would have been impossible.

Table of Contents

List of Tables

List of Figures

Chapter 1

Introduction

1.1 Purpose and Scope

The purpose of this study is to examine the use of a modified Riks-Wempner method on a nonlinear moving contact problem and to study how the convergence of the solutions varies with mesh refinement.

In previous analyses, Chan and Barker (1985) have successfully incorporated the effects of large rotation and displacement, elastic-plastic material, and moving contact algorithm to describe the behavior of sheet pile interlocks. During the development of the previous finite element program, emphasis was on the correct formulation of the moving contact problem. Less emphasis was placed on the solution process and convergence. It has been found that the modified Newton-Raphson approach used in the previous program works well in solving nonlinear equilibrium equations when the contact surfaces stick together, however, some difficuties were encountered when the contact surfaces begin to slide. In an attempt to more deeply study the behavior of sheet pile interlocks under tensile load, the modified Riks-Wempner method was adopted and used in this study.

Detailed description of the modified Riks-Wempner method is given in Chapter II. To increase the efficiency of the computer program, some numerical techniques used in ABAQUS (Hibbit et al, 1984) were incorporated in the program. To describe the application of the modified Riks-Wempner method on a moving contact problem, an overview of the moving contact algorithm is also provided in the chapter. In the last part of the chapter, four test problems, including a buried pipe problem, were studied to verify the validity of the modified Riks-Wempner method applied to non-contact and contact problems.

Chapter III discusses the relation between the convergence of a contact problem and mesh refinement. The effect of curved side elements and regular shaped elements on convergence of solution in simulating the problems with curved boundaries is stated in this chapter. This is followed by a verification of the Hertz contact problem.

In Chapter IV, an updated finite element program is used to model a simple pull-test on PS32 sheet pile interlocks. The results of the PS32 sheet pile analysis, which contain load-deformation behavior, deformed meshes at different load steps, possible pattern of failure mode, elastic-plastic behavior of the interlock connection and statics check of load transfer, are presented and discussed in this chapter.

Chapter V contains conclusions and discussions obtained from the analysis. A few recommendations arising from this study are suggested for future studies.

1.2 Literature Review on Numerical Techniques of Nonlinear Analysis

As presented in many papers, the prediction of nonlinear responses has been extensively studied and a number of numerical solution techniques have been developed.

Among these techniques, the Newton-Raphson method (Tillerson, Stricklin, and Haisler, 1973), with various modifications, is widely used to trace nonlinear load paths of structures. However, in the vicinity of a critical point, as the tangent stiffness matrix approaches a singularity, the method tends to diverge. To overcome this problem, several methods have been proposed.

Bergan (1979) introduced the "current stiffness parameter" to guide the suppressing iterations in the critical zone. At a prescribed value of the stiffness parameter the iteration procedure is discontinued. After that, pure incrementation is used. If the Euclidean norm of the displacement increments exceeds a certain prescribed limit, load and displacements are linearly scaled back. Negative diagonal elements may be detected here, in which case negative load increments are applied. After the stiffness parameter reaches its prescribed value again, the iteration procedure is resumed. The limit point is located by a zero value of the stiffness parameter. This techniques requires very small load increments to avoid drifting away from the equilibrium path.

Wright and Gaylord (1968) developed an artificial spring method which was applied to arch systems and shell structures by Sharifi and Popov (1971) and Ramm (1980), respectively. This technique is based on the observation that a snap-through problem may be transformed into one with a positive definite characteristic if linear artificial springs are added to the system. Numerical experiments shows that this method is only successful in real snap-through problems where the springs can keep the destabilizing structure alive. For local failure it may not be successful.

Argyris (1965) used a prescribed single displacement component as a controlling parameter and the corresponding load level is taken as unknown. Several authors have given some modifications to this method (Pian and Tong, 1970; Zienkiewicz, 1971; Sabir and Lock, 1973; Nemat- Nasser and Shatoff, 1973). However, this method fails whenever the structure snaps back from one load level to a lower one. Furthermore, some knowledge of the failure mode is required for a proper choice of the controlling displacement. It might even be necessary to change the prescribed parameter.

An initial type solution technique called "Homotopy Method", which traces equilibrium curves by solving a differential equation, has been studied and compared to the standard Newton-Raphson method by Hansen (1981). The homotopy method is based on an algorithm that permits mapping of the solution to n nonlinear algebraic equations of $n+1$ variables (Watson, 1979).

The iterative technique of modified Riks-Wempner method was independently introduced by Riks (1972) and Wempner (1971). Riks (1972) proposed an incremental approach which features Newton's method and a special parameter, which is the arc-length of the equilibrium path, controlling the progress of the computations along the equilibrium path to be computed. Wempner (1971) introduced a generalized arc-length in a configuration-load space to modify the method of incremental loading. Then the iteration path follows a plane normal to the tangent, and the new point is the intersection of the normal to the tangent with the equilibrium path. This method, with some numerical techniques, will be implemented as the new equation solver for the moving contact algorithm in this study.

1.3 Literature Review on Solution Methods of Contact Problems

Recently, an increasing interest in contact problems and its application in various engineering fields have resulted in many solution algorithms being presented in the literature. Some of these solution methods are briefly reviewed in the following.

Chan and Tuba (1971) used the over-relaxation method and treated the frictional contact force as an unknown. The contact status of each possible contact point was assumed at first and updated by iterations until the assumed status and the computed status become the same at each contact point.

Francavilla and Zienkiewicz (1975) used a reduced flexibility matrix to solve the frictionless contact problem. By modifiying the contact status of any possible contact point, iteratively, the contact force vector can be obtained after the convergence is achieved.

Duvaut and Lions (1976) introduced a variational inequality formulation and the corresponding uniqueness theorems with the classical Coulomb's friction law assuming that the normal contact stress is known apriori.

Kalker (1977) used an alternate variational principle and showed that the solution is unique if the maximum tangential traction on the contact surface is a function of position and time.

Okamoto and Nakazawa (1979) incorporated the contact constraint equation to the global equation such that the global stiffness matrix displacement vector and force vector are extended by the contact constraint. They increased the external force by an amount which causes a change in the contact status of only one nodal point at a time.

In addition to static contact, Lee and Kamemura (1979, 1981) used a part of the flexibility matrix to solve static and dynamic contact problems. During the iterations, the contact status of each point was updated until the assumed contact status agree with the computed result at each possible point.

Sachdeva and Ramakrishnan (1981) obtained normal and tangential components of the frictional contact force vector by using the modified flexibility matrix. They assumed the contact status of each possible contact point and revised it until the assumed status and the computed result become the same.

Oden and Pires (1981, 1982, 1983) used the penalty method to solve the frictional contact problems, and introduced nonlocal friction laws instead of classical Coulomb's friction laws to demonstrate the convergence of the solution for elastostatic contact problems. The variational principles for boundary-value problems in elasticity, existence and uniqueness of solutions to the nonlocal and nonlinear problems were also discussed in their articles.

Katona (1983) combined the contact constraint condition with global equation. By incorporating the additional contact constraints, the global stiffness matrix, displacement vector, and force vector are extended. The contact constraints are assumed at first and updated by iterations until convergence is obtained. He also presented a special decision table to decide the contact status and the corresponding contact constraint equation.

Torstenfelt (1983, 1984) used the incremental loading techniques similar to Okamoto and Nakazawa (1979) and regarded the frictional contact force vector as unknown. Again, the load increment, which changes the contact status of only one nodal point, was obtained by iterations.

Lee, K. (1985) developed a numerical solution which guarantees the convergence to the corresponding exact solution for two-dimensional linear elastic frictional contact problems. He used the current gap vector and an incremental form of Coulomb's friction law to describe the frictional contact condition. An error vector is also defined and incorporated into the frictional contact condition. The frictional contact problem is solved by an iteration scheme, and the norm of the error vector is reduced monotonically as the iteration proceeds until the exact solution is obtained.

Bathe and Chaudhary (1985) incorporated a contact constraint equation in the global equation. In their formulation, the total variational function is obtained by summing the usual incremental potential and the incremental potential of the contact forces. This approach was adopted to model the moving contact problem by Chan and Barker (1985), since it allows node to internode contact. It is also followed in this study.

1.4 Literature Review on Convergence of the Finite Element Method near a Curved Boundary

Although it has been stated in many books (Cook, 1982; Reddy, 1984) that the solution of the finite element analysis will converge to the exact solution with an increase in mesh refinement, it is not assumed when the given domain of a problem is not represented with proper elements.

Babuska (1961) used inscribed polygons to model a disk and found that the solution did not converge uniformly to the exact solution as the number of polygons approach to ∞ .

Rao and Rajaiah (1968) used a numerical analysis based on polynomial approximation and verified the finding of Babuska (1961), which has been referred to as the "Babuska Paradox".

Zlamal (1973) constructed a general curved element of an isoparametric nature for second order problems and used it along the curved part of the boundary only. It was found that the result obtained by constructing a curved element is better than that obtained by approximating the curved boundary piecewise by polynomials. The improvement of the accuracy of partial derivatives at points lying close to or on the curved boundary is remarkable. A justification of the curved elements in the finite element method is also presented in the literature (Zlamal, 1974).

Krauthammer (1979) made an attempt to show the problems arising from using straight boundary elements for curved boundary models. It was found that solutions of problems by the finite element method, when curved boundaries are present in the model, may not be accurate. The "Babuska Paradox" was also demonstrated by analyzing the Kirsch problem.

1.5 Literature Review on Analysis of Sheet Pile Interlocks

Straight-web sheet piles are designed primarily for use in cellular cofferdams, in which the tension value of the interlock is the prime consideration. Therefore, the strength of the piling can affect the radius of a cofferdam and plays an important role in designing a cellular structure. However, only a few papers dealing with the analysis of pull-out strength of sheet piles interlocks can be found.

Bower (1973) described theoretical studies of interlock behavior and the development of equations for predicting the interlock strength. In addition to the theoretical analysis, he also conducted a number of pullout tests. The examination of tested interlocks established that pullout oc-

curs after large plastic rotations plastic hinges occur in both the thumb and finger of the interlock. It is also indicated that the pullout strength is proportional to the strain-hardening stress and is affected to an even greater degree by a change in finger thickness.

Kay, J. N. (1975) conducted pullout tests on sheet pile interlocks to develop the frequency distribution diagrams for interlock strength. Consideration of these distributions give the designer a basis for a probabilistic approach to design and provide a better feeling for the material property than from the representation of a minimum ultimate strength of 16 kips/inch. However, the results are based on conventional laboratory test procedures and the adequacy in representing field conditions is questionable.

Barker and Oliver (1985) performed six sets of three specimens for two different types of sheet piles. It was found that the tests verify that the classical use of 0.3 for the static coefficient of friction provides a reasonable estimate of the sheet pile interlock shear strength.

In an attempt to develop an analytical tool for predicting the interlock stability of a cell, Chan and Barker (1985) developed a finite element computer program to analyze the interlock behavior. In previous study, the nonlinear moving contact algorithm with elastic-plastic material response and large displacement and rotation is used to model the tensile test of a sheet pile interlock connection. Two sets of analyses are performed on both PS32 and PSX32 sheet piles. The first set assumes no sliding among the contact regions in the interlocks, whereas the second set allows sliding among contact surfaces. It was found that the maximum displacements increase when sliding is allowed at contact regions.

Chapter 2

Modified Riks/Wempner Method

2.1 Introduction

The Riks/Wempner method was introduced independently by Riks (1979) and Wempner (1971), and has been shown by Holzer, et al (1981) to be an effective technique for tracing an equilibrium path beyond a limit point into a postbuckling range. The modified Riks/Wempner method searches for a new equilibrium point by moving away from the previous equilibrium point along a tangent to the equilibrium path for a specified arc length, Δs . By iteration along a normal to the tangent, a new equilibrium point is obtained. (See Fig. 2.1 and 2.2)

Crisfield (1981) recommends an alternative method in which the normal plane is replaced by a sphere with the center at the current equilibrium point and radius Δs. In this study, only iteration along a normal will be considered. The presentation of the modified Riks-Wempner method in this chapter follows that of Holzer et al (1981).

2.2 Stability of Equilibrium

The principle of virtual work states that a continuous body is in equilibrium if the virtual work of all forces acting on the body is zero in a virtual displacement :

$$\delta W = \delta W_E + \delta W_I = 0 \tag{2.1}$$

where

δW_E = virtual work resulting from external forces

δW_I = virtual work resulting from internal forces

= $-\ \delta U$, where U is the strain energy of the system

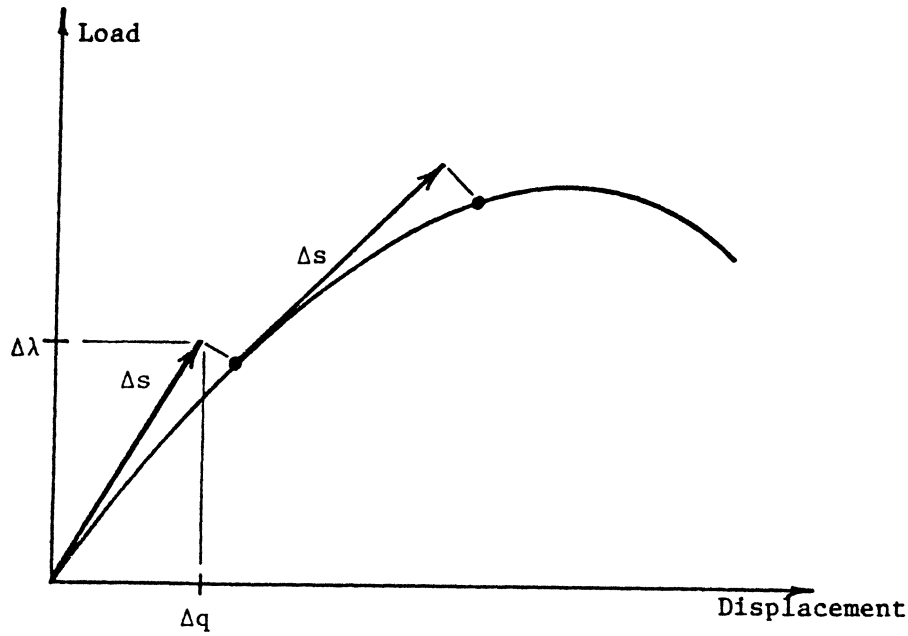

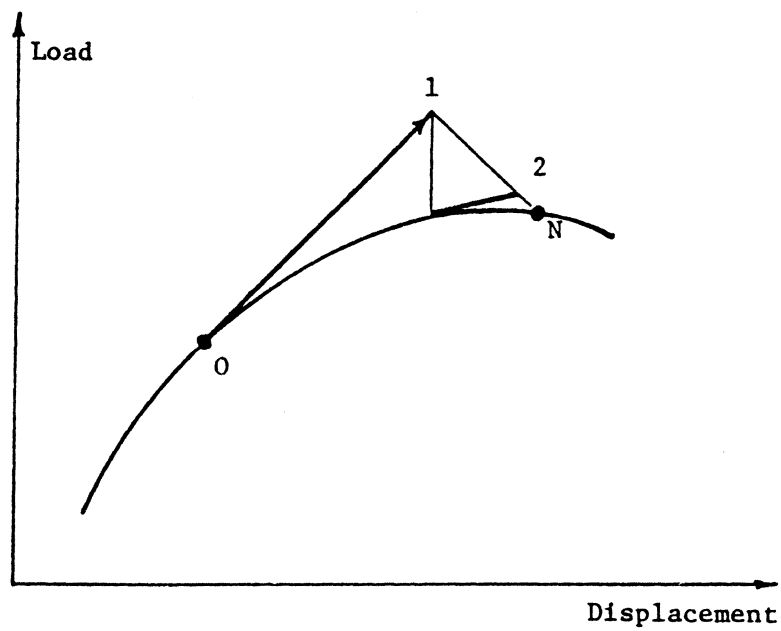

Figure 2.1. The Riks-Wempner Method

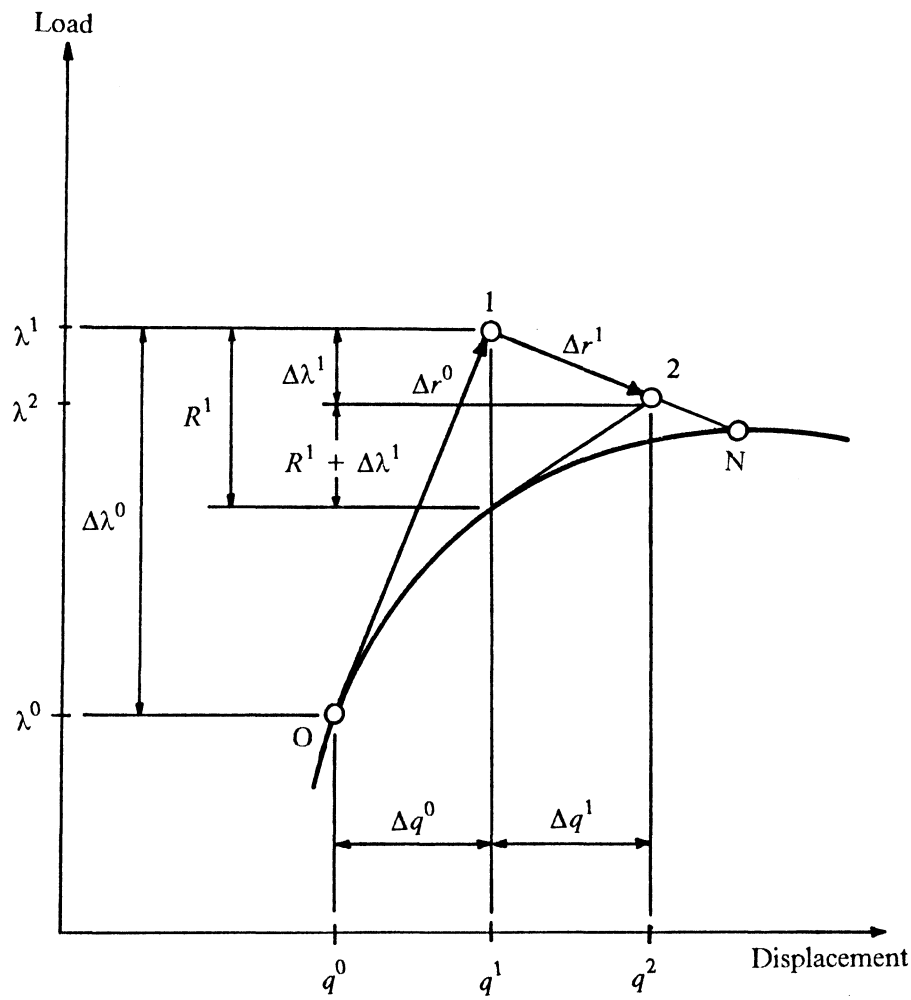

Figure 2.2. Iteration from Point O to Point N

δW_E and δU are determined to be

$$\delta W_E = \delta q^T Q = \lambda \delta q^T \overline{Q} = \sum_{i=1}^{n} \lambda \delta q_i \overline{Q}_i \tag{2.2}$$

$$\delta U = \sum_{i=1}^{n} \frac{\partial U}{\partial q_i} \delta q_i \tag{2.3}$$

where

q = Generalized displacement vector

λ = Loading parameter

Q = Generalized load vector

$\overline{Q}$ = Constant load distribution vector

n = Number of generalized displacements (Degree of freedom)

Substitution of Eqs. 2.2 and 2.3 into Eq. 2.1 yields

$$\delta W = \sum_{i=1}^{n} (\lambda \overline{Q}_i - \frac{\partial U}{\partial q_i}) \delta q_i = 0 \tag{2.4}$$

By the principle of virtual work, since δq_i are arbitrary and independent, Eq. 2.4 yields

$$R_i(q, \lambda) = \lambda \overline{Q}_i - \frac{\partial U}{\partial q_i} = 0 \qquad i = 1,2 \ldots n \tag{2.5}$$

The set of all points (q, λ) satisfying Eq. 2.5 defines equilibrium paths in the load-deflection space. Let (q^k, λ^k) represent the k^{th} approximation to the solution (q, λ). By using the truncated Taylor series expansion of Eq. 2.5, we obtain

$$R_i(q^k, \lambda^k) = \frac{\partial R_i(q^k, \lambda^k)}{\partial \lambda} \Delta\lambda^k + \sum_{j=1}^{n} \frac{\partial R_i(q^k, \lambda^k)}{\partial q_j} \Delta q_j^k = 0 \tag{2.6}$$

or

$$R_i^{k+1} = R_i^k + \Delta\lambda^k \overline{Q}_i - \sum_{i=1}^{n} K_{ij}^k \Delta q^k = 0 \tag{2.7}$$

where

$$R_i^k = R_i(q^k, \lambda^k) \tag{2.8}$$

$$K_{ij}^k = \frac{\partial^2 U(q^k)}{\partial q_i \partial q_j} \tag{2.9}$$

Eq. 2.7 in vector form is

$$K^k \Delta q^k = \Delta\lambda^k \overline{Q} + R^k \tag{2.10}$$

where

$$q^{k+1} = q^k + \Delta q^k \tag{2.11}$$

$$\lambda^{k+1} = \lambda^k + \Delta\lambda^k \tag{2.12}$$

Eqs. 2.10-2.12 are the recurrence relations of the modified Riks/Wempner method where

K^k = Tangent stiffness matrix at q^k

R^k = Unbalanced force vector at q^k, λ^k

2.3 Generalized Arc Length

Let

$$K\Delta q = \Delta\lambda \overline{Q} \tag{2.13}$$

be defined at the known equilibrium point, the starting point of the Riks/Wempner method where the unbalanced force vector, R, is zero. $\overline{Q}$ is the constant load distribution vector. The solution of Eq. 2.13, Δq, and $\Delta\lambda$ define the tangent vector at the starting point

$$t = \Delta r = \begin{bmatrix} \Delta q \\ \Delta\lambda \end{bmatrix} \tag{2.14}$$

which is shown in Fig. 2.2. Accordingly,

$$\Delta s = |t| = \left[\Delta q \Delta q + (\Delta\lambda)^2\right]^{1/2} \tag{2.15}$$

where

$$|t| = (t \cdot t)^{1/2} = \text{Length of the tangent vector t}$$

$$t \cdot t = t^T t = \text{Inner product of t with itself}$$

Eq. 2.15 is called the constraint equation and the generalized arc length Δs can be computed for a specified load increment, $\Delta\lambda$, at the starting point. If Δs is specified at the starting point, we can calculate $\Delta\lambda$ by

$$\Delta\lambda = [(\Delta s)^2 - \Delta q \Delta q]^{1/2} \tag{2.16}$$

Using Eq. 2.10 and Eq. 2.15, we can solve for (n + 1) unknowns, Δq^k and $\Delta\lambda^k$. If we let

$$\Delta q = \Delta\lambda \Delta q^I \tag{2.17}$$

where Δq^I is the solution of the equation

$$K\Delta q^I = \overline{Q} \tag{2.18}$$

the generalized arc length is obtained in terms of $\Delta\lambda$ and Δq^I by writing the constraint equation :

$$\Delta s = \Delta\lambda(\Delta q^I \Delta q^I + 1)^{1/2} \tag{2.19}$$

Ramm (1980) suggests that the number of iterations in future load steps can be controlled by scaling Δs in the form

$$\Delta\hat{s} = \Delta s\,(\frac{\hat{I}}{I})^{1/2}$$

where

$\hat{I}$ = Number of desired iterations

I = Number of iterations required in the previous step.

2.4 The First Step

The first trial solution for a new equilibrium point is defined by the tangent vector at the known equilibrium point

$$t^0 = \Delta r^0 = \begin{bmatrix} \Delta q^0 \\ \Delta\lambda^0 \end{bmatrix} \tag{2.20}$$

Specifically,

$$q^1 = q^0 + \Delta q^0 \tag{2.21a}$$

$$\lambda^1 = \lambda^0 + \Delta\lambda^0 \tag{2.21b}$$

Using Eq. 2.18, $\Delta\lambda^0$ is expressed by

$$\Delta\lambda^0 = \pm \frac{\Delta s}{(\Delta q^{0I} \cdot \Delta q^{0I} + 1)^{1/2}} \tag{2.22}$$

where Δq^{0I} is the solution of

$$K^0 \Delta q^{0I} = \overline{Q} \tag{2.23}$$

and

$$\Delta q^0 = \Delta\lambda^0 \Delta q^{0I} \tag{2.24}$$

In Eq. 2.22, the plus sign indicates loading and the minus sign unloading.

2.5 Iteration on the Normal Plane

The linearized equilibrium equations, Eq. 2.10 and the constraint equation , were originally solved simultaneously and the symmetry and bandedness of the tangent stiffness matrix, K, was destroyed. In order to overcome these difficulties, Wessels (1980) recommended a two-step procedure (see Fig. 2.3).

In the two-step procedure, the incremental vector Δr^k from k to (k + 1) is decomposed as

$$\Delta r^k = \begin{bmatrix} \Delta q^k \\ \Delta\lambda^k \end{bmatrix} = \Delta\lambda^k \begin{bmatrix} \Delta q^{kI} \\ 1 \end{bmatrix} + \begin{bmatrix} \Delta q^{kII} \\ 0 \end{bmatrix} \tag{2.25}$$

or

$$\Delta q^k = \Delta\lambda^k \Delta q^{kI} + \Delta q^{kII} \tag{2.26}$$

where Δq^{kI} and Δq^{kII} are the solutions of

$$K^k \Delta q^{kI} = \overline{Q} \tag{2.27a}$$

$$K^k \Delta q^{kII} = R^k \tag{2.27b}$$

According to the condition of normality, the scalar product of the tangent vector t^0 and the vector Δr^k must vanish :

$$(t^0)^T \Delta r^k = 0 \tag{2.28}$$

The unknown load increment $\Delta\lambda^k$ is determined by using Eqs. 2.20, 2.25, 2.28 :

$$\Delta\lambda^k = -\frac{(\Delta q^0 \cdot \Delta q^{kII})}{(\Delta q^0 \cdot \Delta q^{kI} + \Delta\lambda^0)} \tag{2.29}$$

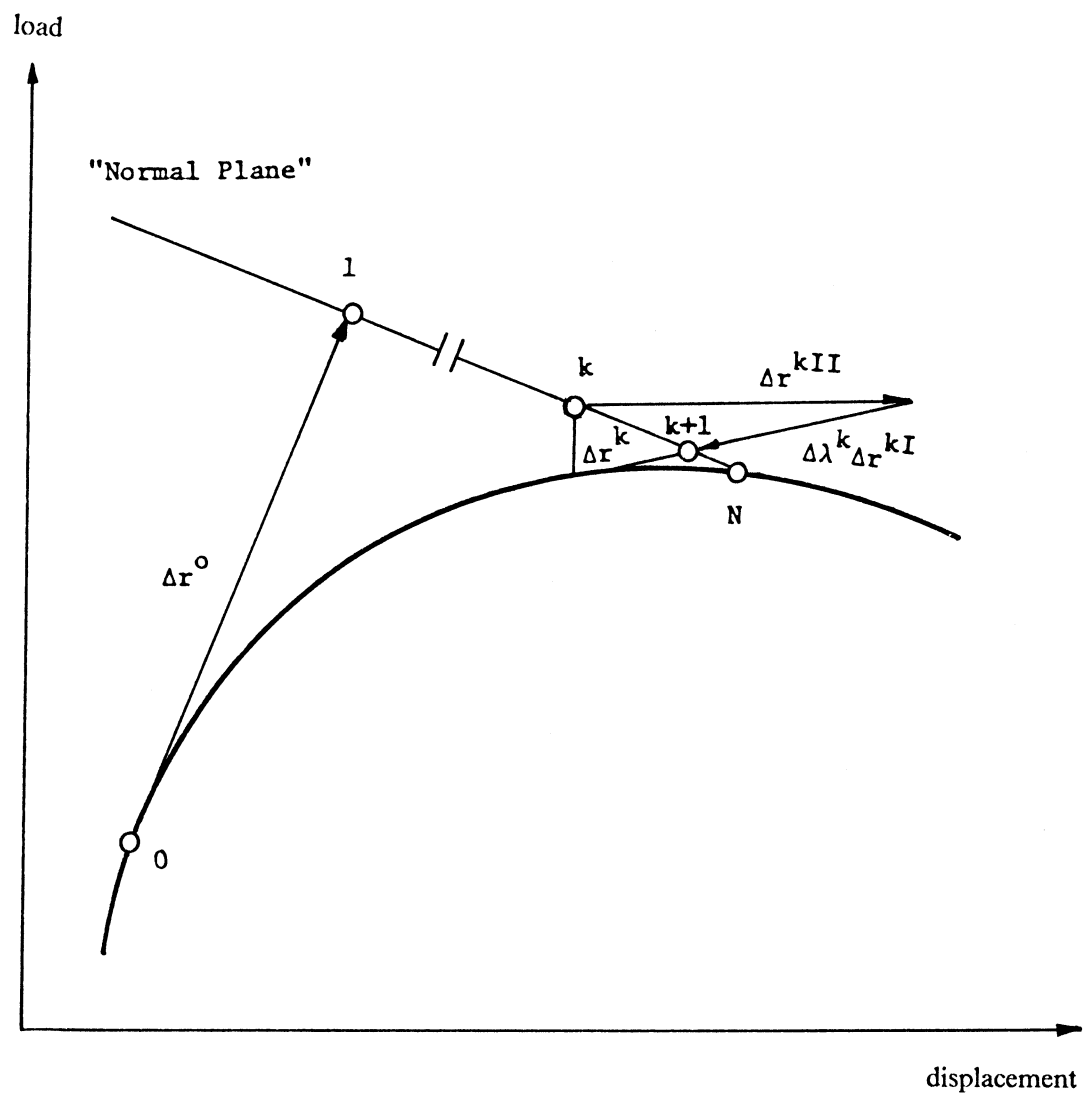

Figure 2.3. Normal Plane Iteration with Two-Step Procedure

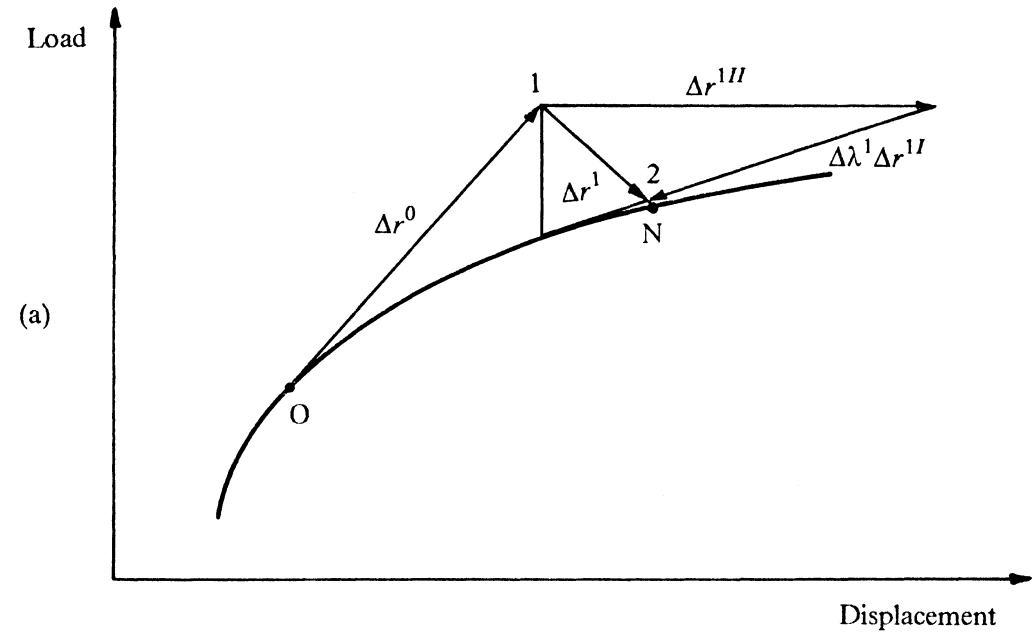

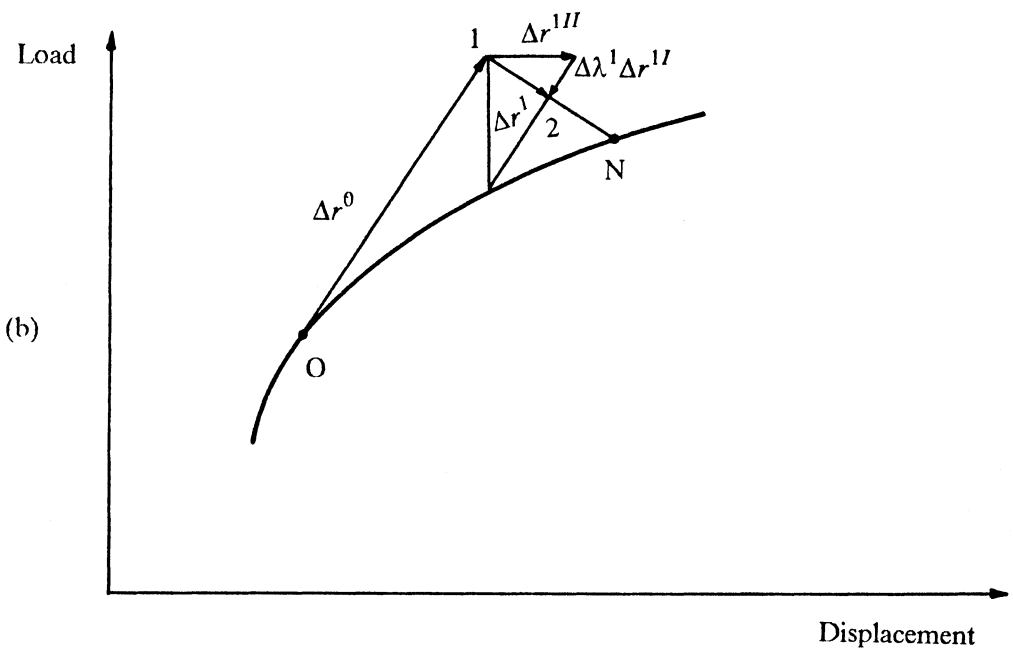

Figure 2.4. Normal Plane Iteration (a) With and (b) Without Updating

Eq. 2.29 is for the case where the tangent stiffness matrix is updated for each iteration (see Fig.2.4a). Alternatively, the tangent stiffness matrix is updated only for the first iteration (see Fig.2.4b)

$$K^k = K^0 \tag{2.30}$$

and

$$\Delta q^{kI} = \Delta q^{0I} \tag{2.31}$$

Because the unbalanced force vector at the starting point is zero, $\Delta q^{0II} = 0$ Therefore, Eq. 2.26 yields

$$\Delta q^{0I} = \frac{\Delta q^0}{\Delta \lambda^0} \tag{2.32}$$

Eqs. 2.31 and 2.32 give

$$\Delta q^{kI} = \Delta q^{0I} = \frac{\Delta q^0}{\Delta \lambda^0} \tag{2.33}$$

By substituting Eq. 2.33 into Eq. 2.29, $\Delta\lambda^k$ for iteration on a normal plane without updating the stiffness matrix is obtained :

$$\Delta \lambda^k = - \frac{\Delta \lambda^0 \Delta q^0 \cdot \Delta q^{kII}}{\Delta q^0 \cdot \Delta q^0 + (\Delta \lambda^0)^2} \tag{2.34}$$

The improved solution for the next equilibrium point is

$$q^{k+1} = q^k + \Delta q^k \tag{2.35}$$

$$\lambda^{k+1} = \lambda^k + \Delta \lambda^k \tag{2.36}$$

where Δq^k and $\Delta\lambda^k$ are determined by Eqs. 2.26 and Eq. 2.29 (or 2.34), respectively.

2.6 Determination of the Sign for Loading or Unloading

In Eq. 2.22, we must determine the correct sign of $\Delta\lambda^0$ to eliminate the problems encountered with the Newton-Raphson method when tracing around limit points since the plus sign indicates loading and the minus sign unloading.

In ABAQUS, Hibbit et al (1984) suggest using the inner product of $[\Delta^i q, \Delta^i\lambda]$ and $[\Delta^{i+1}q^0, \Delta^{i+1}\lambda^0]$ to decide the sign for every load step, i.e., the sign is determined such that the inner product between the current initial vector and the previous increment is always positive (see Fig. 2.5), where

$\Delta^i q$ = Incremental displacement from $(i-1)^{th}$ to i^{th} equilibrium point

$\Delta^i\lambda$ = Incremental load factor from $(i-1)^{th}$ to i^{th} equilibrium point

$\Delta^{i+1}q^0$ = Current initial displacement obtained from Eq. 2.23 and Eq. 2.24 at the beginning of $(i+1)^{th}$ load step

$\Delta^{i+1}\lambda^0$ = Current initial increment of load factor computed from Eq. 2.22 at the beginning of $(i+1)^{th}$ load step

2.7 Convergence Criteria

To terminate the iterative process, many control variables have been recommended and used by different authors (Cook, 1981; Bathe and Cimento, 1979). In this study, three solution variables suggested by Bathe and Cimento (1979) were used for the termination of the iterations. These are the displacements, the unbalanced forces, and the internal energy.

The convergence criterion of displacement is stated as :

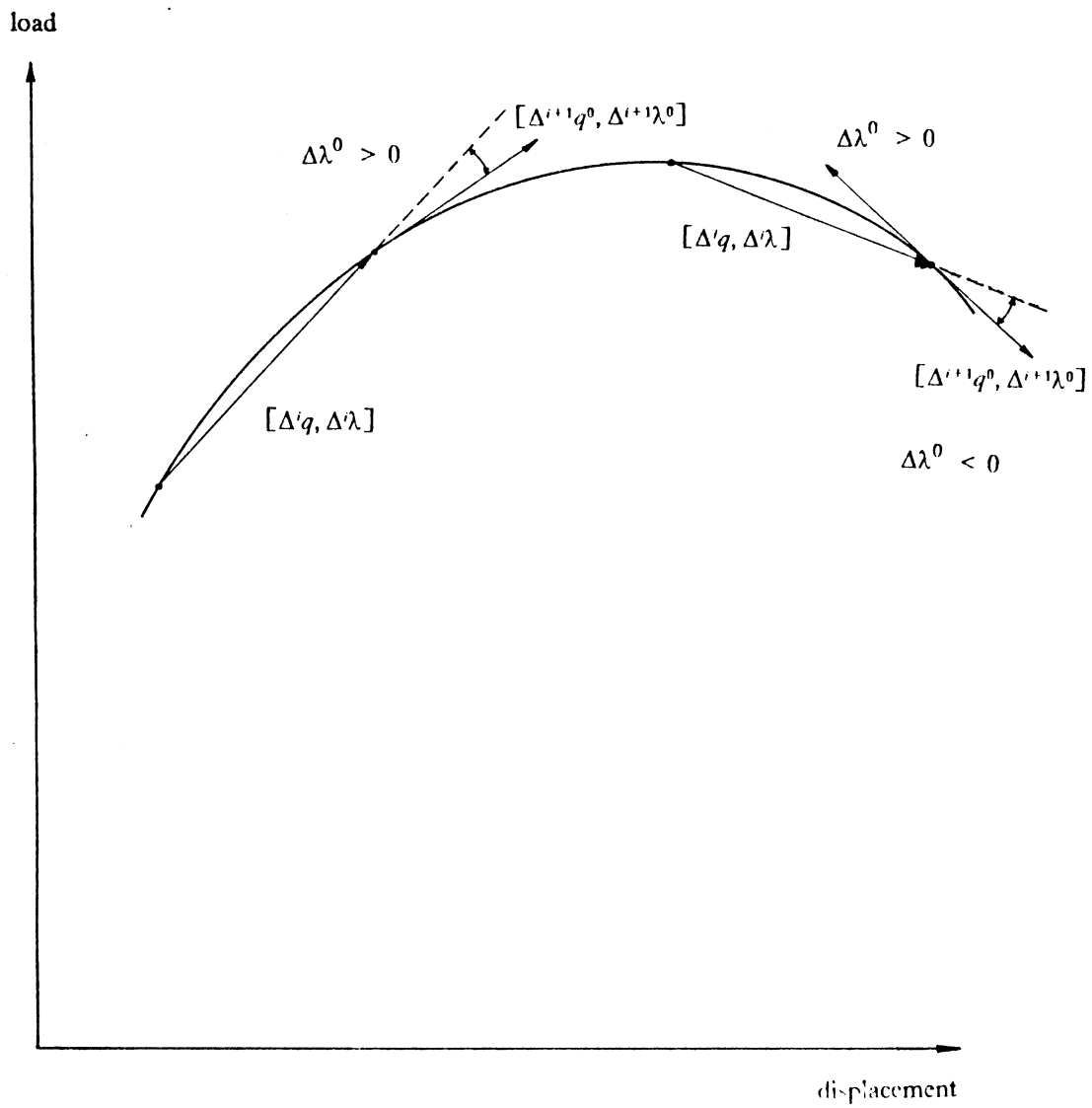

Figure 2.5. Determination of the Sign in Eq. 2.22

$$\frac{\|\Delta^{n+1}U^{(i)}\|}{\|^{n+1}U\|} \leq \varepsilon_D \tag{2.37}$$

where

$\|\Delta^{n+1}U^{(i)}\|$ is the Euclidean norm of the incremental displacements in i^{th} iteration of $(n+1)^{th}$ load step

$\|^{n+1}U\|$ is the Euclidean norm of the total displacements at $(n+1)^{th}$ load step.

Since ^{n+1}U is not known in advance, it is approximated by $^{n+1}U^{(i)}$

ε_D is a displacement convergence tolerance.

The unbalanced force criterion requires that the norm of the unbalanced load vector be within a preset tolerance ε_F of the original load increment:

$$\|^{n+1}R^{(i)} - {}^{n+1}F^{(i)}\| \leq \varepsilon_F \|^{n+1}R^{(1)} - {}^{n}F\| \tag{2.38}$$

where

${}^{n+1}R^{(1)}$ and ${}^{n+1}R^{(i)}$ are the total external force vector at 1^{st} and i^{th} iteration of $(n + 1)^{th}$ load step, respectively

${}^{n+1}F^{(i)}$ is the internal nodal force vector in i^{th} iteration of $(n + 1)^{th}$ load step

${}^{n}F$ is the internal nodal force vector obtained in n^{th} load step (i.e., previous load step)

ε^{F} is a prescribed force convergence tolerance.

The convergence criterion based on internal energy is given as :

$$\frac{\Delta^{n+1}U^{(i)T}({}^{n+1}R^{(i)} - {}^{n+1}F^{(i-1)})}{\Delta^{n+1}U^{(1)T}({}^{n+1}R^{(1)} - {}^{n}F)} \leq \varepsilon_{E} \tag{2.39}$$

where

$\Delta^{n+1}U^{(i)}$ are the incremental displacements in i^{th} iteration of $(n+1)^{th}$ load step; in the modified Riks-Wempner method, this is the solution obtained from Eq. 2.26

$\Delta^{n+1}U^{(1)}$ are the incremental displacements of 1^{st} iteration of $(n+1)^{th}$ load step

${}^{n+1}R^{(1)}$ and ${}^{n+1}R^{(i)}$ are the total applied force vector in 1^{st} and i^{th} iteration of $(n+1)^{th}$ load step, respectively

${}^{n+1}F^{(i-1)}$ is the internal nodal force vector in $(i-1)^{th}$ iteration of $(n+1)^{th}$ load step

${}^{n}F$ is the internal nodal force vector in n^{th} load step (i.e., previous load step).

2.8 Numerical Techniques on Computer Implementation

The solution procedure has been incorporated in the finite element program by Chan and Barker (1985) to handle both nonlinear plane strain and plane stress problems. To increase the efficiency of the solution process, some numerical techniques in ABAQUS (Hibbit et al., 1984) were adopted in the current program.

According to ABAQUS, if after a specified number of iterations the solution has not converged, the increment size of arc length Δs is reduced by a factor of four. If this results in a smaller increment than the user has specified as a minimum, the iteration is terminated. If convergence is achieved in less than a specified number of iterations in two consecutive increments, the increment size is increased by a factor of 1.5, up to the maximum value prescribed by the user on the data card.

The N-S diagram (Holzer, 1985) for the modified Riks-Wempner algorithm is shown in Figure 2.6.

While $\lambda <$ maximum prescribed value

Generate K_T^0

Solve $K_T^0 \Delta q^{0I} = \bar{Q}$ for Δq^{0I}

If this is first pass by the point

Then	else
Prescribe $\Delta\lambda^0$	Decide SIGN ($\pm$)
$\Delta s = \Delta\lambda^0 (\Delta q^{0I} \cdot \Delta q^{0I} + 1)^{1/2}$	$\Delta\lambda^0 = \dfrac{SIGN\, \Delta s}{(\Delta q^{0I} \cdot \Delta q^{0I} + 1)^{1/2}}$

$\Delta q^0 = \Delta\lambda^0 \Delta q^{0I}$

$q^1 = q^0 + \Delta q^0$

$\lambda^1 = \lambda^0 + \Delta\lambda^0$

Compute internal forces due to deformations, F

While not converged

$Q^k = \lambda^k \bar{Q}$

$R^k = Q^k - F^k$

Generate K_T^k

Solve $K_T^k \Delta q^{kI} = \bar{Q}$ for Δq^{kI}

Solve $K_T^k \Delta q^{kII} = R^k$ for Δq^{kII}

$$\Delta\lambda^k = \frac{-(\Delta q^0 \cdot \Delta q^{kII})}{(\Delta q^0 \cdot \Delta q^{kI} + \Delta\lambda^0)}$$

$q^{k+1} = q^k + \Delta q^k$

$\lambda^{k+1} = \lambda^k + \Delta\lambda^k$

Compute F

Test for convergence

Record values at new equilibrium point

Scale Δs by $\Delta s \left(\hat{I}/I\right)^{\frac{1}{2}}$

Figure 2.6. Modified Riks-Wempner Algorithm

2.9 Application of the Modified Riks-Wempner Method to Contact Algorithm

The formulation of the contact algorithm adopted in this study was developed by Bathe and Chaudhary (1985). A brief summary is given to provide an overview of the formulation and the application of the modified Riks-Wempner method to this formulation.

When considering the effect of contact forces, the incremental total potential of the contact forces is added to the usual variational functional. That is,

$$\Pi_1 = \Pi - \sum_k W_k \tag{2.40}$$

where

$\sum_k W_k$ is the incremental potential of the contact forces

Π_1 is the total variational function

Π is the usual incremental total potential leading to the incremental equilibrium equation without contact condition, which is described as (Bathe, 1982)

$$([{}_n^nK_L] + [{}_n^nK_{NL}])[\Delta u] = [{}^{n+1}R] - [{}_n^nF] \tag{2.41}$$

in which

K_L and K_{NL} are the linear and nonlinear stiffness matrices, u is the incremental nodal displacement vector, R is the sum of the externally applied body and surface forces, and F is the equivalent force vector of the internal stresses.

Details of the terms in Eq. 2.41 can be found in a previous report by Chan and Barker (1985).

Since equilibrium iteration is used within each load increment, the value of W_k is written for iteration (i) in $(n + 1)^{th}$ load step. At this stage of the analysis, the response of the system at n^{th} step has been calculated and (i-1) iterations have been performed for the solution at $(n + 1)^{th}$ step. After W_k is established, a first variation of the potential is carried out and the corresponding contributions give additional terms to Eq. 2.41. However, the original terms in Eq. 2.41 will remain unchanged.

In evaluating the contribution of W_k , it is necessary to know whether the contact surface is sticking or sliding. A node k of the contact body is said to come into contact with a segment AB of the target body when penetration occurs within the target. This is illustrated in Figure 2.7, where the location of contact on surface AB is not known. If during an iteration a tensile force is found acting on the contact node, debonding occurs and the contact force is set to be zero. The motion of the contact bodies is governed by Columb friction with μ_s the coefficient of static friction and μ_k the coefficient of kinetic friction. Denoting t_n as the compressive normal traction along the contact surface, the motion of the contact point is indicated by the following equations :

$$\text{sticking} \quad t_t \leq \mu_s t_n \tag{2.42}$$

$$\text{sliding} \quad t_t = \mu_k t_n \tag{2.43}$$

The direction of the tangential traction will always be opposite to the direction of sliding. If t_t drops below the kinetic friction force, sticking is said to take place again.

To construct the finite element equations for the contacting system, the stationarity of the contact potential is invoked. Since there are two variables involved, Δu and $\Delta\lambda$, two sets of Euler equations are obtained. These are discretized into finite element equations and can be given as

$$\begin{bmatrix} {}^{n+1}K_T^{(i-1)} & {}^{n+1}K_C^{(i-1)} \\ {}^{n+1}K_C^{(i-1)} & 0 \end{bmatrix} \begin{bmatrix} \Delta u^{(i)} \\ \Delta\lambda_c^{(i)} \end{bmatrix} = \begin{bmatrix} {}^{(n+1)}R^{(i)} \\ 0 \end{bmatrix} - \begin{bmatrix} {}^{n+1}F^{(i-1)} \\ 0 \end{bmatrix} + \begin{bmatrix} {}^{n+1}R_C^{(i-1)} \\ {}^{n+1}\Delta_C^{(i-1)} \end{bmatrix} \tag{2.44}$$

where

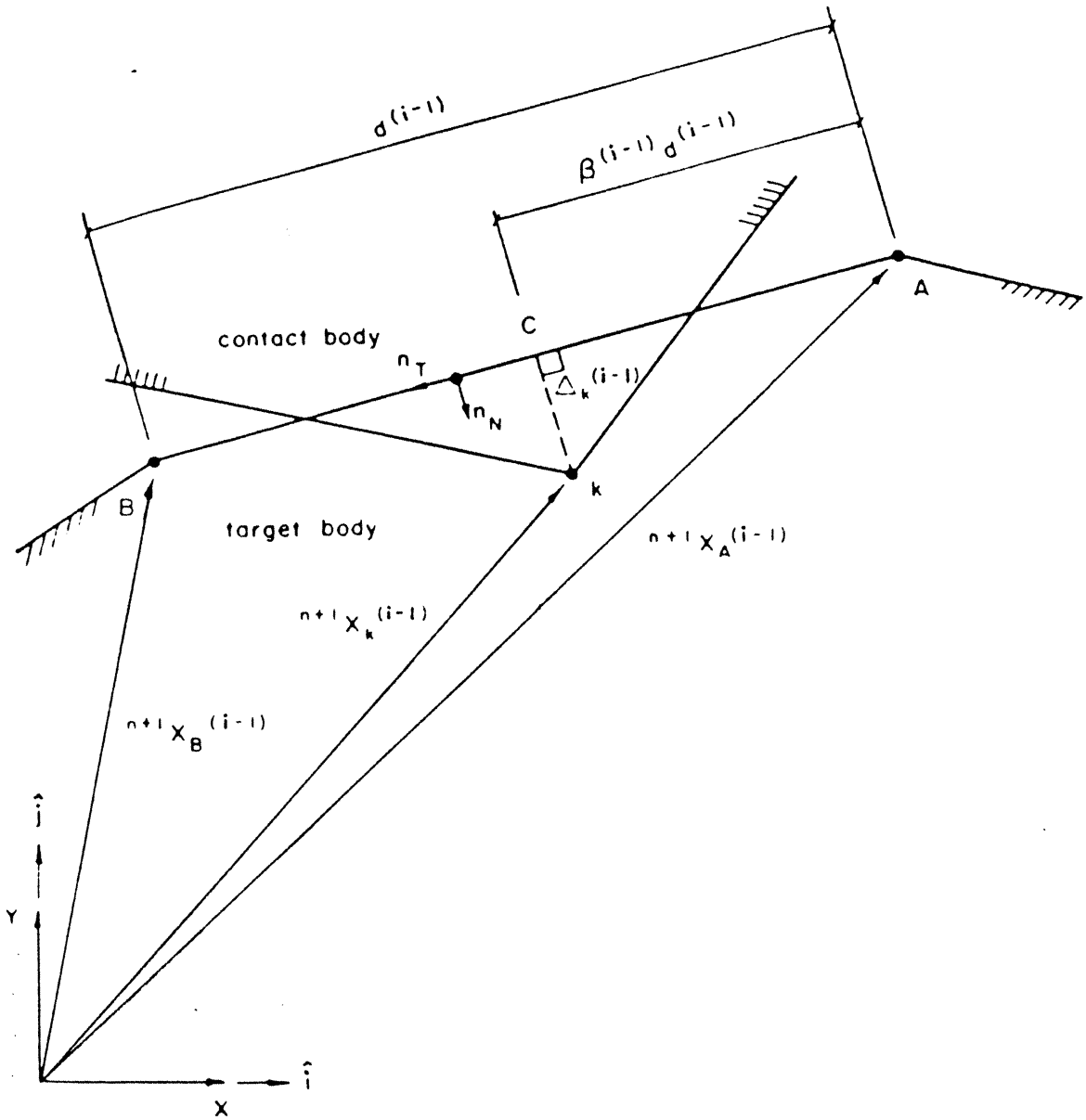

Figure 2.7. Schematic Representation of a Contact Point

$\Delta u^{(i)}$ is the incremental displacement vector in iteration (i); of dimension ($NEQ \times 1$)

$\Delta \lambda_c^{(i)}$ is the incremental contact force vector in iteration (i); ($NEQC \times 1$)

$K_T^{(i-1)}$ is the sum of the linear and nonlinear stiffness matrices of Eq. 2.41 after iteration (i-1); ($NEQ \times NEQ$)

$K_C^{(i-1)}$ is the contact stiffness matrix, for the effect of contact conditions after iteration (i-1); ($NEQT \times NEQT$)

$R_C^{(i-1)}$ is the updated contact force vector after iteration (i-1); ($NEQ \times 1$)

$\Delta_C^{(i-1)}$ is the overlap vector; ($NEQC \times 1$)

NEQ = total number of displacement degrees of freedom

NEQC = total number of incremental contact constraint equations

NEQT = NEQ + NEQC .

When the modified Riks-Wempner method is used to solve Eq. 2.44, the two-step procedure of Eq. 2.25 to 2.27b is given as

$$\Delta r^k = \begin{bmatrix} \Delta u^k \\ \Delta \lambda^k \end{bmatrix} = \Delta \lambda^k \begin{bmatrix} \Delta u^{kI} \\ 1 \end{bmatrix} + \begin{bmatrix} \Delta u^{kII} \\ 0 \end{bmatrix} \tag{2.45}$$

where

Δu^{kI} and Δu^{kII} are the solutions of

$$\begin{bmatrix} K_T & K_C \\ K_C & 0 \end{bmatrix} \begin{bmatrix} \Delta u^{kI} \\ \Delta \lambda_c^I \end{bmatrix} = \begin{bmatrix} \overline{Q} \\ \Delta_C^I \end{bmatrix} \tag{2.46}$$

$$\begin{bmatrix} K_T & K_C \\ K_C & 0 \end{bmatrix} \begin{bmatrix} \Delta u^{kII} \\ \Delta \lambda_c^{II} \end{bmatrix} = \begin{bmatrix} R \\ 0 \end{bmatrix} - \begin{bmatrix} F \\ 0 \end{bmatrix} + \begin{bmatrix} R_C \\ \Delta_C^{II} \end{bmatrix} \tag{2.47}$$

Because the contact problem involves nodal displacements and contact forces, both must be within acceptable tolerances. The convergence criteria on both the change in total internal energy and the change in contact forces were used for the termination of the iteration.

The convergence criteria are given as (Bathe and Chaudhary, 1985; Chan and Barker, 1985)

$$\frac{\Delta U^{(i)T}({}^{n+1}R^{(i)} + {}^{n+1}R_c^{(i-1)} - {}^{n+1}F^{(i-1)})}{\Delta U^{(1)T}({}^{n+1}R + {}^{n}R_c - {}^{n}F)} < ETOL \tag{2.48}$$

$$\frac{\|\Delta R^{(i-1)} - \Delta R^{(i-2)}\|}{\|\Delta R^{(i-1)}\|} < RCTOL \tag{2.49}$$

for incremental internal energy and contact forces, respectively, where

${}^{n+1}R^{(i)}$ is the total applied force vector in i^{th} iteration of $(n+1)^{th}$ load step

${}^{n+1}R_c^{(i-1)}$ is the contact force vector in $(i-1)^{th}$ iteration of $(n+1)^{th}$ load step

${}^{n+1}F^{(i-1)}$ is the internal nodal force vector in $(i-1)^{th}$ iteration of $(n+1)^{th}$ load step

$\Delta U^{(i)}$ is the incremental displacement vector after i^{th} iteration

$\Delta U^{(1)}$ is the incremental displacement vector after 1^{st} iteration of each load step, in the modified Riks-Wempner method, this is the solution obtained from Eq. 2.24

${}^{n}R_c$ is the contact force vector obtained in the n^{th} load step (i.e., previous load step)

${}^{n}F$ is the internal nodal force vector in the n^{th} load step (i.e., previous load step)

$\|\Delta R^{(i-1)}\|$ is the norm of all the components in unbalanced force vectors obtained after $(i-1)^{th}$ iteration corresponding to the contact forces.

The N-S diagram for modified Riks-Wempner algorithm on contact problem is shown in Figure 2.8.

2.10 Test Problem 1

A tip-loaded cantilever investigated by Tang (1980) was modeled by the eight-node elements (see Fig.2.9). The purpose of this test problem is to verify the application of the modified Riks-Wempner method on elastic-plastic buckling of cantilever beams.

While λ < maximum prescribed value		
Generate K_T^0 and K_c^0		
Solve Eq. (2.44) for Δq^{0I}		
If this is first pass by the point Then		else
Prescribe $\Delta\lambda^0$		Decide SIGN ($\pm$)
$\Delta s = \Delta\lambda^0(\Delta q^{0I} \cdot \Delta q^{0I} + 1)^{1/2}$		$\Delta\lambda^0 = \dfrac{SIGN\ \Delta s}{(\Delta q^{0I} \cdot \Delta q^{0I} + 1)^{1/2}}$
$\Delta q^0 = \Delta\lambda^0 \Delta q^{0I}$		
$q^1 = q^0 + \Delta q^0$		
$\lambda^1 = \lambda^0 + \Delta\lambda^0$		
Compute internal forces due to deformations, F		
Update contact conditions due to deformations		
Compute contact forces for updated contact conditions		
While not converged		
$Q^k = \lambda^k \bar{Q}$		
$R^k = Q^k - F^k + R_c^k$		
Generate K_T^k and K_c^k		
Solve Eq. (2.46) for Δq^{kI}		
Solve Eq. (2.47) for Δq^{kII}		
$\Delta\lambda^k = \dfrac{-(\Delta q^0 \cdot \Delta q^{kII})}{(\Delta q^0 \cdot \Delta q^{kI} + \Delta\lambda^0)}$		
$q^{k+1} = q^k + \Delta q^k$		
$\lambda^{k+1} = \lambda^k + \Delta\lambda^k$		
Compute internal forces, F		
Update contact conditions		
Compute contact forces		
Test convergence for internal energy and contact forces		
Record values at new equilibrium point		
Scale Δs by $\Delta s\,(\hat{I}/I)^{1/2}$		

Figure 2.8. Modified Riks-Wempner Algorithm on Contact Problems

The transverse load and tip deflection for different load steps are plotted in Figure 2.10. Since the material is assumed to be rigid-plastic with strain hardening (Tang, 1980), it can be seen that the tip deflection asymptotically approaches the length of the cantilever. The equilibrium curve shows an excellent agreement with the numerical result by Tang (1980).

2.11 Test Problem 2

The second test problem is a cantilever subjected to a uniformly distributed load (see Fig.2.11), which has been studied by many authors using the Newton-Raphson method (Bathe and Cimento, 1979; Katzenberger, 1983; Chan and Barker, 1985). This problem was selected to verify the capability of the program for handling a distributed load.

Katzenberger (1983) has indicated that the solution will converge to an incorrect value if the external load is a function of the configuration and the external load is neglected in the modeling process. In this study, the structure was modeled by five eight-node elements. Both the configuration-independent and follower load were applied. The result shows that the deflection under follower load is larger than that under configuration-independent load (see Fig.2.12). Comparing with the analytical result by Holden (1972) and numerical result by Katzenberger (1983) for configuration-independent and follower load, respectively, the load-displacement curves generated by the current program are the same as those presented in the literature.

2.12 Test Problem 3

The third test problem is a shallow circular arch under uniform pressure. The configuration, initial load increment, material and geometric properties are shown in Figure 2.13. Both five and ten eight-node isoparametric plane stress elements were used for one half of the arch.

The results are plotted in Figure 2.14 as non-dimensional load ($\bar{p}$) versus deflection ($\frac{w}{R}$), where

$$\bar{p} = \frac{12\beta^2 R^3}{\pi^2 E h^3} p$$

β is half of open angle of the arch (in radians)

R is radius of middle plane of the circular arch

p is the distributed pressure along the arch

E is Young's modulus

h is depth of cross section for the arch

The plot obtained is similar to those given by Sharifi and Popov (1971) and Ramm (1980) (see Fig. 2.14). However, a comment must be made here. While testing this problem, an attempt was made to study the difference between the results obtained from two different meshes. It was found that the five-element model needs a more strict convergence tolerance to get results similar to those of the ten-element model. Figure 2.15 shows an incorrect representation of the load-deflection curve, which was obtained from the five-element model using the same convergence tolerance as the ten-element model. After replacing the convergence tolerance, which is one-tenth of that used in the ten-element model, the five-element model gives a satisfactory result (see Fig. 2.16).

2.13 Test Problem 4

To illustrate the validity of the modified Riks-Wempner algorithm applied to a contact problem, the buried pipe problem of Bathe and Chaudhary (1985) is analyzed.

Figure 2.17 shows a pipe buried in soil and subjected to the overburden pressure p_0 . In this analysis, both the pipe and the soil are considered to be linear elastic media having the following properties :

Pipe, Young's modulus = $20.7 \times 10^7\ kpa$

Poisson's ratio = 0.30

Moment of inertia = $2.533 \times 10^{-7}\ m^4$

Mean radius = $0.84\ m$

Soil, Young's modulus = $18.4 \times 10^3\ kpa$

Poisson's ratio = 0.33

The objective of this test is to predict tractions along the pipe-soil interface under different frictional conditions.

In this study, eight-node elements are used to model the soil and the pipe. The finite element mesh is shown in Figure 2.17. Three different values of friction coefficients ($\mu = 0, \mu = 0.25, \mu = \infty$) are used to investigate the problem and the results are shown in Figure 2.18. For the extreme cases, $\mu = 0\ and\ \mu = \infty$, the exact analytical solutions have been obtained by Burns (1965) :

For $\mu = 0$,

$$f_N = p_0(0.952 + 0.019 \cos 2\theta)$$

For $\mu = \infty$,

$$f_N = p_0(0.952 - 0.261 \cos 2\theta)$$

$$f_T = 0.555 p_0 \sin 2\theta$$

As seen from the figure, the numerical results of two cases, $\mu = 0$ and $\mu = \infty$, are very similar to the analytic solution. However, no analytical solution is available to compare with the calculated result for $\mu = 0.25$.

Cross Section :

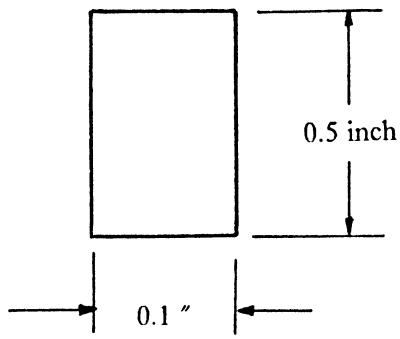

$A = 0.05\ inch^2$

E = 30000000 psi

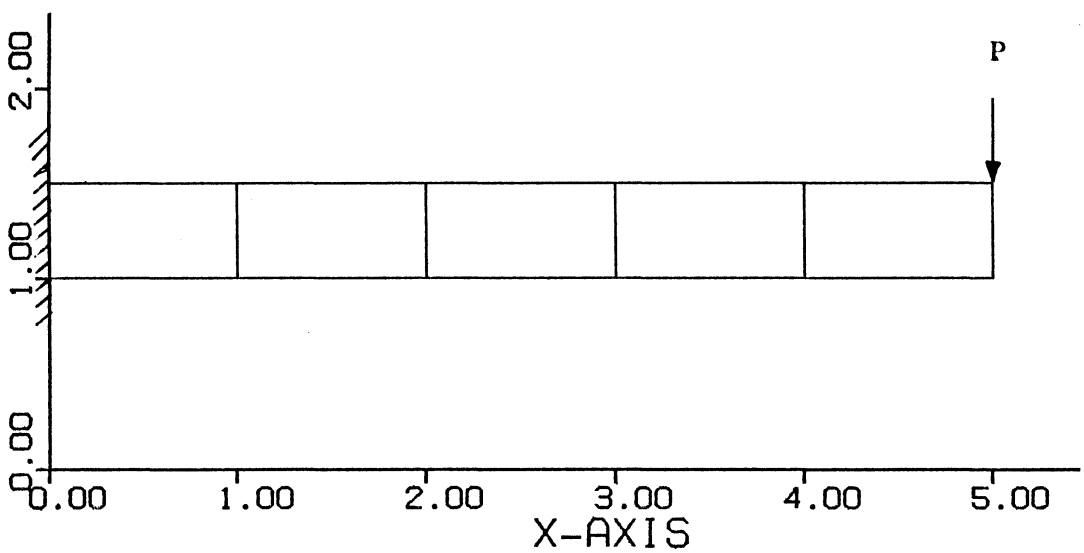

Figure 2.9. Test Problem 1

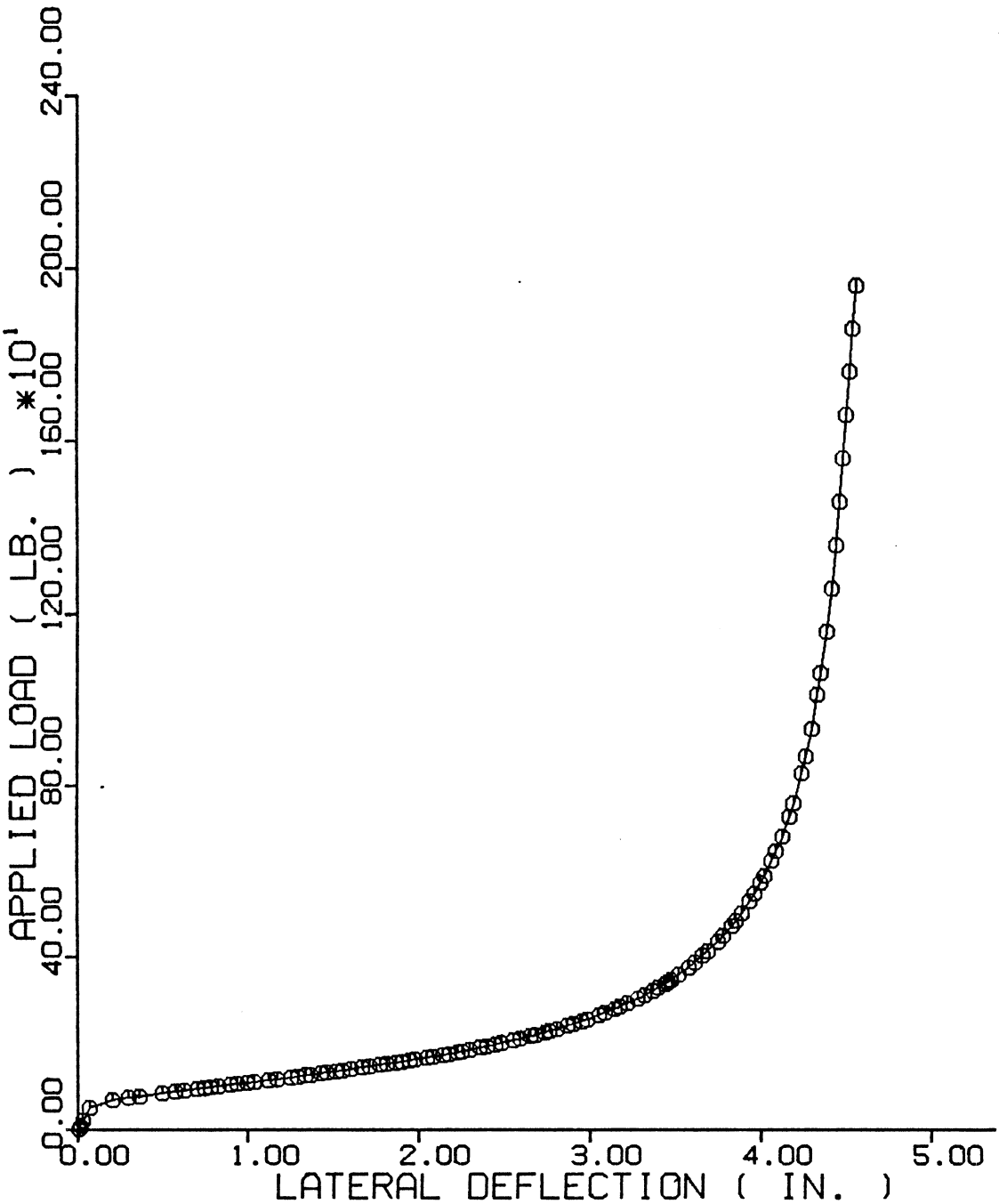

Figure 2.10. Result of Test Problem 1

Cross Section :

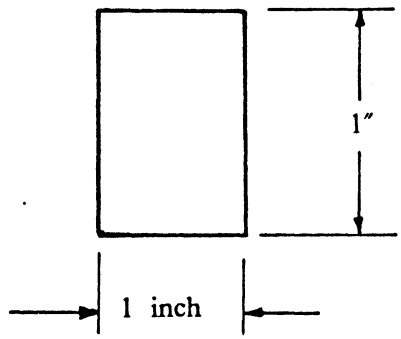

A = 1 $inch^2$

E = 30000000 psi

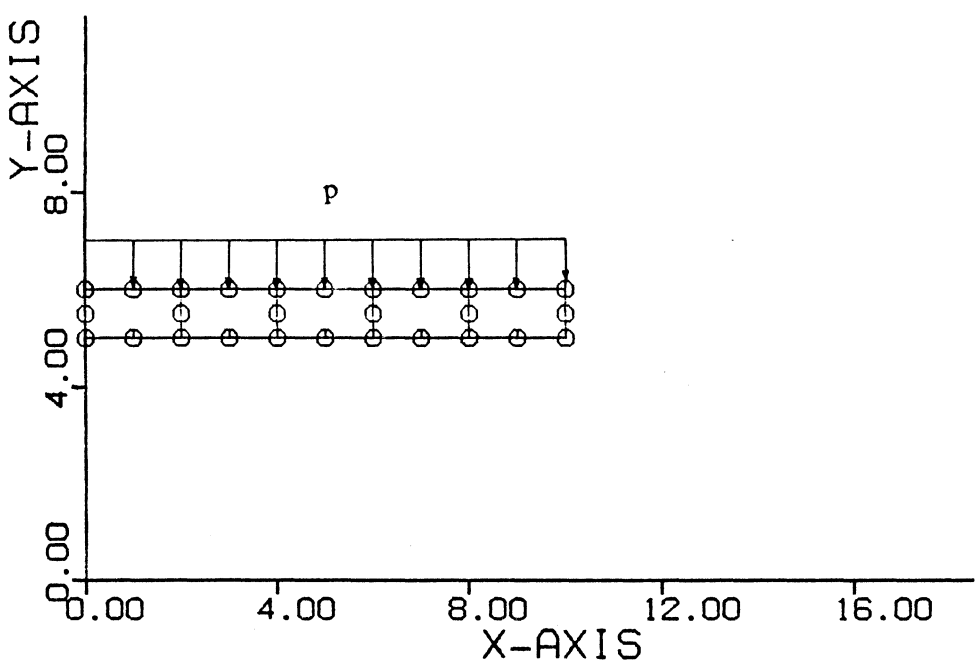

Figure 2.11. Test Problem 2

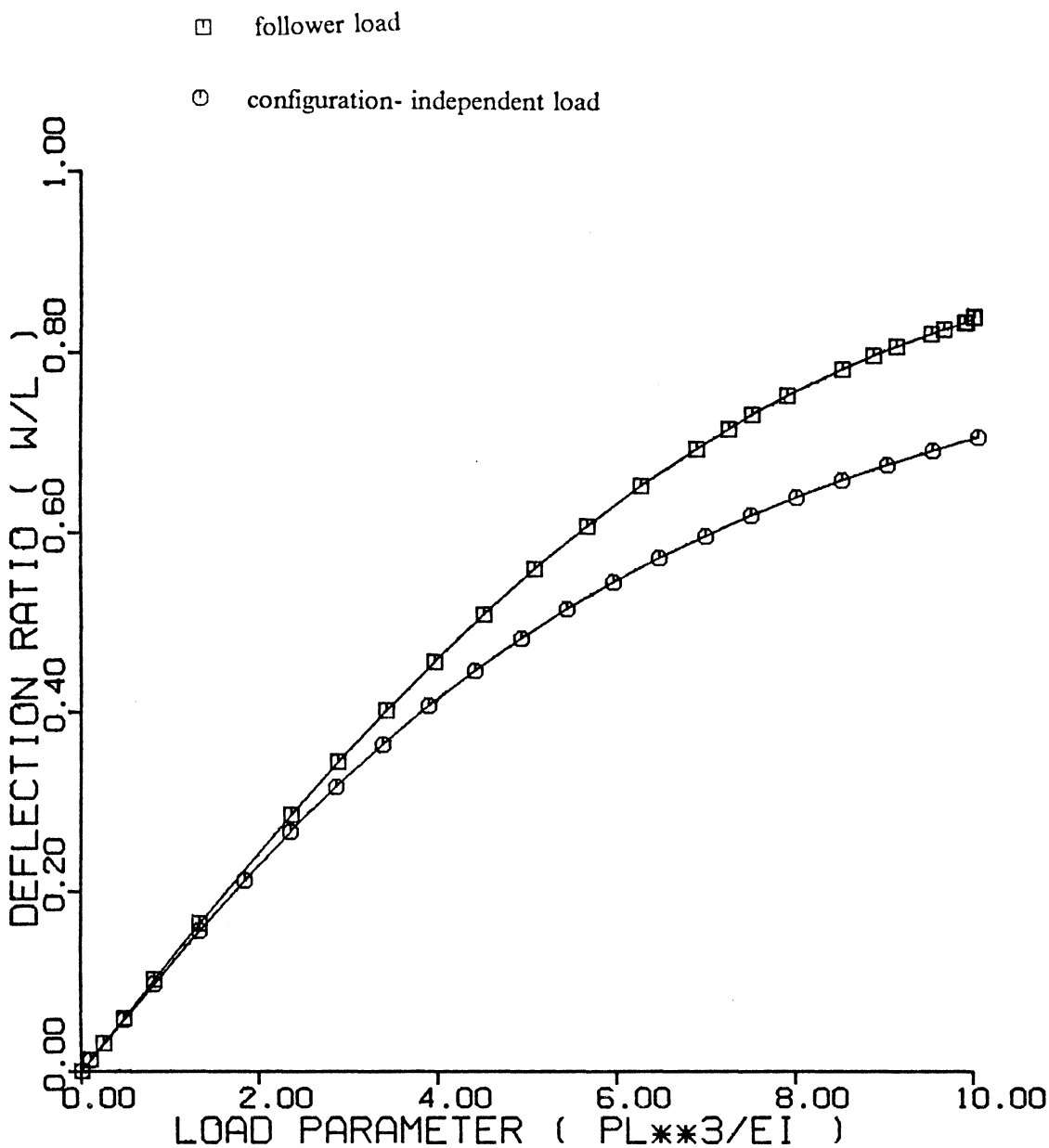

Figure 2.12. Result of Test Problem 2

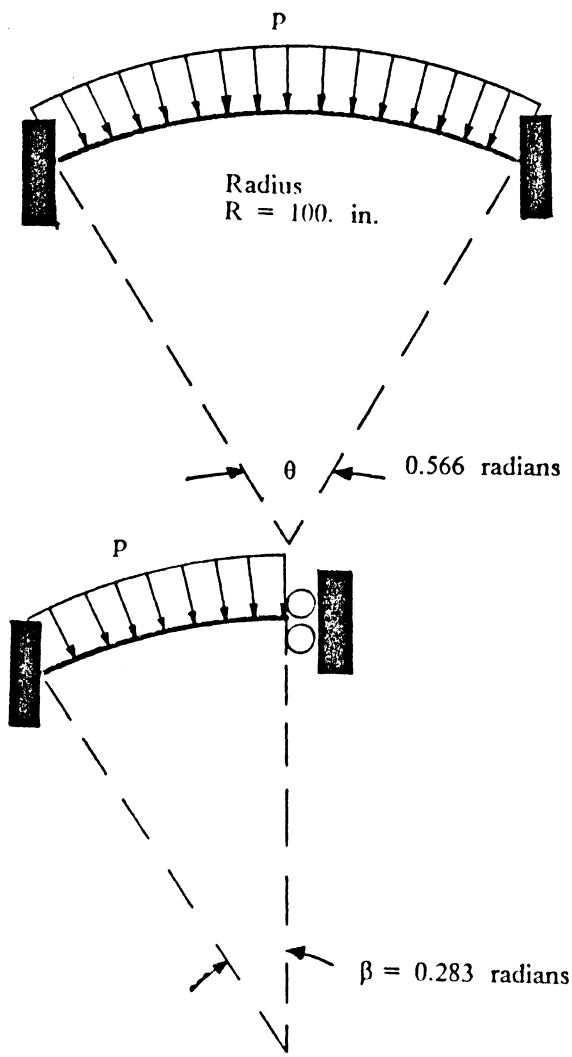

h = 2 in.

A = 2 in^2

E = 10000 Ksi

$\Delta\lambda^0$ = 0.3

Figure 2.13. Test Problem 3

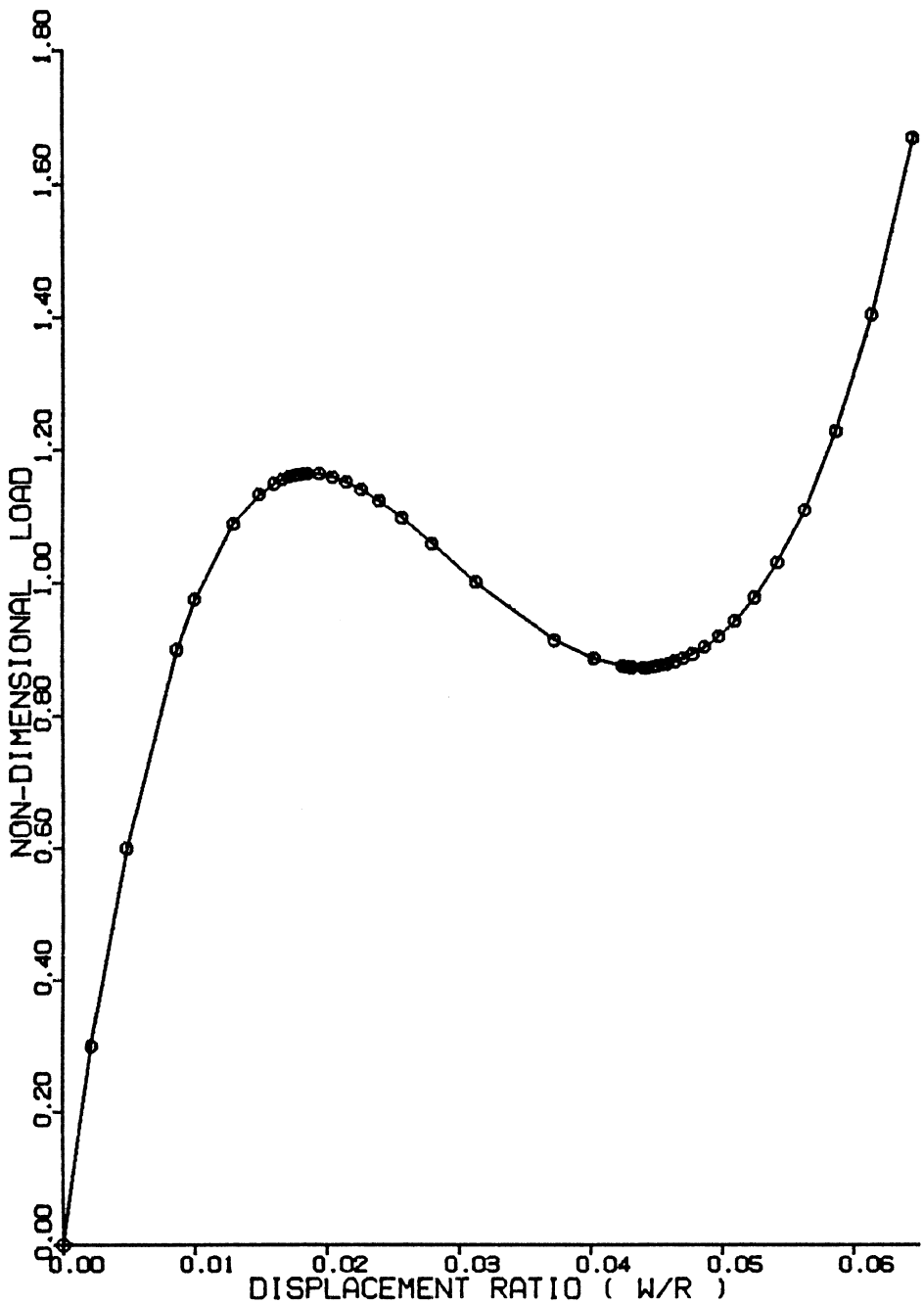

Figure 2.14. Result of Ten-Element Model

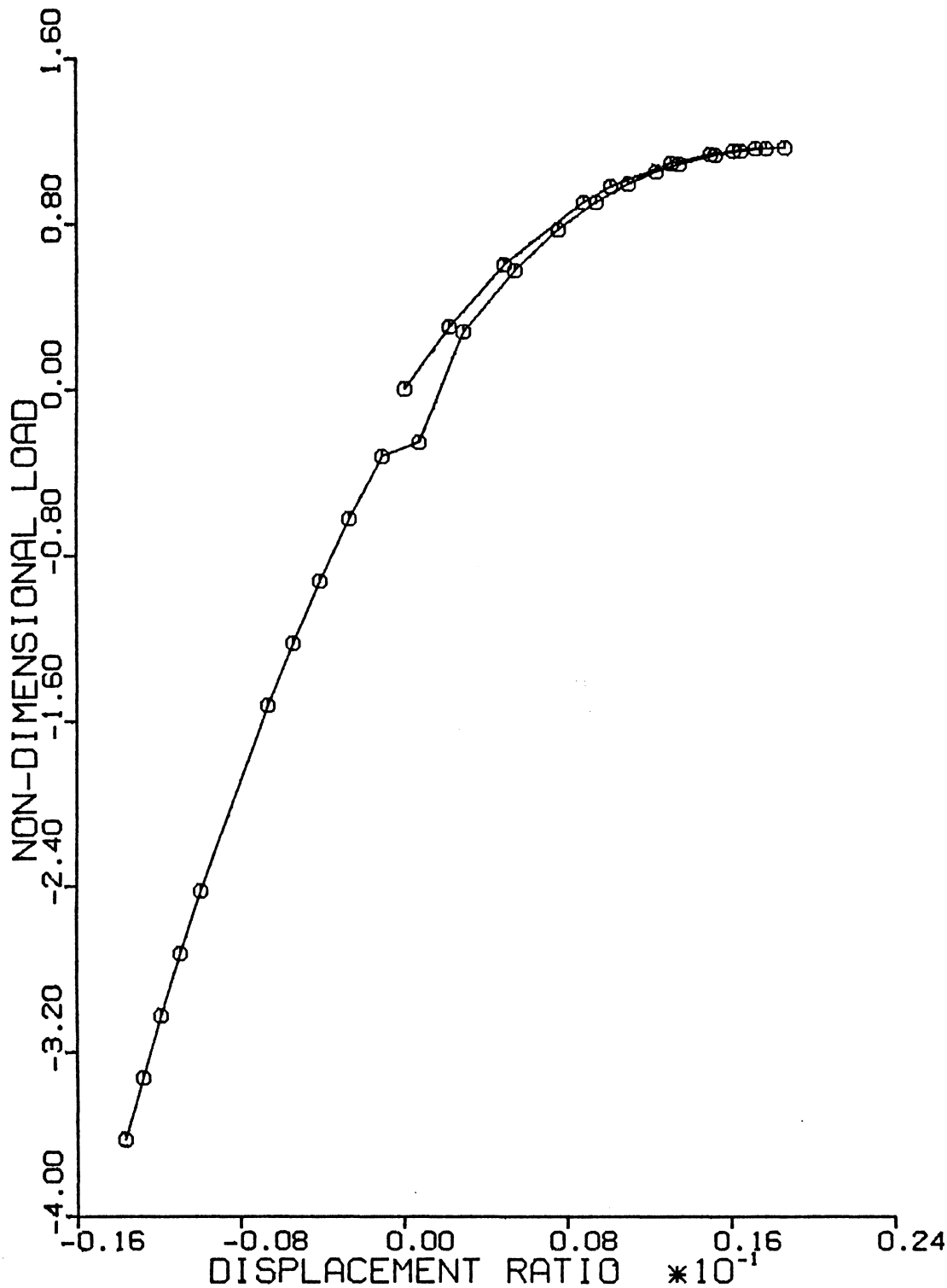

Figure 2.15. Wrong Representation of Load-Deflection Curve

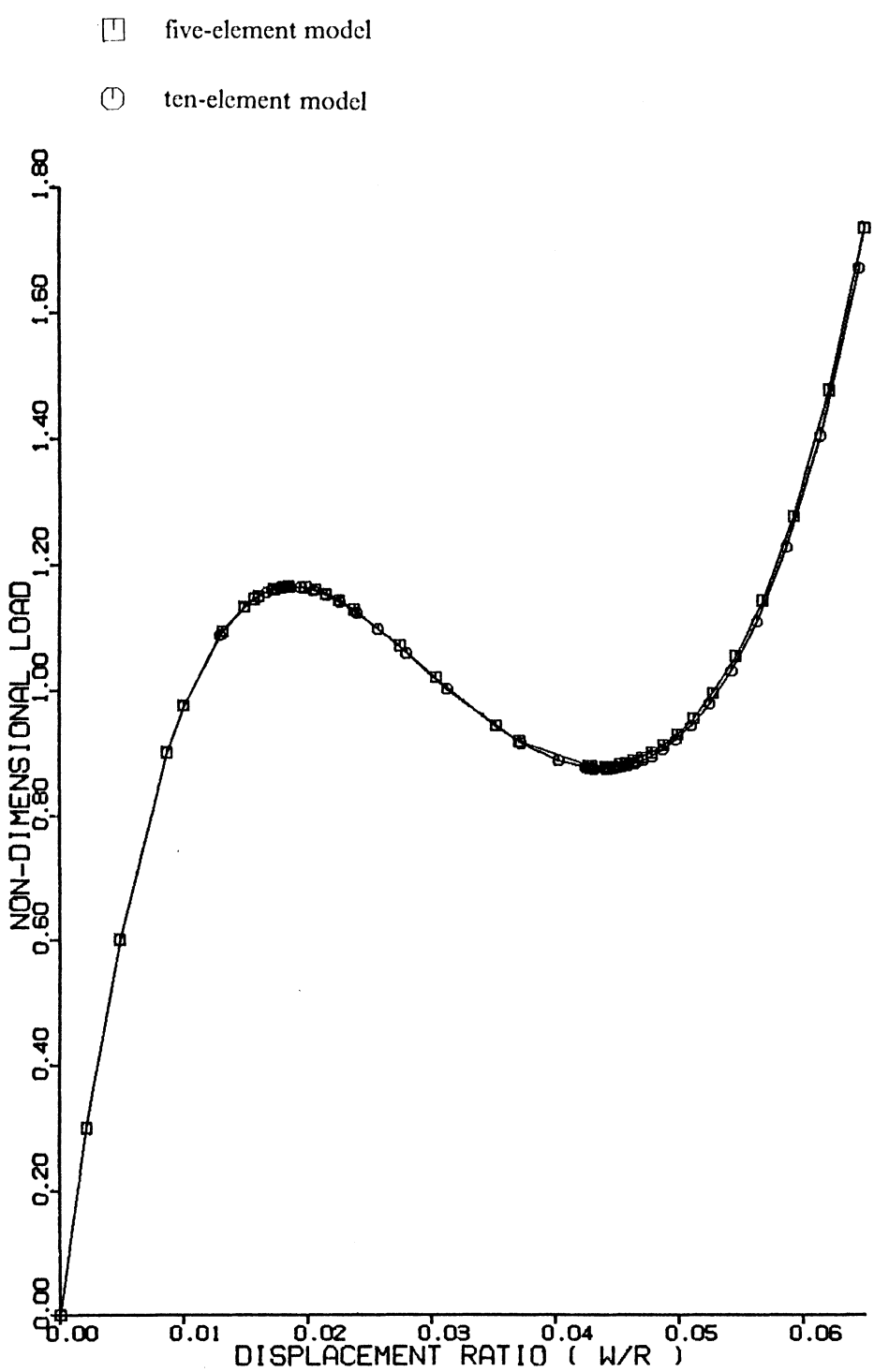

Figure 2.15. Comparison of Five and Ten-Element Model

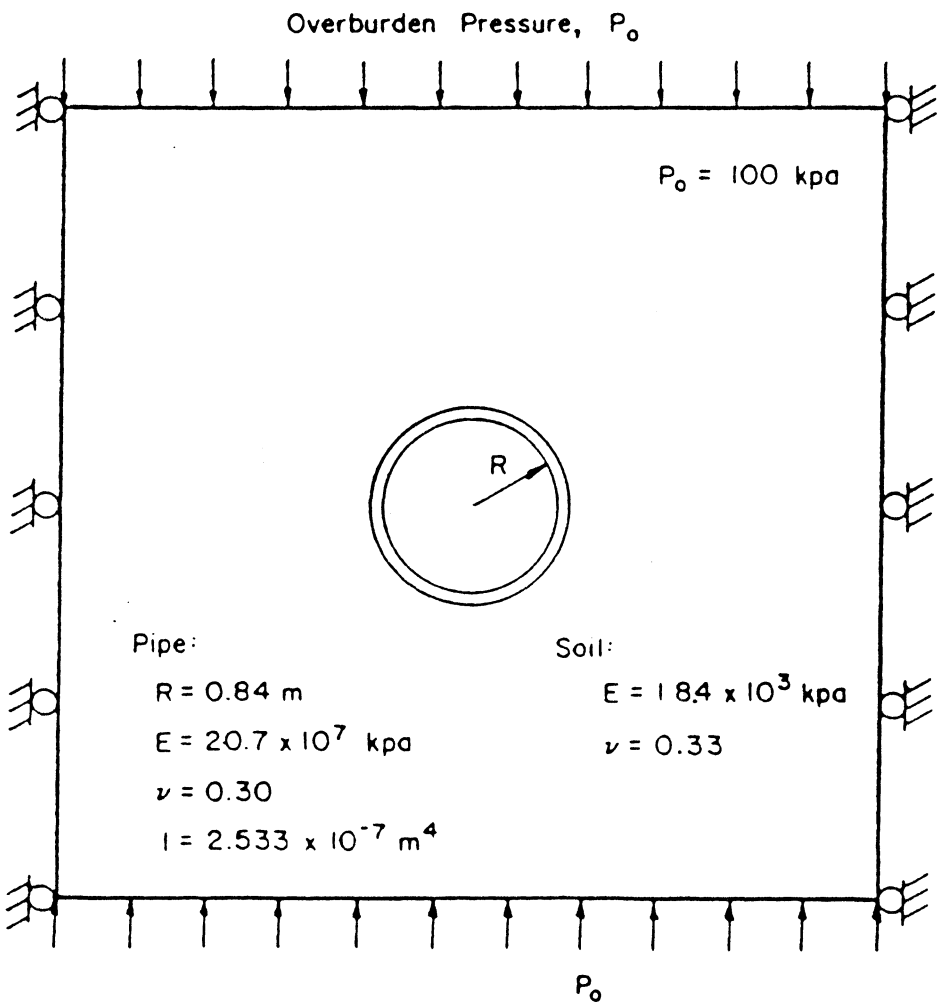

Figure 2.17. Buried Pipe under Overburden Pressure

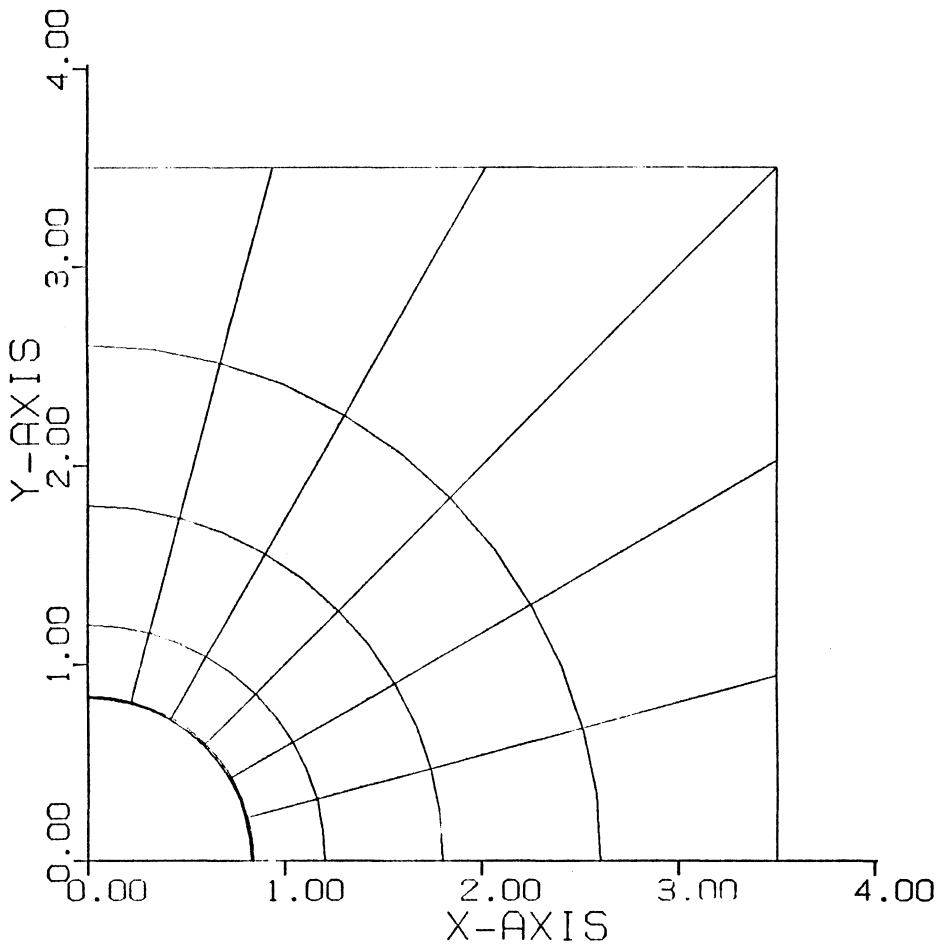

Figure 2.18. Finite Element Mesh for Buried Pipe

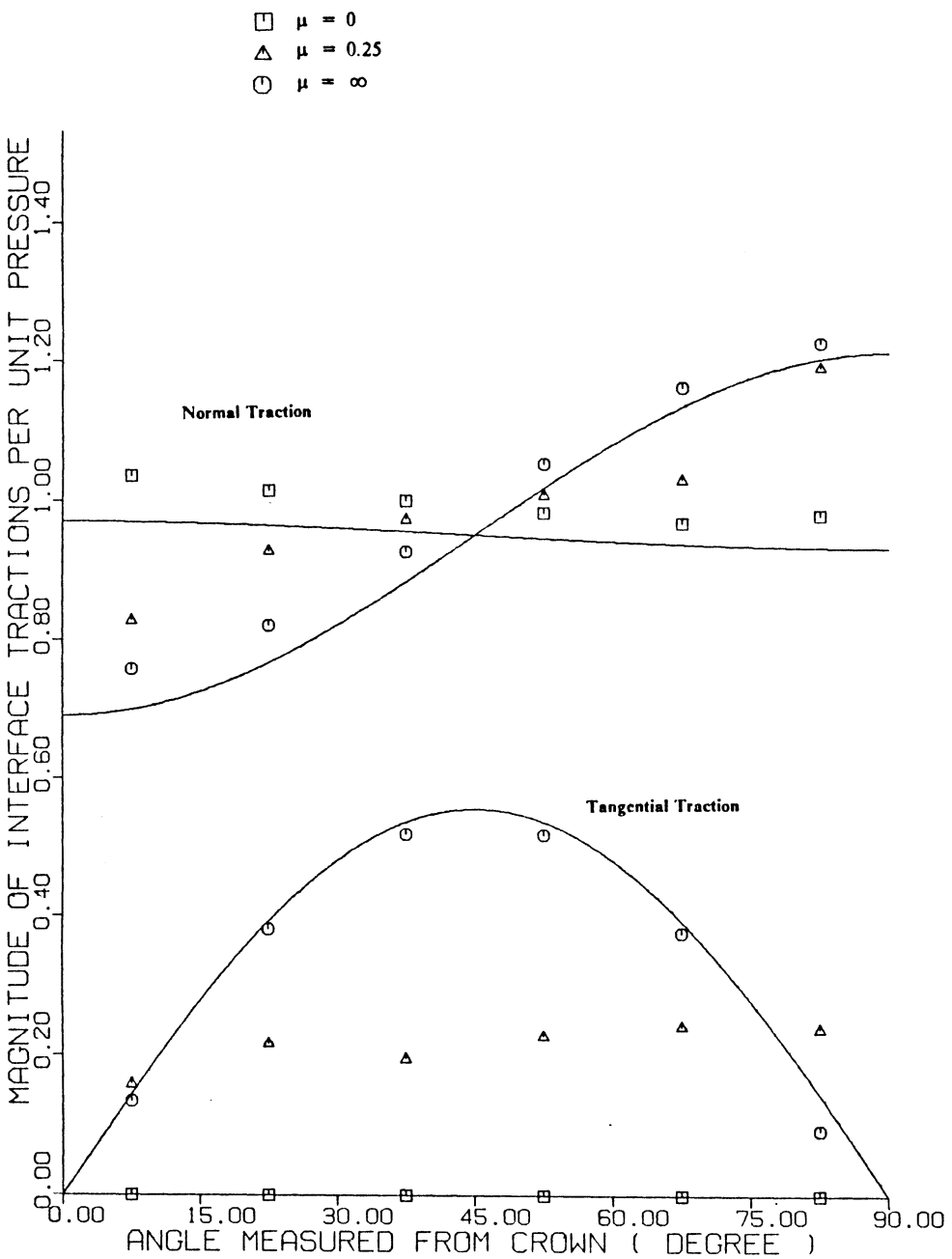

Figure 2.19. Result of Buried Pipe under Overburden Pressure

Chapter 3

Mesh Refinement and Convergence for Contact Problem

3.1 Straight Boundary and Curved Boundary

When the finite element method is used to solve a given problem, the first step is to discretize the continuum, i.e., divide the continuum into elements. Although the number and the type of elements to be used usually depend on the judgement and experience of the analyst, attention should be given to the problem that contains a curved boundary.

In problems with straight line boundaries, we can expect to get a desired accuracy by increasing the number of elements. However, the finite element solution may not be accurate when using straight-line elements to approximate the curved boundary (Krauthammer, 1979). Birkhoff (1969), and Strang and Fix (1974) have shown that a "Boundary Layer Effect" exists in such cases, and the solutions in the direction normal to the boundary "will almost always converge to the wrong answer". As indicated by Krauthammer (1979), the numerical accuracy for some problems may not come up with the geometrical accuracy.

To evaluate the accuracy of the finite element method near a curved boundary, Krauthammer (1979) has successfully demonstrated the differences between the actual curved boundary problem and the simulated boundary model by analyzing the "Kirsch problem" (see Fig. 3.1). He divided the model into two parts. The first, defined as "region A", is the area between the boundary of the hole and a curved line parallel to the boundary of the hole. The second part of the model is the area outside "region A". By changing the configuration of the elements inside "region A" (see Fig .3.2), the errors resulting from a boundary layer effect were obtained.

The analytical solution is given in the book by Timoshenko and Goodier (1951) as follows :

$$\sigma_r = \frac{T}{2}(1 - \frac{a^2}{r^2}) + \frac{T}{2}(1 + 3\frac{a^4}{r^4} - 4\frac{a^2}{r^2}) \cos 2\theta$$

$$\sigma_\theta = \frac{T}{2}(1 + \frac{a^2}{r^2}) - \frac{T}{2}(1 + 3\frac{a^4}{r^4}) \cos 2\theta \qquad (3.1)$$

$$\tau_{r\theta} = \frac{T}{2}(1 - 3\frac{a^4}{r^4} + 2\frac{a^2}{r^2}) \sin 2\theta$$

where

a = Radius of the circular hole

T = Uniaxial tension acting on the plate

θ = Angle between a radius vector, from the center of the hole, and the direction of the tension T

r = Radius vector to any point on the plate

The calculation of the error for each different configuration of the elements within "region A" was performed by (Krauthammer, 1979) :

$$\text{error} = \frac{\sigma_T - \sigma_N}{\max(\sigma_T, 1)} \qquad (3.2)$$

where

σ_T represents theoretical solution

σ_N represents numerical solution

In Table 3.1, it can be seen clearly that when using curved isoparametric elements on the curved boundary, fewer elements are needed and better accuracy can be obtained.

Zlamal (1973) also indicated that the use of elements with curved sides along the curved part of the boundary can give a significant improvement of the accuracy for the solution.

As a conclusion to their discussion (Zlamal, 1973; Strang and Fix, 1974; and Krauthammer, 1979), it has been recommended that one has to place special elements, which are more compatible to the curvature of the boundary, near the curved boundary. One type of these elements is the quadratic isoparametric element used in this study.

Table 3.1

Results of Different Configurations for Region 'A' (Krauthammer, 1979)

Stage	Fig.	Max. error σ_θ , (%)	Angle (deg)	Max. error σ_r , (%)	Angle (deg)
1	3.2a	16.4	84.5	> 100.0	40.3
2	3.2b	1.1	83.5	22.0	83.5
3	3.2c	4.1	87.5	4.0	17.5
4	3.2d	3.4	45.0	3.9	60.0
5	3.2e	< 1.0	all	< 1.0	all

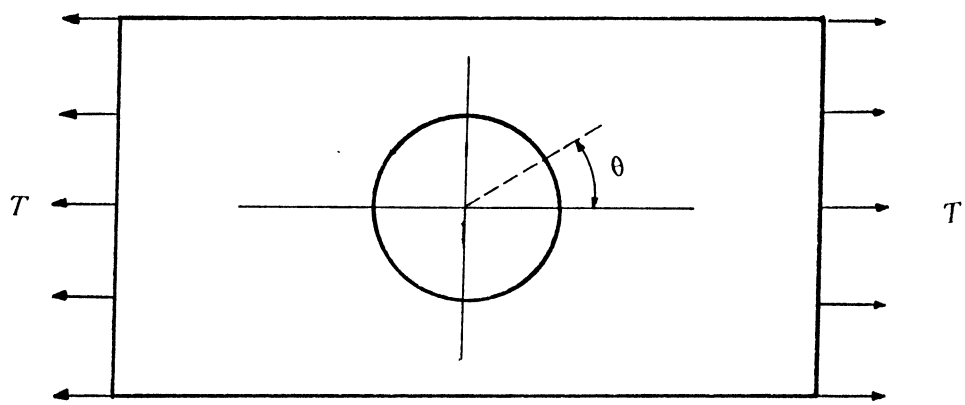

Figure 3.1. Kirsch Problem

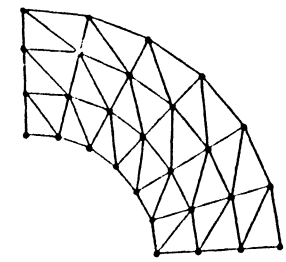

(a) 36 CST Elements

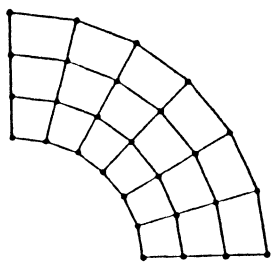

(b) 18 LSQ Elements

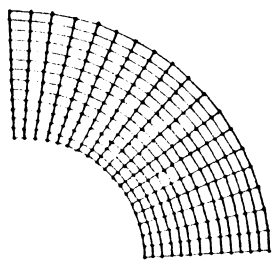

(c) 234 LSQ Elements

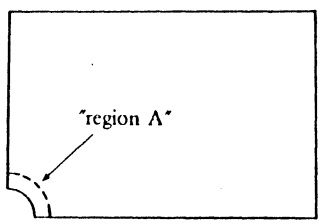

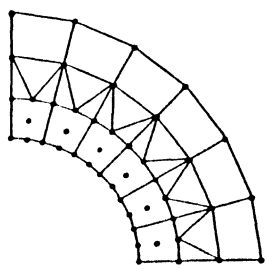

(d) 6 Isoparametric Elements

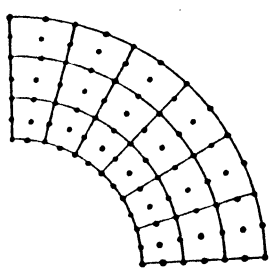

(e) 18 Isoparametric Elements

Figure 3.2. Finite Element Models by Krauthammer (1979)

3.2 Isoparametric Elements in Finite Element Analysis

Elements in which the geometry and the displacements are interpolated in the same way are called isoparametric elements. As discussed in many modern textbooks on the finite element method (Strang and Fix, 1974; Cook, 1981; Reddy, 1984), isoparametric elements are more commonly used due to the ease and efficiency of calculation in the finite element implementation. Once mastered with one type of element, it can be easily applied to most other isoparametric elements. Especially, as discussed in the previous section, the isoparametric formulation permits the generation of elements with curved sides yet maintains interelement compatibility. By writing many element configurations into one subroutine, one can also have the elements of "mixed" type (Zienkiewicz, 1968), i.e., the elements which contain one, two, or no mid-side nodes (see Fig.3.3). Due to this versatility, isoparametric elements are effective in two- and three-dimensional analysis and nonstructural applications.

As is well-known, the choosing of element types and nodes of each element is based on many factors, such as: ease of programming, computer cost, geometry of the structure, characteristics of the problem, and accuracy. In Table 3.2 (Zienkiewicz, 1968) , it can be easily seen that the use of simple triangular elements results in poorer accuracy than the use of rectangular elements, though the geometry of the structure can be exactly represented by both elements. Also, it is noted that as the number of the nodes on rectangular elements increases from 4 to 8, accuracy is greatly improved. But only little improvement of accuracy was achieved by increasing the mid-side nodes on rectangular elements from 8 to 12.

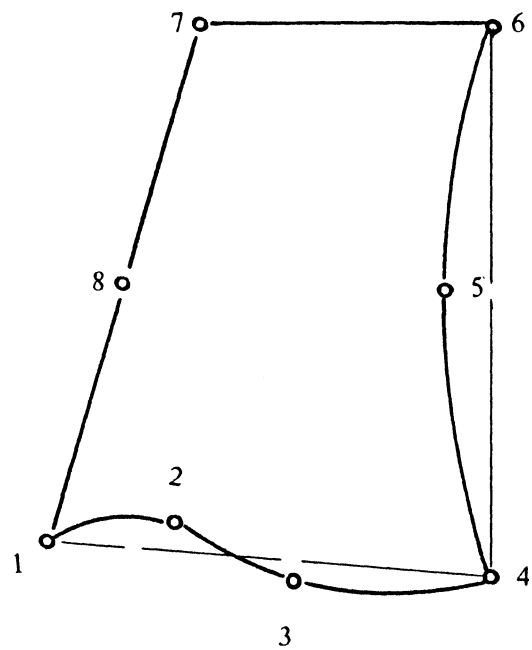

Figure 3.3. Elements of "Mixed" Type

Table 3.2

Four Elements Used to Represent a Cantilever (Zienkiewicz, 1968)

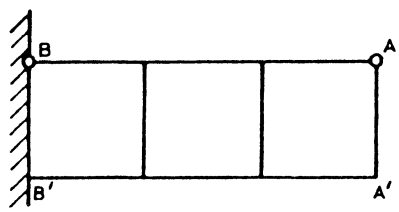

TYPE OF ELEMENT	VERTICAL LOAD OF A		COUPLE AT A A'	
	MAX DEFL AT AA'	MAX STRESS BB'	MAX DEFL AT AA'	MAX STRESS BB'
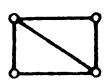	·26	·19	·22	·22
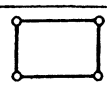	·65	·56	·67	·67
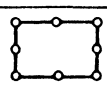	·99	·99	1·00	1·00
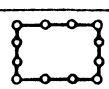	1·00	1·00	1·00	1·00
EXACT	1·00	1·00	1·00	1·00

The global coordinates and displacements of quadratic isoparametric elements are defined as (Zienkiewicz, 1977; Cook, 1981; Bathe, 1982; Reddy, 1984) :

$$x = \sum_{i=1}^{8} N_i x_i$$

$$y = \sum_{i=1}^{8} N_i y_i \qquad (3.3a)$$

$$u = \sum_{i=1}^{8} N_i u_i$$

$$v = \sum_{i=1}^{8} N_i v_i \qquad (3.3b)$$

or in matrix form

$$\begin{Bmatrix} x \\ y \end{Bmatrix}_{2\times 1} = [N]_{2\times 16}\{c\}_{16\times 1} \qquad (3.4a)$$

$$\begin{Bmatrix} u \\ v \end{Bmatrix}_{2\times 1} = [N]_{2\times 16}\{d\}_{16\times 1} \qquad (3.4b)$$

where

$$\{c\} = \{x_1, y_1, x_2, y_2, \ldots, x_7, y_7, x_8, y_8\}$$

$$\{d\} = \{u_1, v_1, u_2, v_2, \ldots, u_7, v_7, u_8, v_8\}$$

$$[N] = \begin{bmatrix} N_1 & 0 & N_2 & 0 \ldots N_7 & 0 & N_8 & 0 \\ 0 & N_1 & 0 & N_2 \ldots 0 & N_7 & 0 & N_8 \end{bmatrix}$$

The shape functions N_i are given as

$$
\begin{aligned}
N_1(\xi, \eta) &= -\frac{1}{4}(1-\xi)(1-\eta)(1+\xi+\eta) \\
N_2(\xi, \eta) &= \frac{1}{2}(1-\xi^2)(1-\eta) \\
N_3(\xi, \eta) &= \frac{1}{4}(1+\xi)(1-\eta)(\xi-\eta-1) \\
N_4(\xi, \eta) &= \frac{1}{2}(1+\xi)(1-\eta^2) \\
N_5(\xi, \eta) &= \frac{1}{4}(1+\xi)(1+\eta)(\xi+\eta-1) \\
N_6(\xi, \eta) &= \frac{1}{2}(1-\xi^2)(1+\eta) \\
N_7(\xi, \eta) &= \frac{1}{4}(1-\xi)(1+\eta)(-\xi+\eta-1) \\
N_8(\xi, \eta) &= \frac{1}{2}(1-\xi)(1-\eta^2)
\end{aligned}
\tag{3.5}
$$

The numbering of nodes and the orientation of local axes ξ, η are shown in Figure 3.4.

By the chain rule, the coordinate transformation of derivatives is

$$
\begin{aligned}
\frac{\partial \varphi}{\partial \xi} &= \frac{\partial \varphi}{\partial x}\frac{\partial x}{\partial \xi} + \frac{\partial \varphi}{\partial y}\frac{\partial y}{\partial \xi} \\
\frac{\partial \varphi}{\partial \eta} &= \frac{\partial \varphi}{\partial x}\frac{\partial x}{\partial \eta} + \frac{\partial \varphi}{\partial y}\frac{\partial y}{\partial \eta}
\end{aligned}
\tag{3.6}
$$

or in vector form

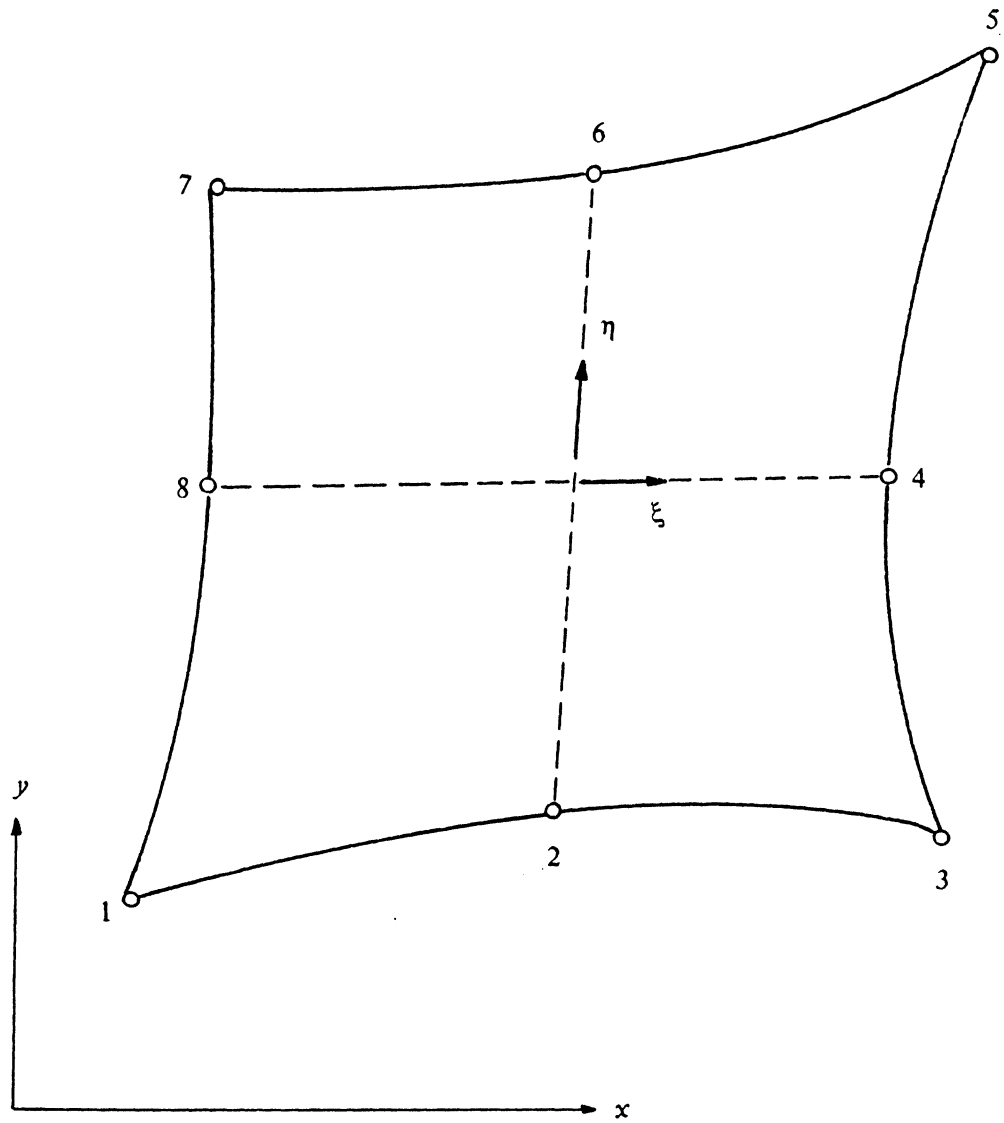

Figure 3.4. Nodal Numbering and Orientation of Load Axes

$$\begin{Bmatrix} \varphi,_\xi \\ \varphi,_\eta \end{Bmatrix} = [J] \begin{Bmatrix} \varphi,_x \\ \varphi,_y \end{Bmatrix} \tag{3.7}$$

where

φ is some function of x and y

$[J]$ is the Jacobian matrix

$$[J] = \begin{bmatrix} \frac{\partial x}{\partial \xi} & \frac{\partial y}{\partial \xi} \\ \frac{\partial x}{\partial \eta} & \frac{\partial y}{\partial \eta} \end{bmatrix} = \sum_{i=1}^{8} \begin{bmatrix} \frac{\partial N_i}{\partial \xi} \cdot x_i & \frac{\partial N_i}{\partial \xi} \cdot y_i \\ \frac{\partial N_i}{\partial \eta} \cdot x_i & \frac{\partial N_i}{\partial \eta} \cdot y_i \end{bmatrix} \tag{3.8}$$

The inverse of the Jacobian matrix can be obtained using standard matrix inversion techniques,

$$[J]^{-1} = \begin{bmatrix} \frac{\partial \xi}{\partial x} & \frac{\partial \eta}{\partial x} \\ \frac{\partial \xi}{\partial y} & \frac{\partial \eta}{\partial y} \end{bmatrix} = \frac{1}{\det J} \begin{bmatrix} \frac{\partial y}{\partial \eta} & -\frac{\partial y}{\partial \xi} \\ -\frac{\partial x}{\partial \eta} & \frac{\partial x}{\partial \xi} \end{bmatrix} \tag{3.9}$$

Rearranging Eq. 3.7, another transformation is obtained :

$$\begin{Bmatrix} \varphi,_x \\ \varphi,_y \end{Bmatrix} = [J]^{-1} \begin{Bmatrix} \varphi,_\xi \\ \varphi,_\eta \end{Bmatrix} \tag{3.10}$$

With the shape functions and formulas of transformation given above, the element stiffness matrix and nodal forces can be formulated by using the Gaussian numerical integration technique. The formulas and assembly process for a system model, which will follow the standard procedures used in general finite element analysis, can be found in books by Bathe (1982), Cook (1981), and

Zienkiewicz (1977). Since it is not the intent of this study to present these and they have been discussed in a previous report (Chan and Barker, 1985), they will not be repeated here.

3.3 Regular and Irregular Elements

Although a given domain can be discretized by different element shapes, some recommendations should be taken when laying out a mesh. That is, keep interior corner angles θ near 90 degrees, and take care of elements aspect ratios such that excessive elongated elements are not used within a mesh (Cook, 1981). In this study, the elements which meet rules stated above are called regular elements, whereas the elements which do not are called irregular elements. Macneal and Harder (1985) indicated that care should be taken when testing is carried out on problems with irregular elements.

In order to study the effect which irregular elements may have on the results of finite element analysis, a cantilever under concentrated load was modelled by two different meshes, mesh A and mesh B, (see Fig. 3.5). In Figure 3.6, the load-deflection curves for irregular meshes were plotted and compared to the result of test problem 1. It can be seen clearly that even if all have equal volume in every mesh, using different shaped elements gives different results. As indicated by Cook (1981), a general quadrilateral element tends to lose accuracy if its form becomes a general quadrilateral rather than a rectangle. Similar conclusions were made by Backlund (1978) and Gifford (1979).

Of course, it is not possible to use standard shapes on all the elements of a mesh, especially for those problems with highly nonlinear geometric boundary. However, it is recommended to avoid unnecessary irregularity within a mesh, particularly when higher accuracy is desired and for those problems which are sensitive to the effect of irregular elements.

3.4 Convergence and Mesh Refinement

The convergence of the results obtained from a finite element analysis is affected by many factors, such as the number, type (e.g., linear, quadratic), shape (e.g., triangular, rectangular), size of elements, and allocation of loads to nodes. Each of these factors may contribute to different or-

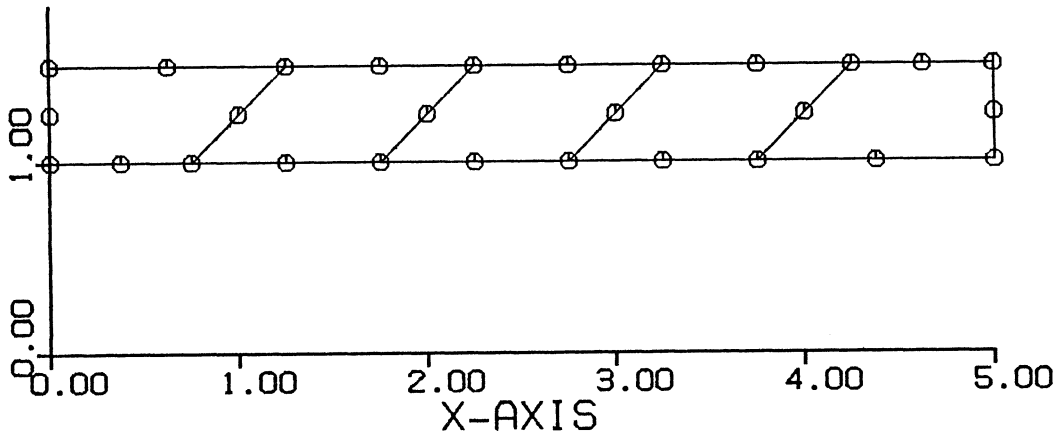

Mesh A

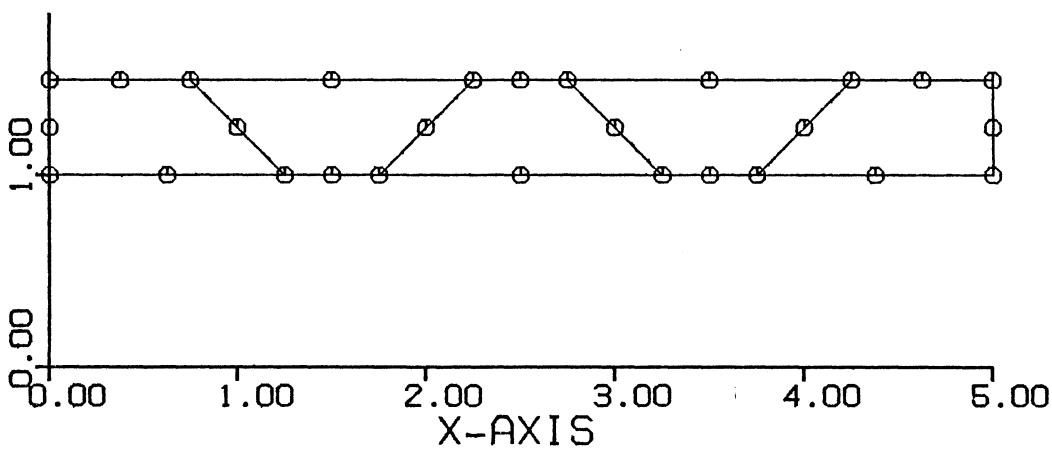

Mesh B

Figure 3.5. Mesh A and Mesh B for Tip-Loaded Cantilever

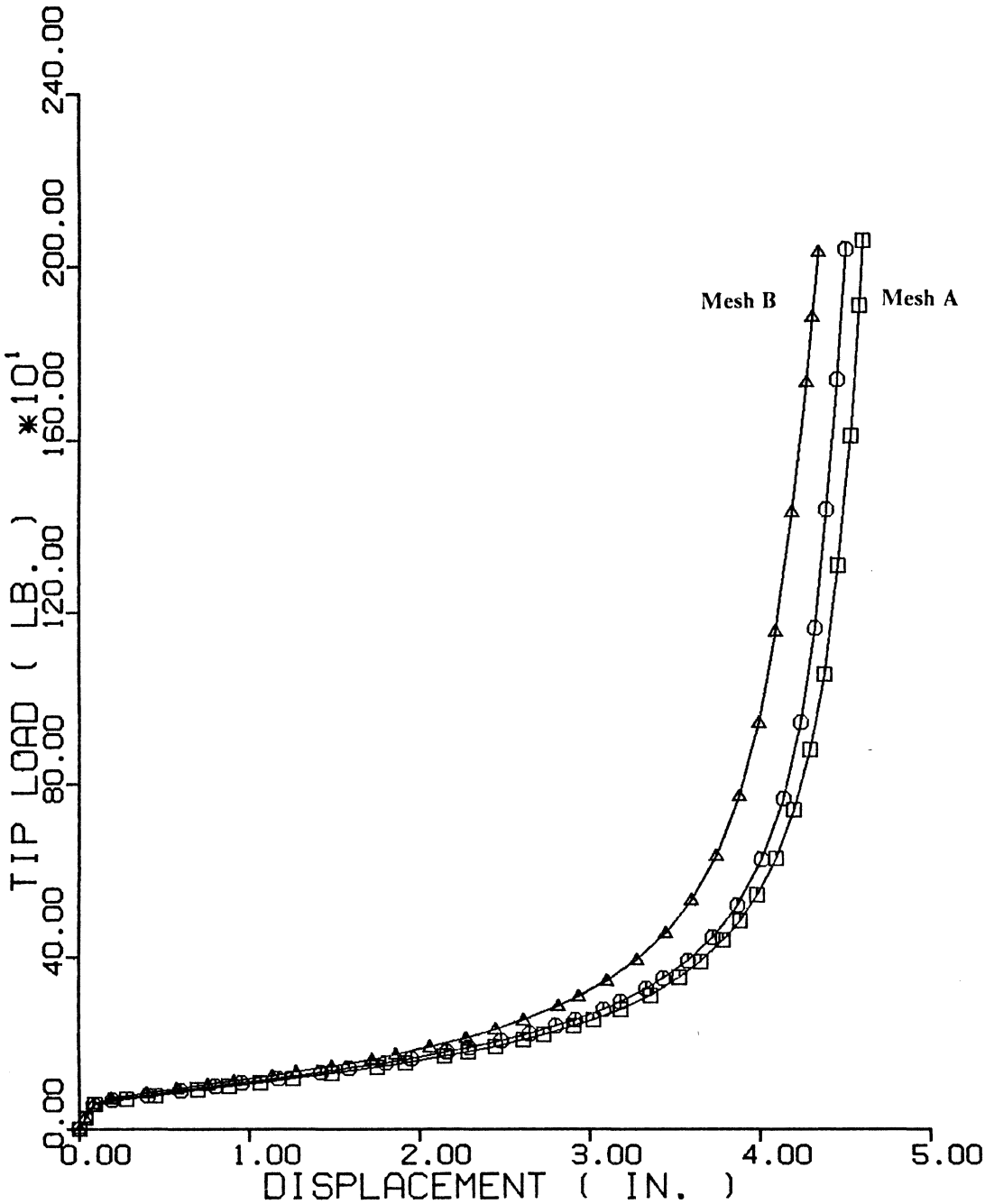

Figure 3.6. Load-Deflection Curves of Mesh A, B, and Test Problem 3

ders of error. Since it is out of the scope of this study to verify the relation between all these factors and convergence, herein is presented only the effect of elements with curved boundary and regular shape on convergence of refined mesh.

The example chosen to demonstrate the effect of curved boundary and regular elements is the Hertz contact problem between an elastic cylinder and rigid block (see Fig. 3.7). The analytical solution, as described in the literature (Timoshenko and Goodier, 1934), is as follows :

For the general case of two elastic bodies in contact, the distribution of pressure q along the width of the surface of contact can be represented by a semi-ellipse. The radii of this semi-ellipse are calculated from :

$$a = \sqrt{\frac{4P'(k_1 + k_2)R_1R_2}{R_1 + R_2}} \tag{3.11}$$

$$b = \frac{2P'}{\pi a} \tag{3.12}$$

where a represents the long radius of an ellipse which is half the width of the surface of contact, b represents the short radius of an ellipse which is the maximum contact pressure at the center of the surface, P' is the applied load, and R_1 and R_2 are radii of the two bodies, respectively.

Constants k_1 and k_2 are defined as :

$$k_1 = \frac{1 - \nu_1^2}{\pi E_1} \tag{3.13}$$

$$k_2 = \frac{1 - \nu_2^2}{\pi E_2} \tag{3.14}$$

where ν_1, ν_2, E_1, E_2 are the Poisson's ratio and Young's modulus of the two bodies, respectively.

Because of double symmetry, only a quarter of the cylinder was modelled by quadratic isoparametric elements. The concentrated load applied at the top of the cylinder was transformed into a distributed load along the upper edge of the quarter cylinder to simulate the real situation

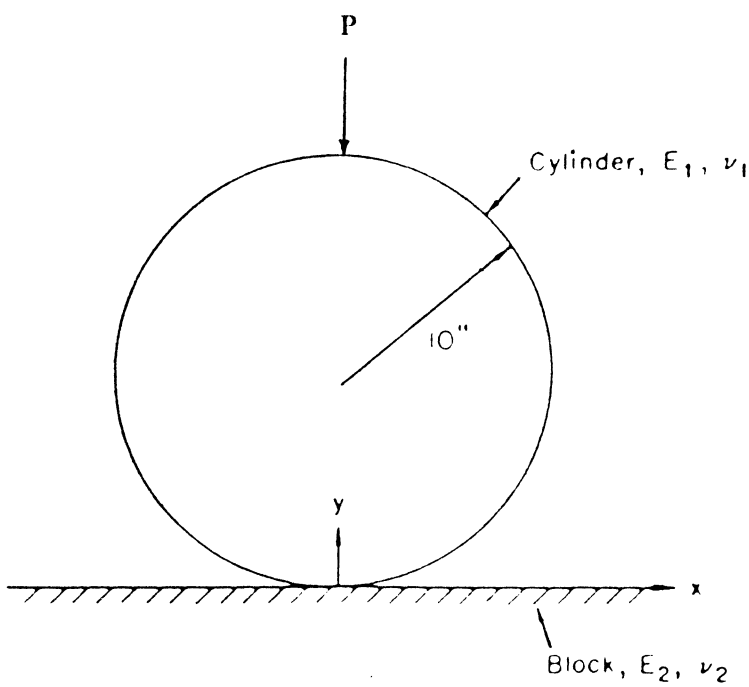

Figure 3.7. Elastic Cylinder and Rigid Block

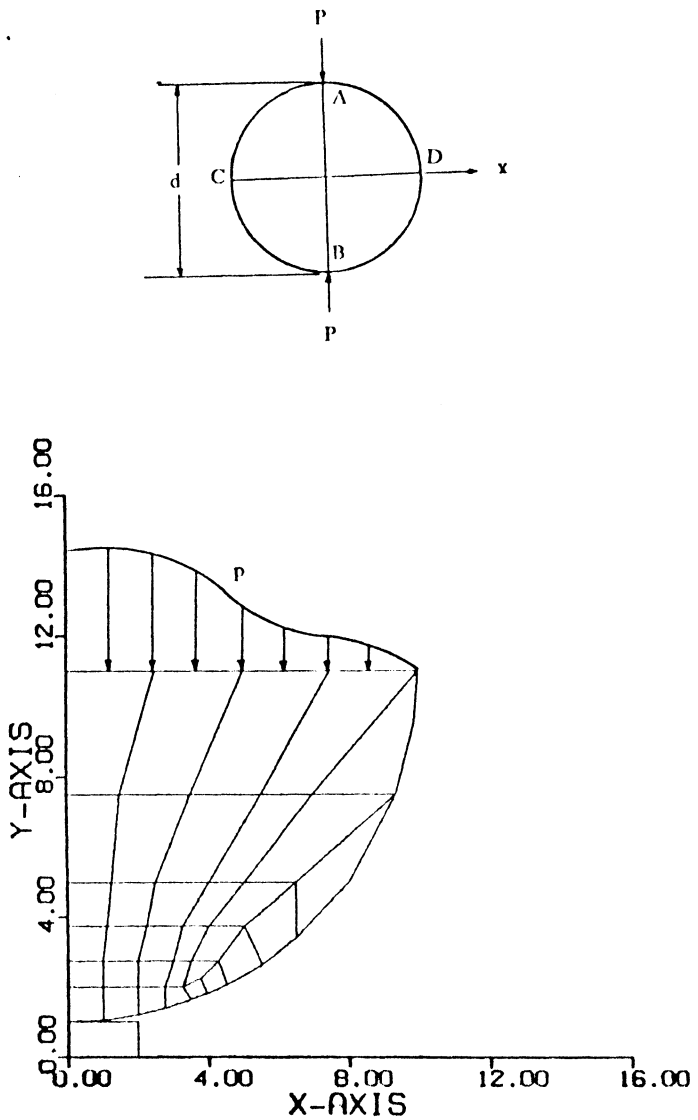

Figure 3.8. Load Distribution of Circular Disk under P

of load distribution. The equation for transformation was given in the book by Timoshenko and Goodier (1934) by

$$\sigma_y = \frac{2P}{\pi d}\left[1 - \frac{4d^4}{(d^2 + 4x^2)^2}\right] \tag{3.15}$$

where

σ_y is the compressive stress along the diameter CD (see Fig. 3.8)

due to the applied load P

P is the two equal and opposite forces acting along the diameter

AB of circular disk

d is the diameter of circular disk

x is the distance from the center of circular disk.

For convenience, the meshes used to model the problem were divided into three groups. The first group contains the meshes with straight line boundary and irregular elements (see Fig. 3.9). In this group, straight line elements were used to model the circular boundary. All the corner nodes of element sides along the boundary layer were placed on the circle , whereas the midside nodes were not. The second group contains the meshes with curved boundary and regular elements (see Fig. 3.10). In this group, curved isoparametric elements were used only near the circular boundary, while more regular straight-line elements were used elsewhere. Both the corner nodes and midside nodes along the boundary layer were placed on the circle. The third group contains the mesh with curved boundary and irregular elements (see Fig. 3.11). In the first two groups, each contains three different meshes, which are named as rough mesh, finer mesh I, finer mesh II, respectively (see Fig.

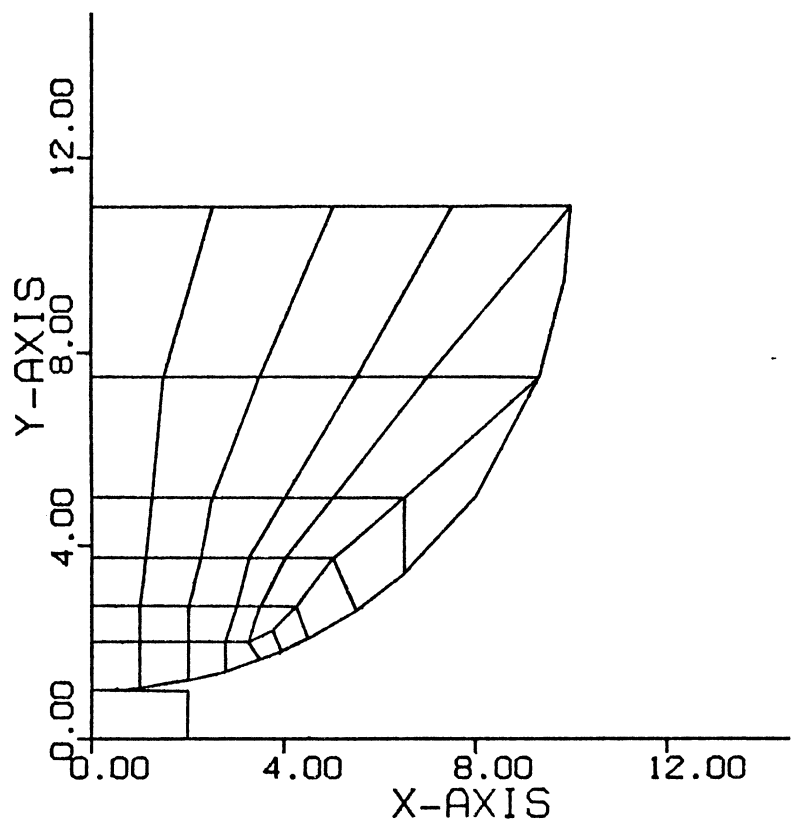

Figure 3.9. Rough Mesh for Group I

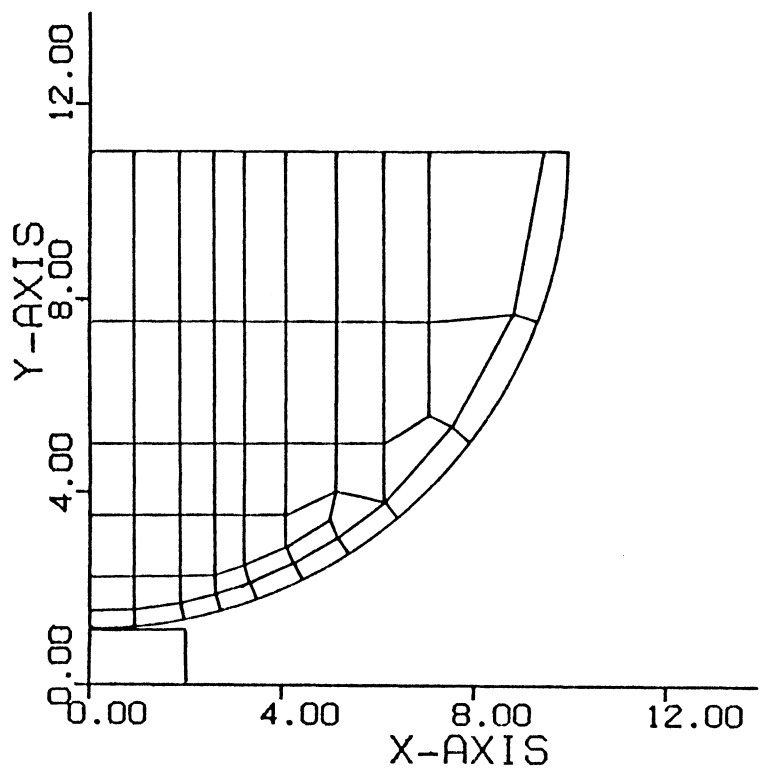

Figure 3.10. Rough Mesh for Group II

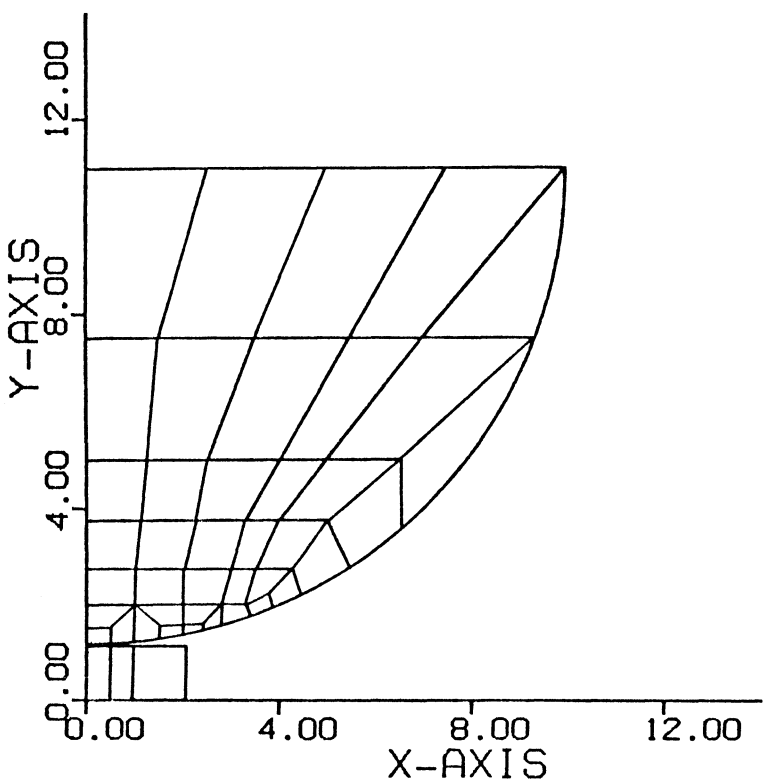

Figure 3.11. Mesh for Group III

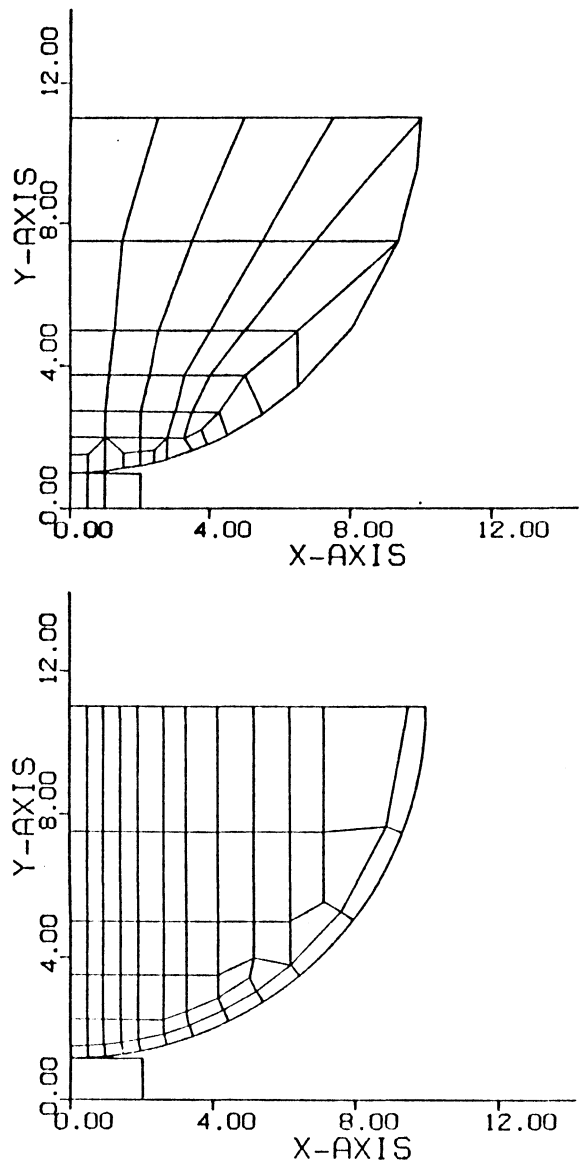

Figure 3.12. Finer Mesh I for Group I and II

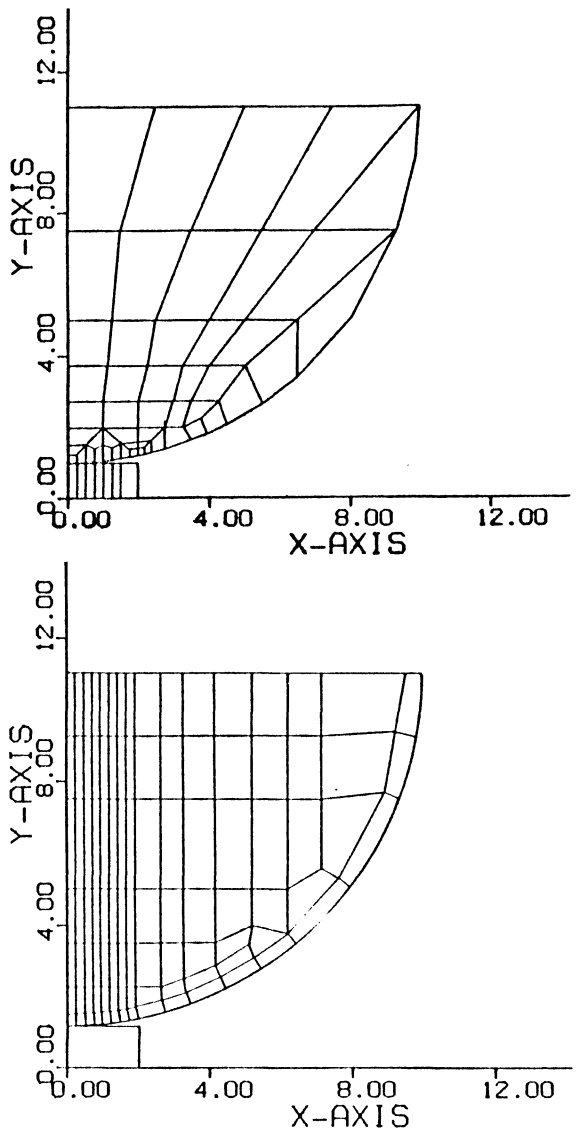

Figure 3.13. Finer Mesh II for Group I and II

3.12 and 3.13). The rule for mesh refinement, "all previous meshes should be contained in the current mesh" (Reddy, 1984), was followed carefully during each stage of refining mesh. In the third group, only one mesh is used. The convergence criteria on both the change in total internal energy and the change in contact forces were used for the termination of the iteration. The values of tolerances, ETOL and RCTOL, used in this problem are 0.001 and 0.01, respectively.

The numerical results obtained from each mesh of the three different groups are presented graphically (see Fig. 3.14, 3.15, 3.16, 3.17). It can be seen from the figures that the difference between group I and group II are small for rough mesh. However, when we attempt to refine the mesh to obtain more finite element solution points and a higher solution accuracy, group II, which used curved elements and more regular elements , is superior to group I. Also, the results obtained from group I demonstrated the "Babuska Paradox" (Krauthammer, 1979), which describes an error associated with modeling a curved boundary by straight-sided elements. Although mesh refinement caused the contact region of the cylinder to have more contact segments and to converge to a circular arc , we should not expect the contact pressure along the contact surface to converge to the exact solution. In fact, the solution of group I meshes became worse when the mesh was refined.

The results of group III shows that, although curved elements were used to model the boundary, the irregular elements may still cause a large error in the solution. This result agrees with the results obtained in the previous section for a cantilever under tip load.

Since the representation and discretization of a given domain depend on the type of problem and the behavior of the solution, it is not the recommendation of this study to use curved elements and regular shaped elements for all geometrically nonlinear problems. However, because of the sensitivity of some problems, it is suggested to use regular shaped elements instead of general shaped elements, and to model a curved boundary with curved elements when the geometry of the problem is known.

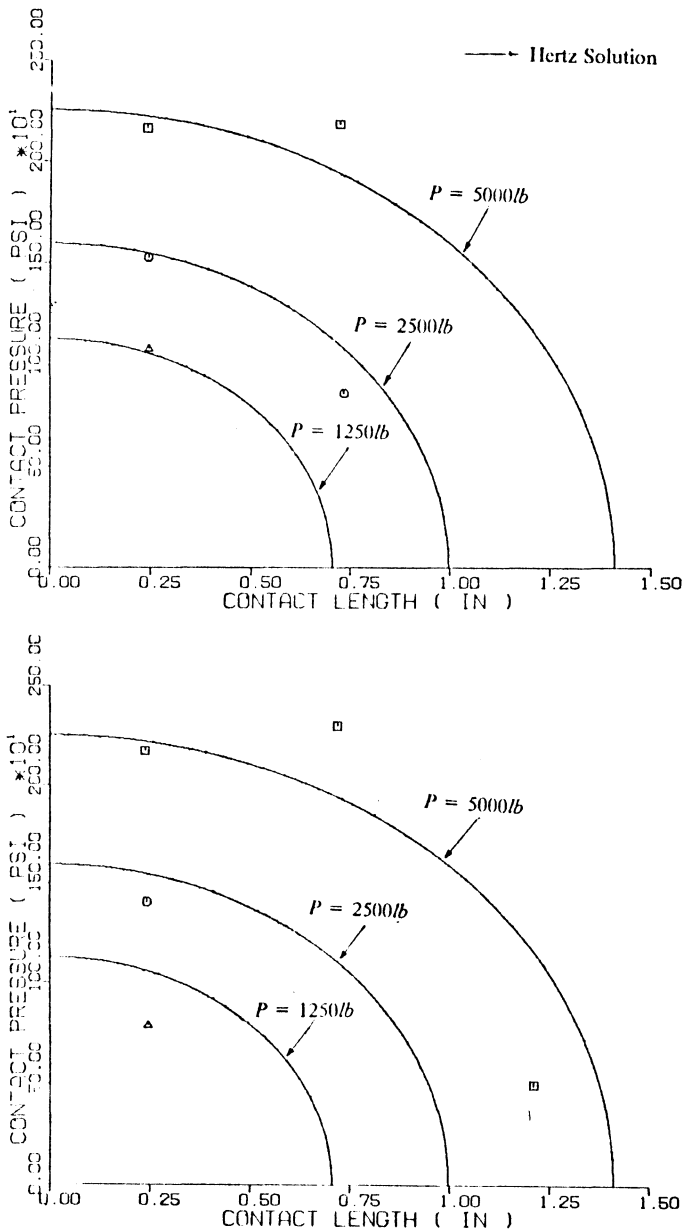

Figure 3.14. Result of Rough Mesh for Group I and II

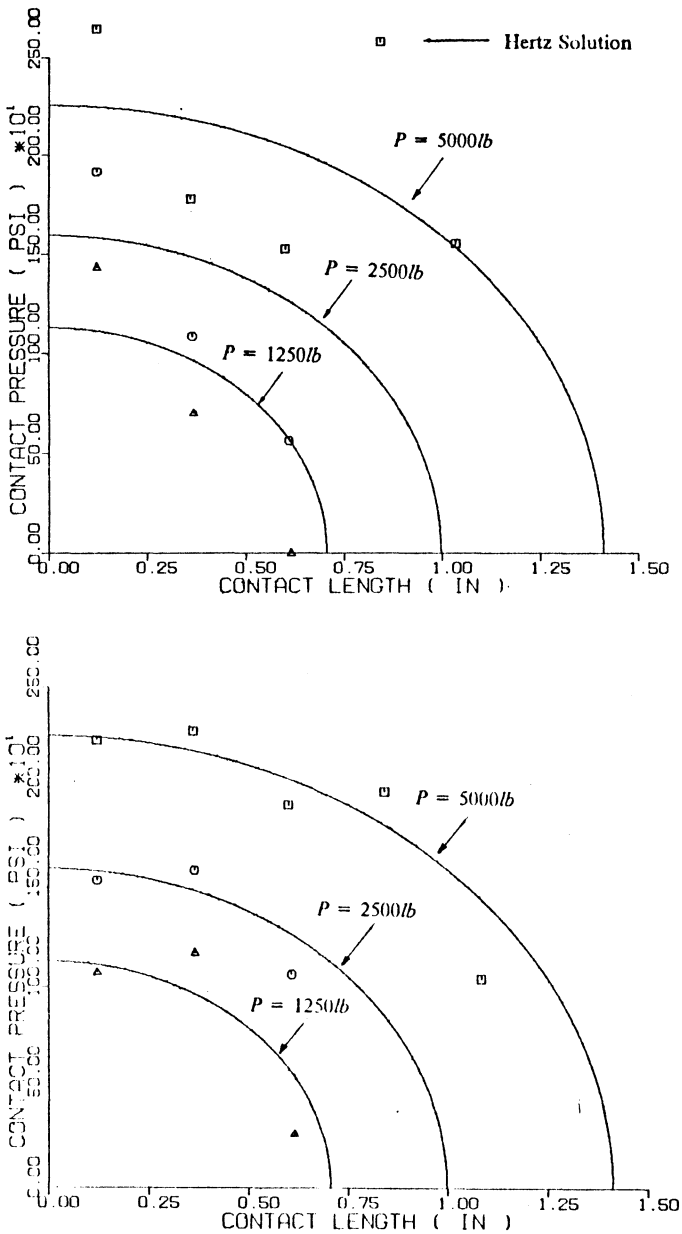

Figure 3.15. Result of Finer Mesh I for Group I and II

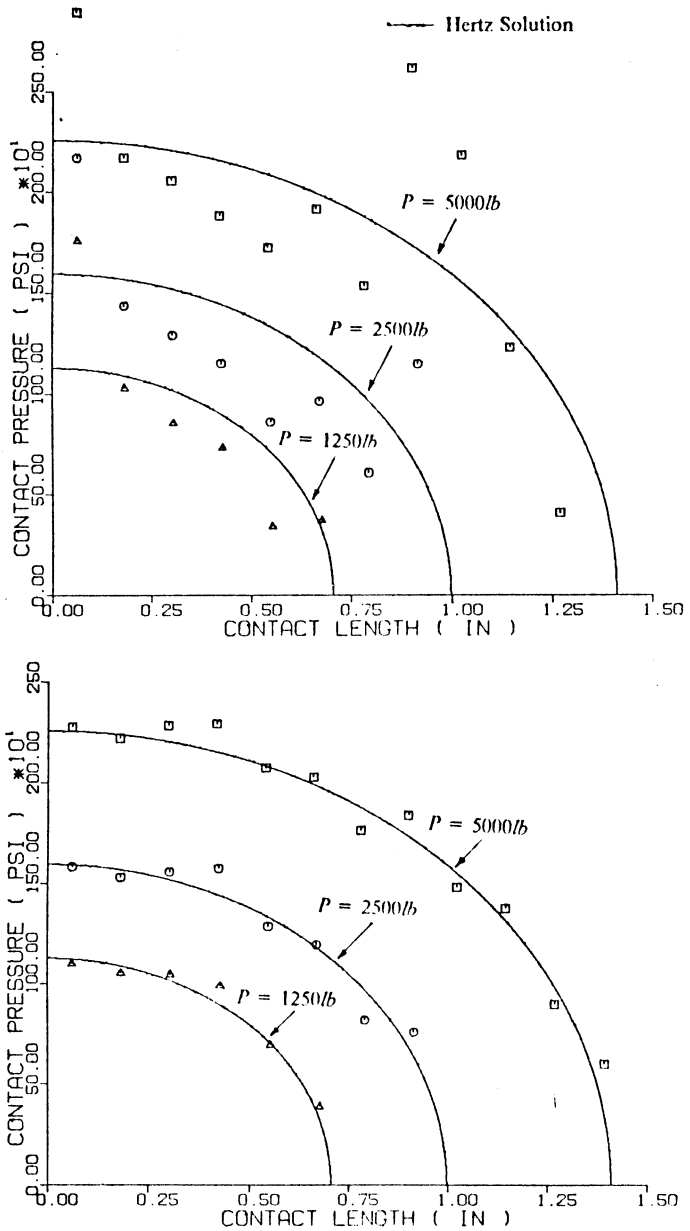

Figure 3.16. Result of Finer Mesh II for Group I and II

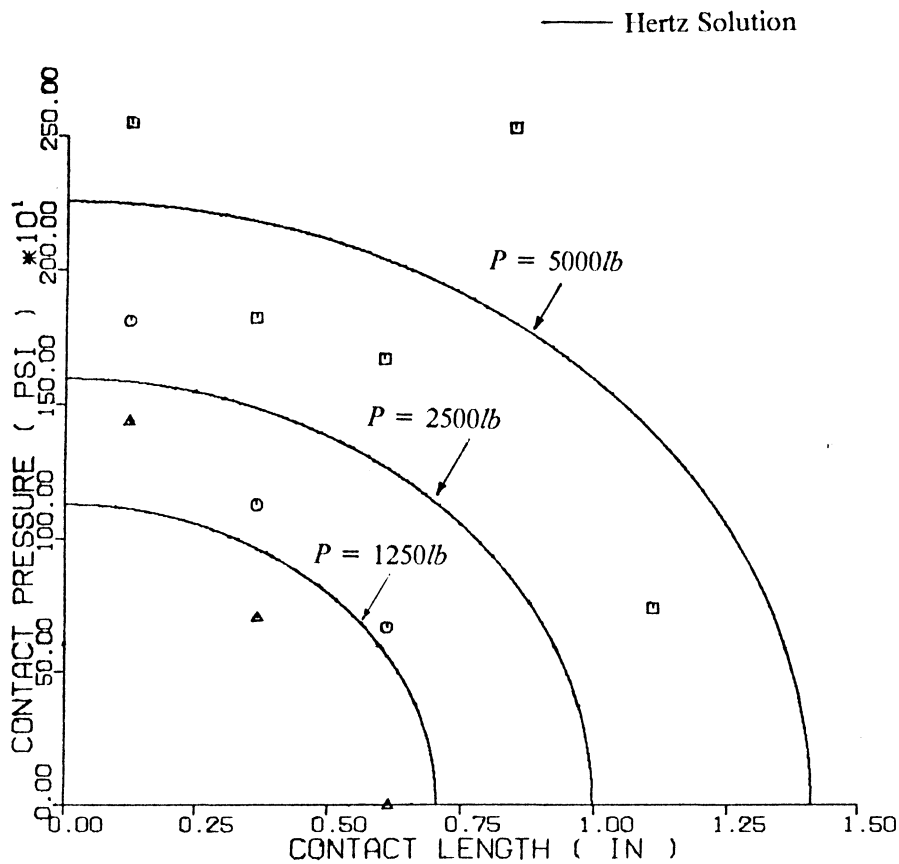

Figure 3.17. Result of Group III

Chapter 4

Analysis of Sheet Pile Interlock

4.1 Introduction

The nonlinear formulation of the moving contact problem with elastic-plastic material response has been applied to a sheet pile interlock connection by Chan and Barker (1985) using the Newton-Raphson method. In that previous report, the load-deflection curve could not be found for an applied load beyond 10.0 kips/inch. An attempt was made to increase the loading, but the solution failed to converge because of excess deformations of the sheet piles. To study the behavior of the sheet pile interlock more completely, the modified Riks-Wempner algorithm described in Chapter II has been implemented as the equation solver for this report.

4.2 Description of Finite Element Model

Since the interlock geometries in field condition vary from one interlock to another, the as-rolled shapes of the interlocks for PS32 published in the Steel Sheet Piling Handbook by United States Steel (1983) (Fig. 4.1) were enlarged and traced carefully. This enlarged shape was used for the finite element discretization.

The eight-node quadratic isoparametric elements were used to model the sheet pile interlocks. Since the detailed dimensions of an interlock were not available, the coordinates of the finite element mesh were scaled from the enlarged drawing of the interlock using the known web dimension as reference. The coordinates of the nodes were measured by an electronic digitizer which could give values up to three decimal places. The data were recorded and stored in an IBM personal computer, and transferred to the mainframe later on. The typical set-up for the axially tensile pull-test of sheet piles and the finite element mesh used to simulate the test are shown in Figures 4.2 and 4.3, re-

spectively. The finite element mesh contained 92 eight-node isoparametric elements with 390 displacement degrees of freedom.

The material properties of the sheet piles used in this study are as followsg, which were reported by Oliver (1985) and used by Chan and Barker (1985) in the previous analysis :

Young's modulus = 29500 *ksi*

Poisson's ratio = 0.3

Yield stress = 44 *ksi*

Strain hardening modulus = 500 *ksi*

The coefficients of friction were chosen as 0.3 for both μ_s and μ_k . This value was recommended in the report by Oliver (1985).

Three contact regions in the interlocks were chosen. Each of these contact regions included three contact-target pairs (Fig. 4.4). The three contact regions were defined as :

(1) Contact segment 1 is comprised of contactor nodes 2, 4, 6

(2) Contact segment 2 is comprised of contactor nodes 7, 9, 11

(3) Contact segment 3 is comprised of contactor nodes 13, 15, 17

This definition is similar to that by Chan and Barker (1985). In the previous analysis, all the contactor nodes were assumed to be in sticking contact at the beginning of the solution of the incremental equilibrium equation (Fig. 4.5). However, only contactor node 2 of contact segment 1, contactor nodes 7, 9, 11 of contact segment 2, and contactor node 13 of contact segment 3 were assumed to be in sticking contact at first. Futhermore, in order to simulate the real constraint sit-

uation of the pull-test, more constraints were provided at the ends of the two sheet piles in the interlocks (Fig. 4.6).

In this study, only the regular strength PS32 sheet pile was analysed. However, a similar procedure can be extended to the analysis of high strength PSX32 sheet pile.

4.3 Results Of Finite Element Analysis

To depict the load-deformation characteristics of the sheet pile interlocks in a pull test, the maximum deflection at the end of the sheet pile on which the load was applied is plotted with the loading and shown in Figure 4.7. In Figure 4.7, the displacement-load plot was compared to the previous result obtained by Chan and Barker using the Newton-Raphson method. Within the range of 8.0 kips/inch, the displacement responses are linear in both cases. As the loading increases, the displacement responses of the previous report quit around 10.0 kips/inch, whereas the plot of the current study continued up to 15.5 kips/inch with a nonlinear relationship beyond the loading of 8.0 kips/inch.

The deformed meshes of the interlocks at different load steps are shown in Figure 4.8-4.12. A magnification factor of 10 is used for the nodal displacements. In the figures, the response of the whole mesh can be seen clearly. Figure 4.12 also indicates the possible modes of contact failure in the interlock connection. The deformed meshes show that the interlocking sheet piles deform by bending until sufficient deformation causes the specimens to separate. This result agrees with the testing result by Bower (1973). An attempt was made to investigate the behavior of the sheet pile interlocks when additional lateral constraints were provided at the tips of the thumbs to prevent the effect of rotation. A similar analysis was made by Chan and Barker (1985), which was named as Case III in the previous report. In Figure 4.13, it can be seen that the load-deformation plot continues up to 20.07 kips/inch when the effect of rotation is dismissed. A comparison with the result using the Newton- Raphson method is also presented in Figure 4.13.

To study the sliding in the connection more closely, the longitudinal and lateral displacements at the five contactor-target nodes of the three contact regions are plotted in Figures 4.14-4.23. From these figures, the behavior of the contactor-target nodes can be seen clearly. When a pair of nodes

are in sticking contact, the nodal displacements are identical for the two nodes. A difference in values can be an indication of either loss in contact or sliding between the two nodes.

In order to investigate the elastic-plastic behavior of the sheet pile interlocks under tensile load, the growth of plastic zones in the interlocks with increase in loading was plotted (Fig.s 4.24-4.29). As the previous report indicated, the thinnest regions on the thumbs of the sheet piles will yield first.

As a final step to study the analytical results from the finite element program, statics checks are carried out at the web sections of the sheet piles. Figure 4.30 and 4.31 compare the stress distribution at various web sections of the sheet piles. It can be seen that excellent statics check is found on the section B-B of the web on which the load is applied (Table 4.1), whereas some differences exist between the resultant axial force and the applied load on the other web section A-A. This is due to the frictional resistance developing between the contact surfaces of the interlocks.

Table 4.1

Statics Check at Web Sections

Load Step	Section A-A (kips/inch)	Section B-B (kips/inch)	Applied Load (kips/inch)
1	1.017	1.000	1.000
2	2.620	2.581	2.581
3	4.643	4.582	4.581
4	6.669	6.583	6.580
5	8.688	8.582	8.580
6	10.71	10.58	10.58
7	12.41	12.58	12.58
8	13.83	14.22	14.21
9	15.17	15.50	15.50

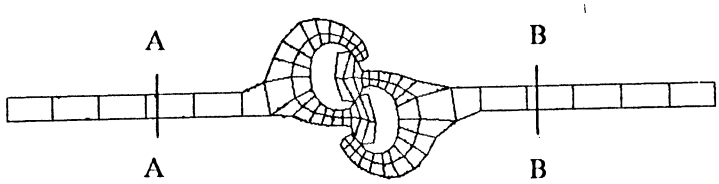

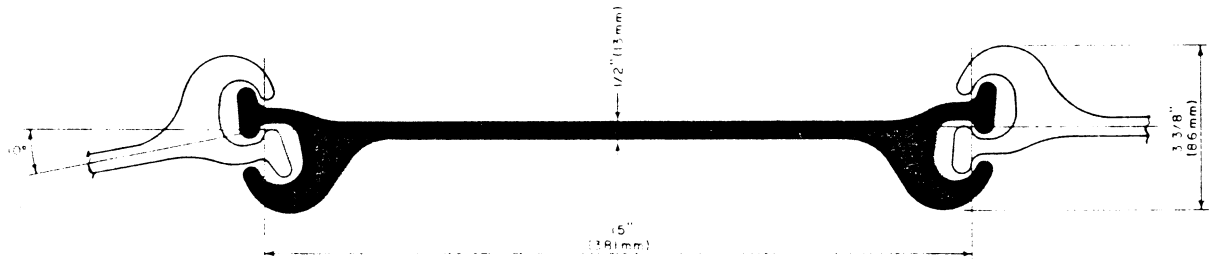

Figure 4.1. PS32 Sheet Pile Interlock (U.S. Steel Handbook)

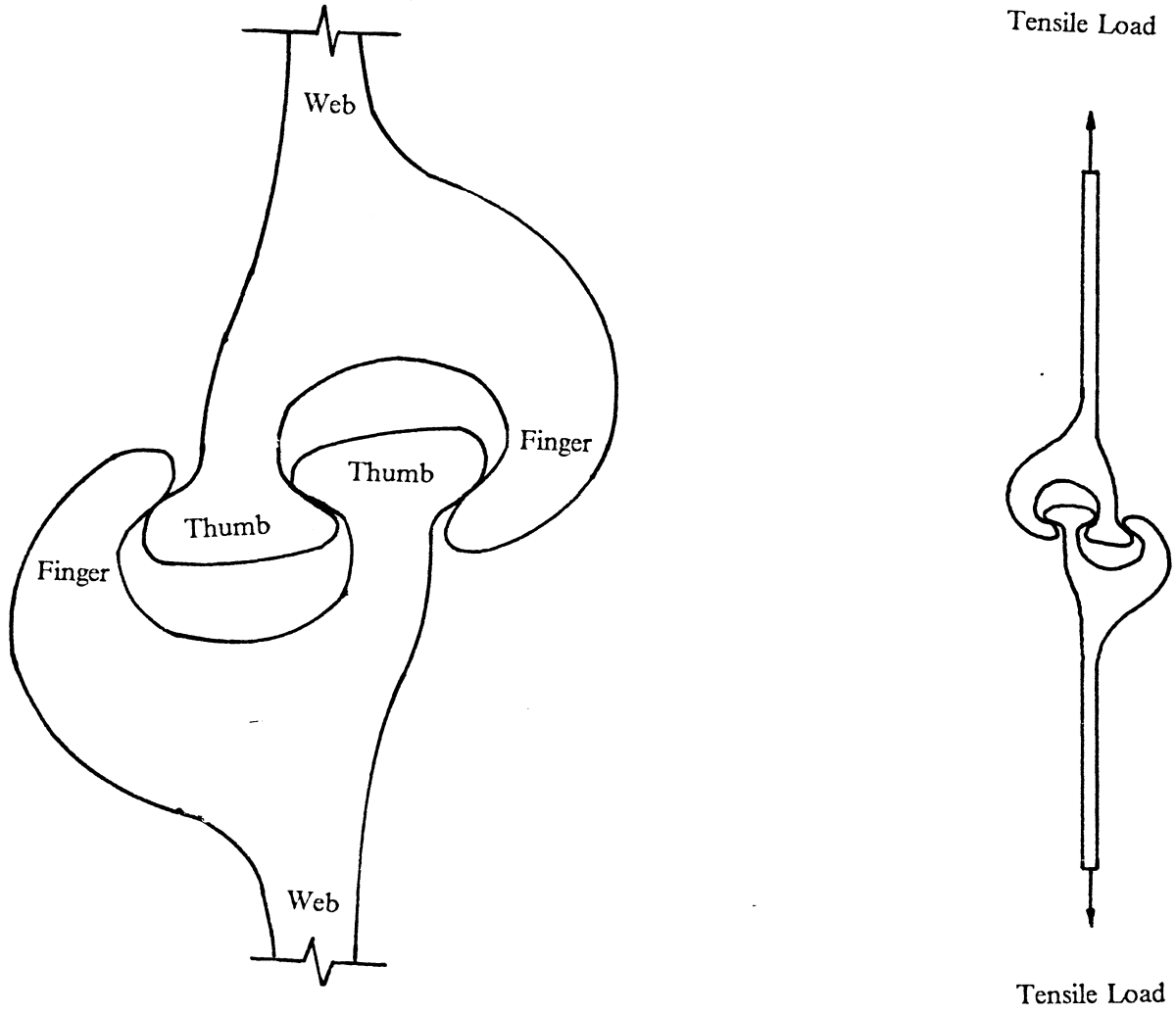

Figure 4.2. Typical Tensile Test of Sheet Pile

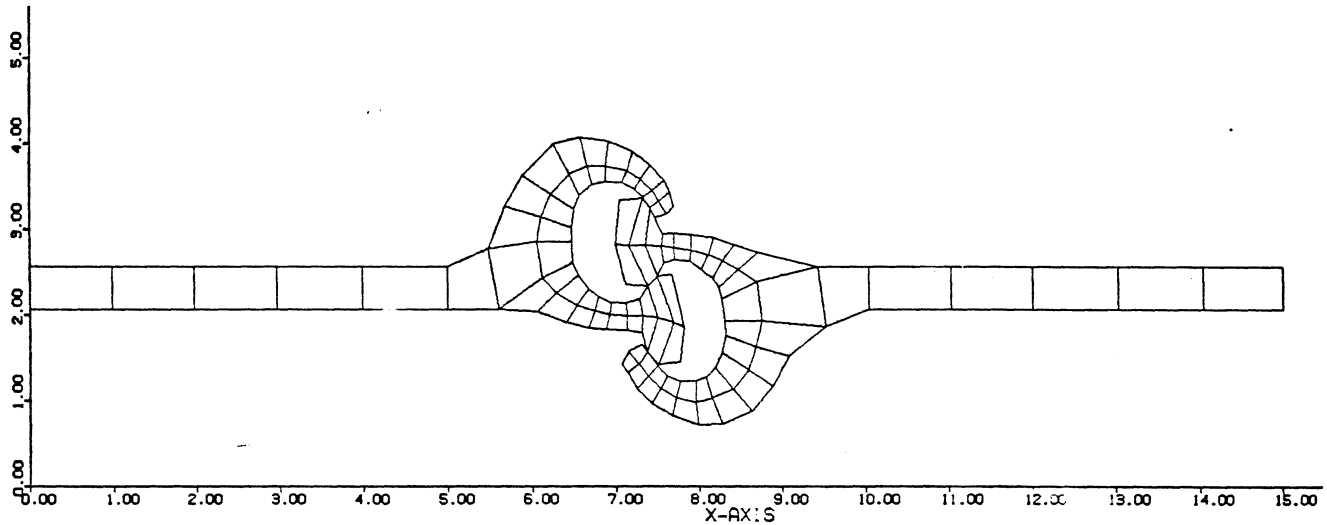

Figure 4.3. Finite Element Mesh for PS32 Sheet Pile

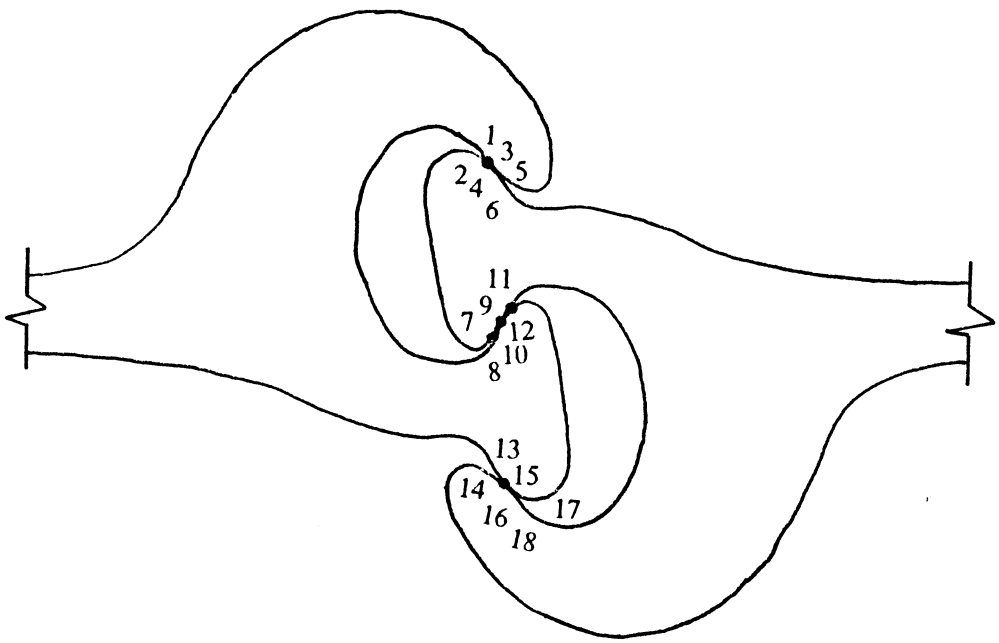

Contactor Nodes : 2, 4, 6
7, 9, 11
13, 15, 17

Target Nodes : 1, 3, 5
8, 10, 12
14, 16, 18

Figure 4.4. Contact Node Pairs in Sheet Pile Interlocks

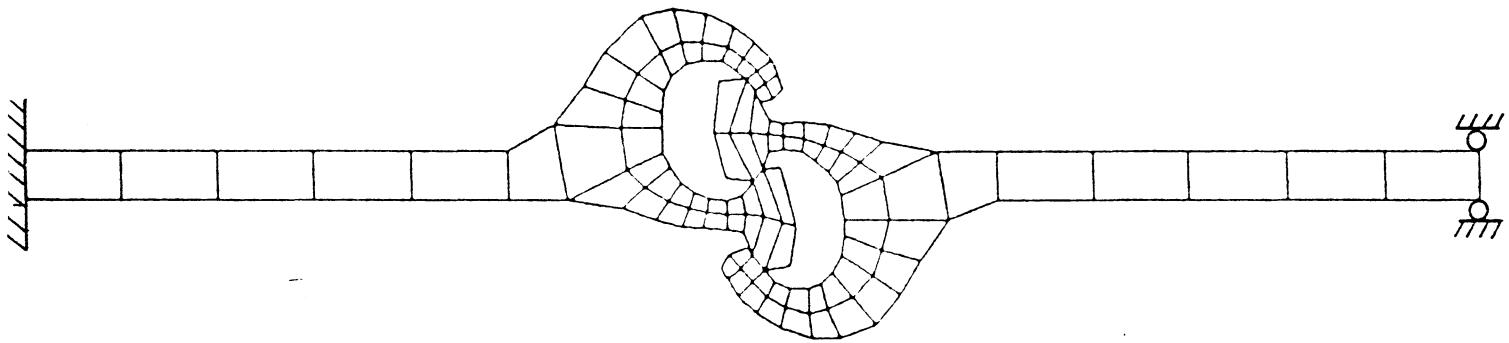

Figure 4.5. Finite Element Model for PS32 by Chan and Barker (1985)

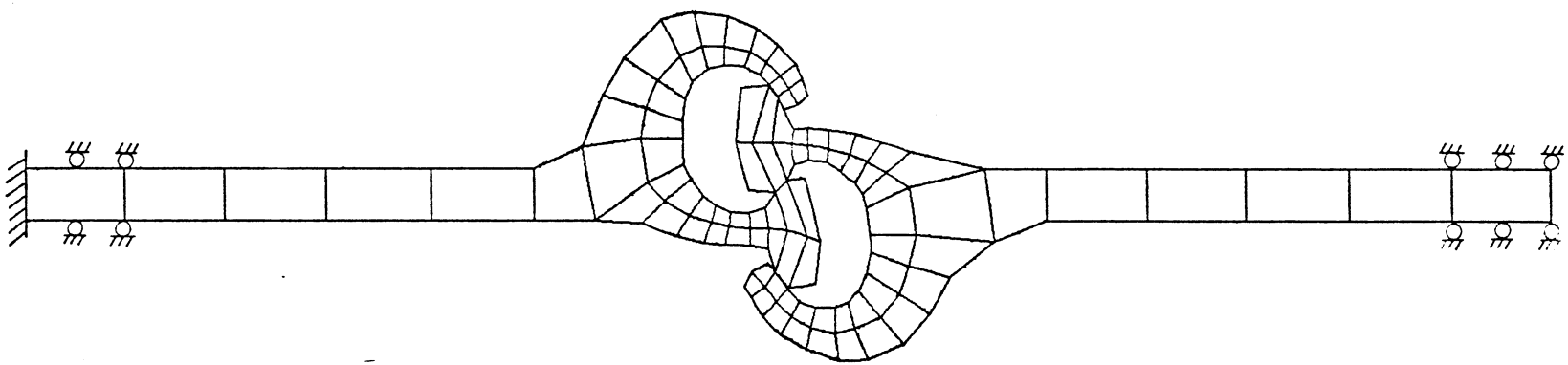

Figure 4.6. New Finite Element Model for PS32 Sheet Pile Interlock

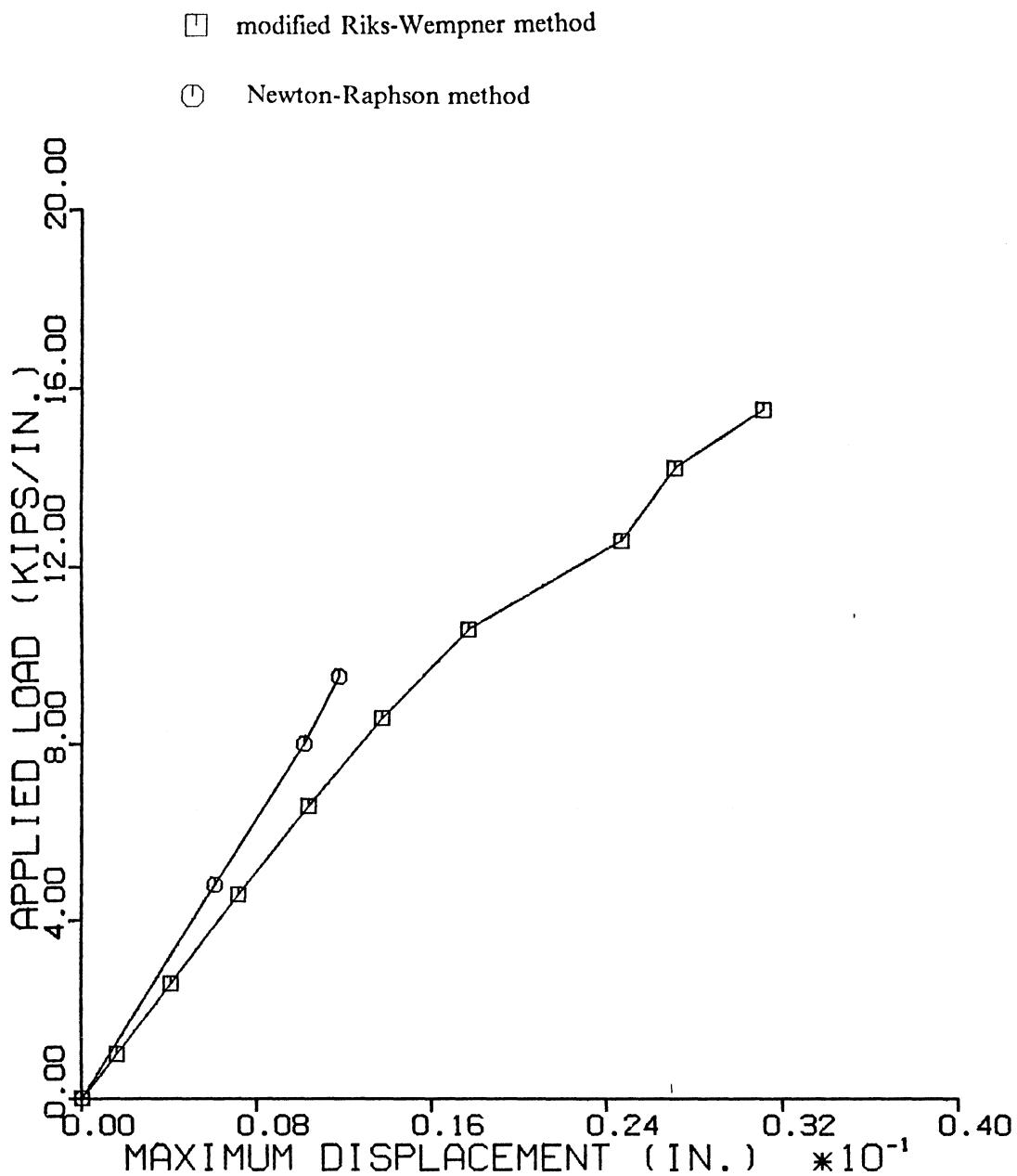

Figure 4.7. Maximum Displacement of PS32 Sheet Pile Interlocks

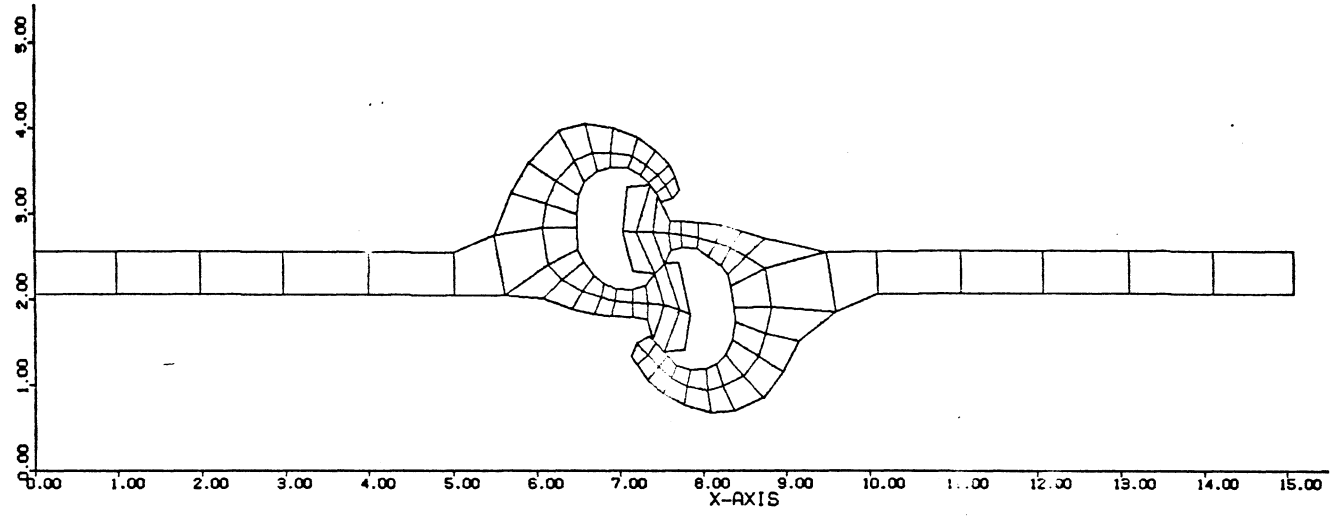

Figure 4.8. Deformed Mesh of PS32 at 2.58 kips/inch

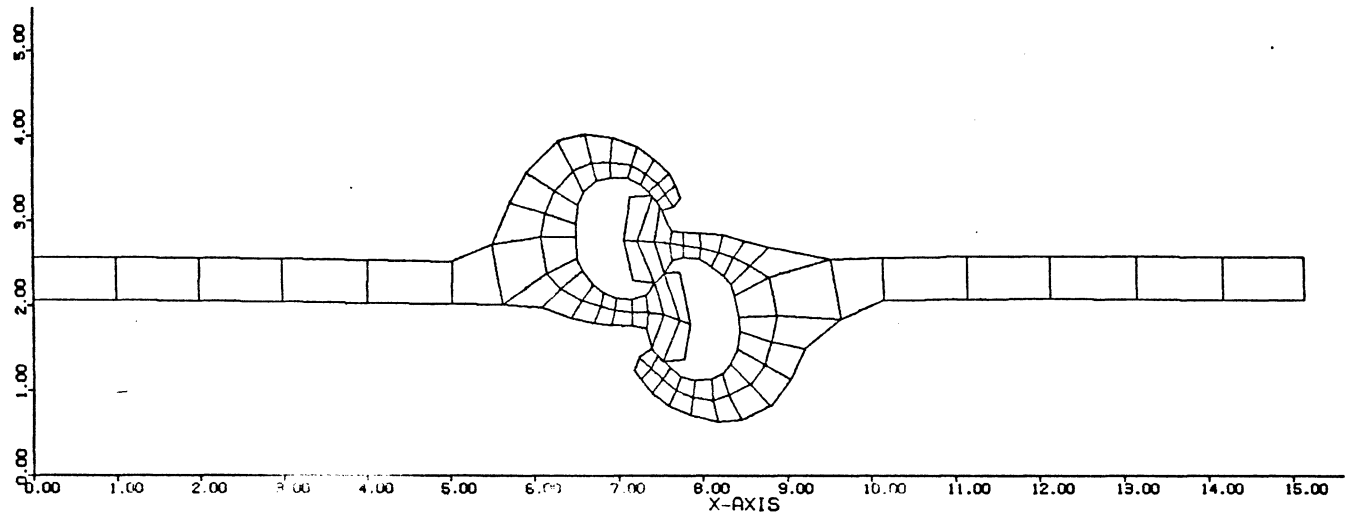

Figure 4.9. Deformed Mesh of PS32 at 6.58 kips/inch

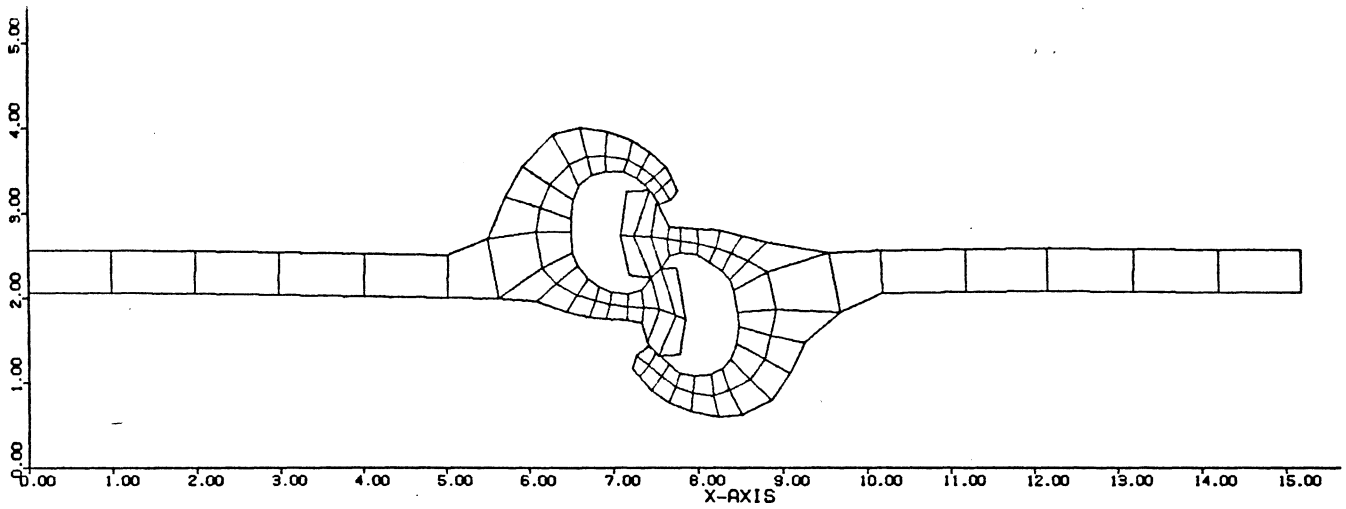

Figure 4.10. Deformed Mesh of PS32 at 10.58 kips/inch

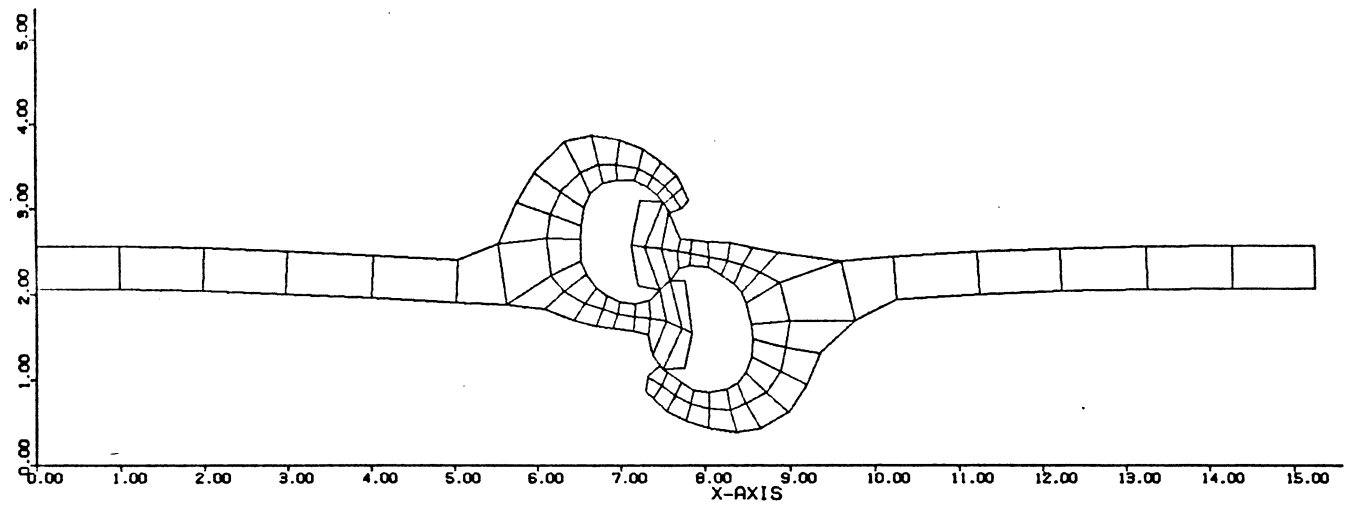

Figure 4.11. Deformed Mesh of PS32 at 14.21 kips/inch

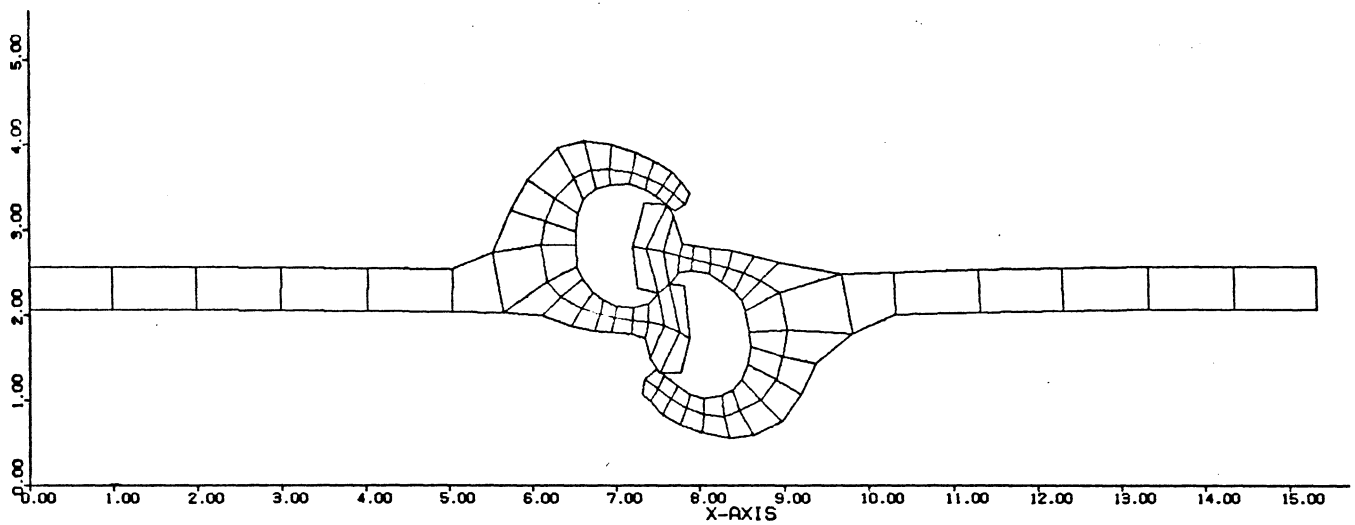

Figure 4.12. Deformed Mesh of PS32 at 15.5 kips/inch

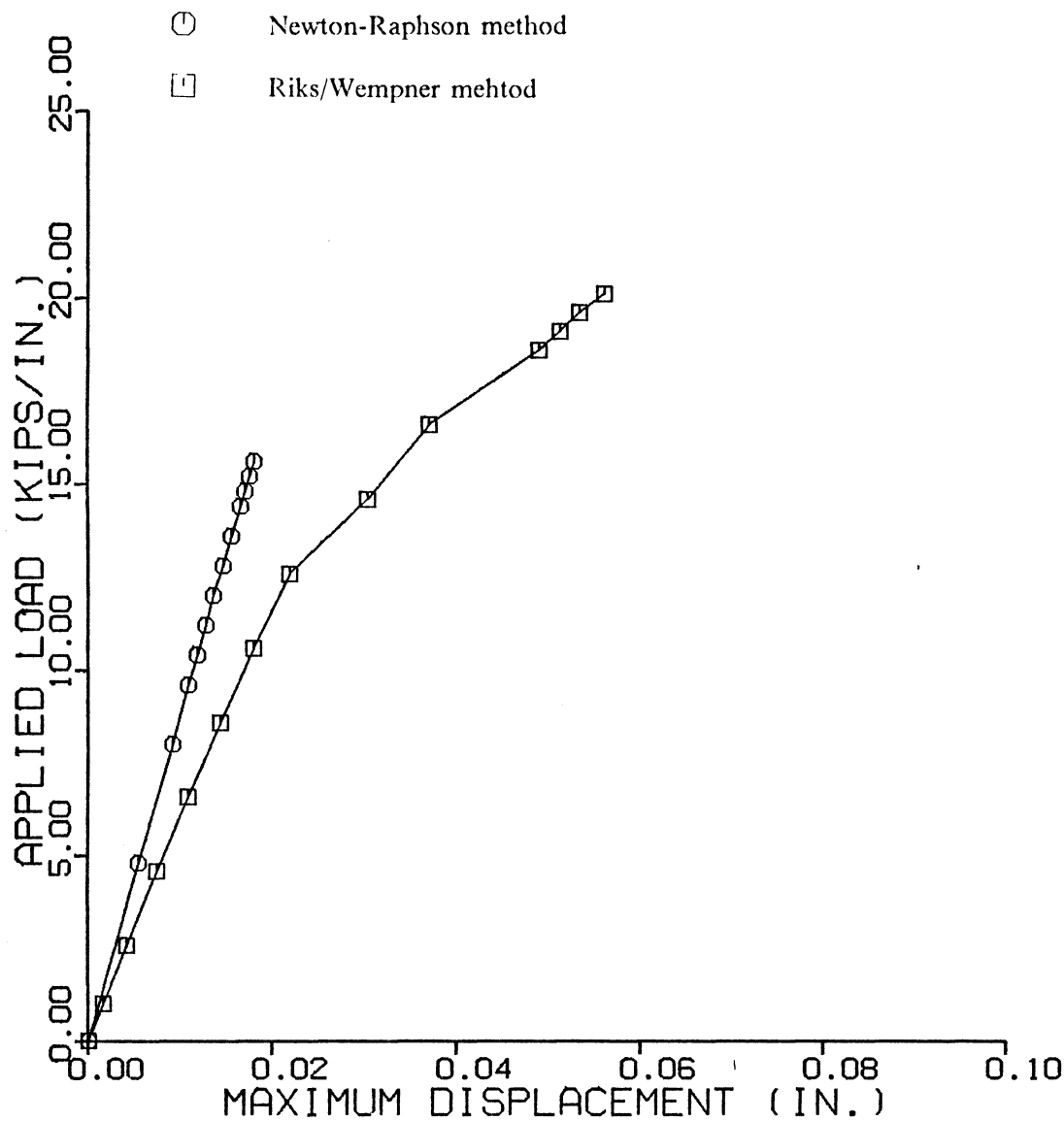

Figure 4.13. Maximum Displacement when Rotation is Dismissed

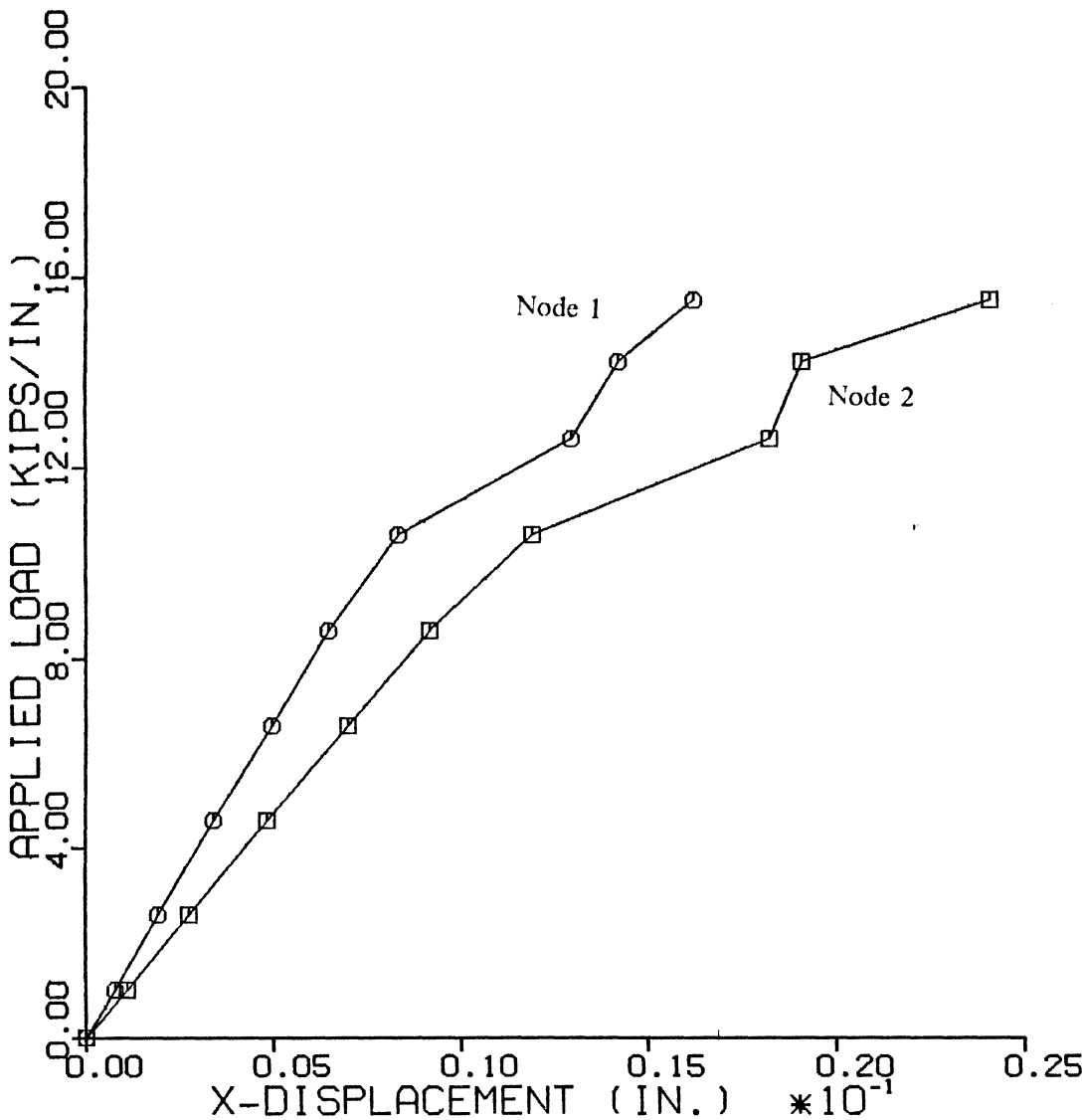

Figure 4.14. Longitudinal Displacement vs. Load for Contact Nodes 1, 2

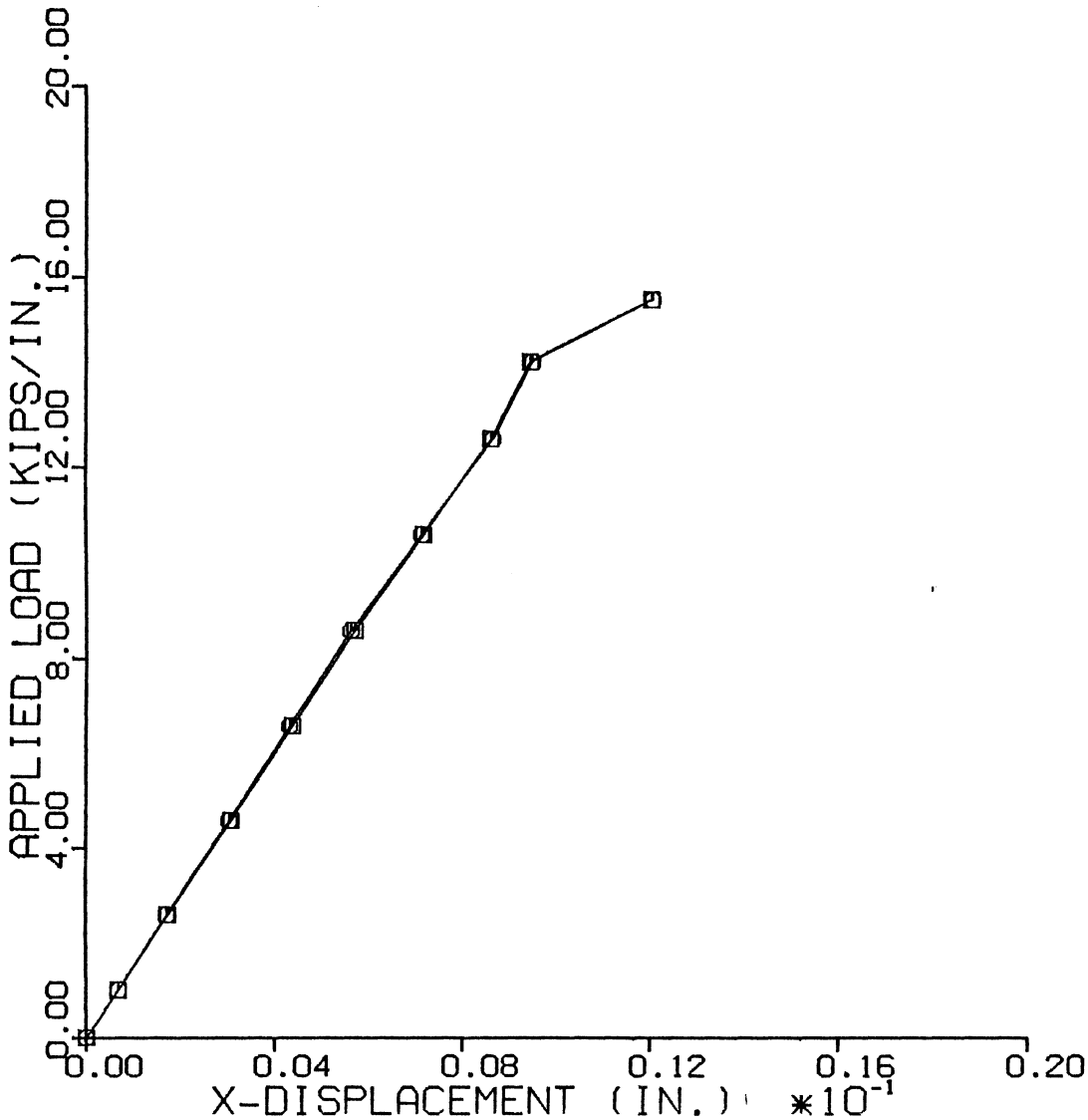

Figure 4.15. Longitudinal Displacement vs. Load for Contact Nodes 7, 8

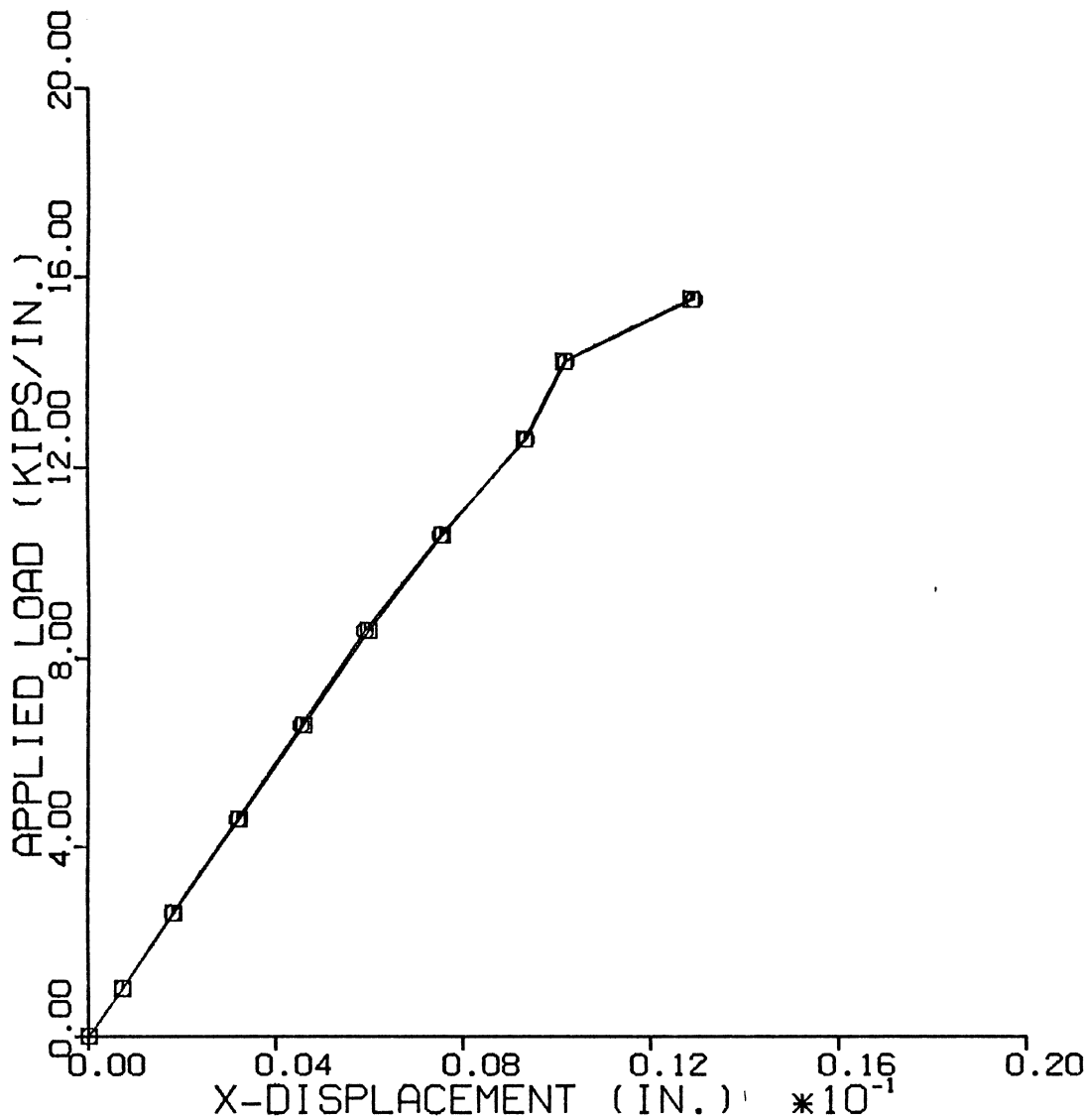

Figure 4.16. Longitudinal Displacement vs. Load for Contact Nodes 9, 10

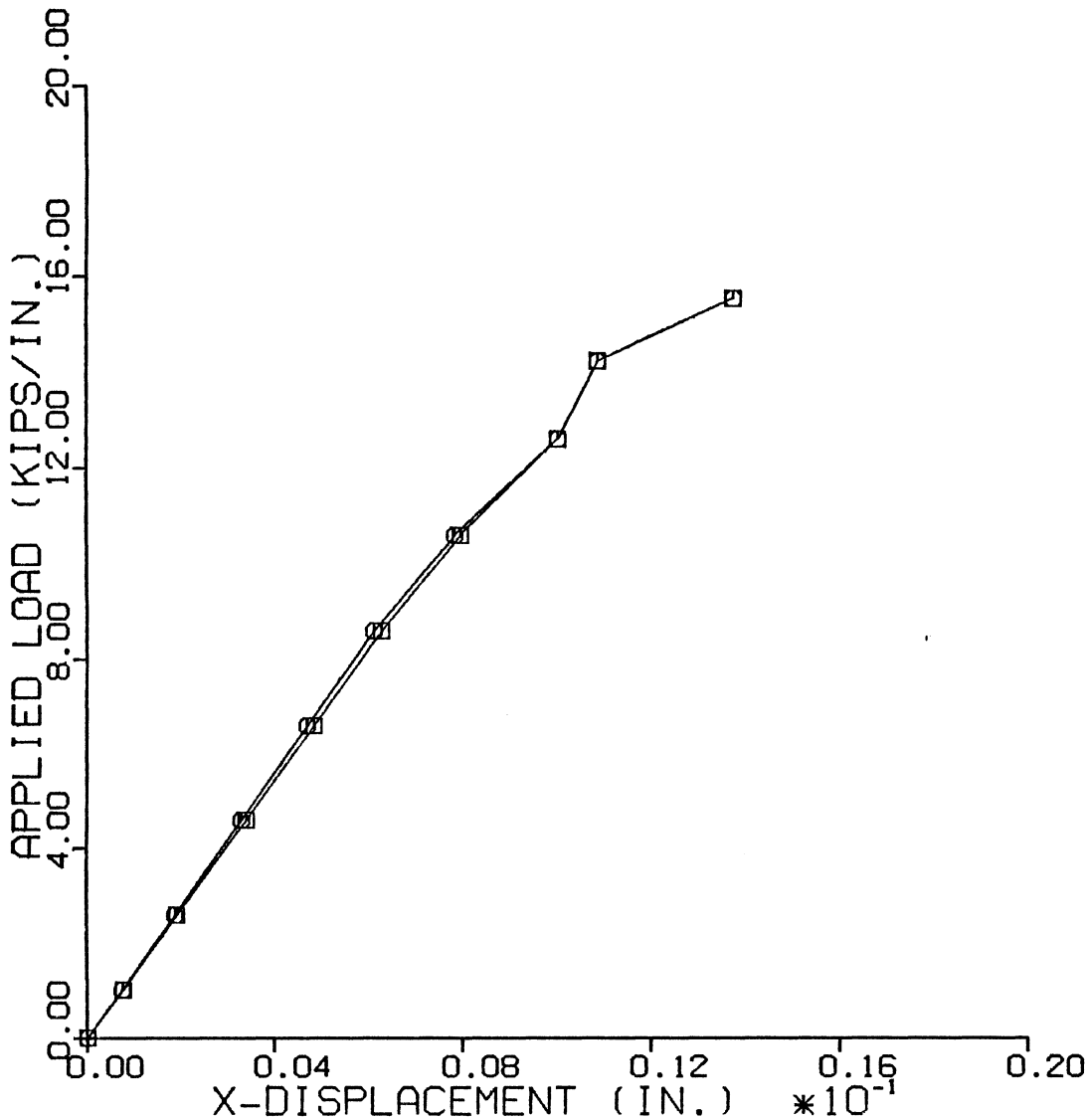

Figure 4.17. Longitudinal Displacement vs. Load for Contact Nodes 11, 12

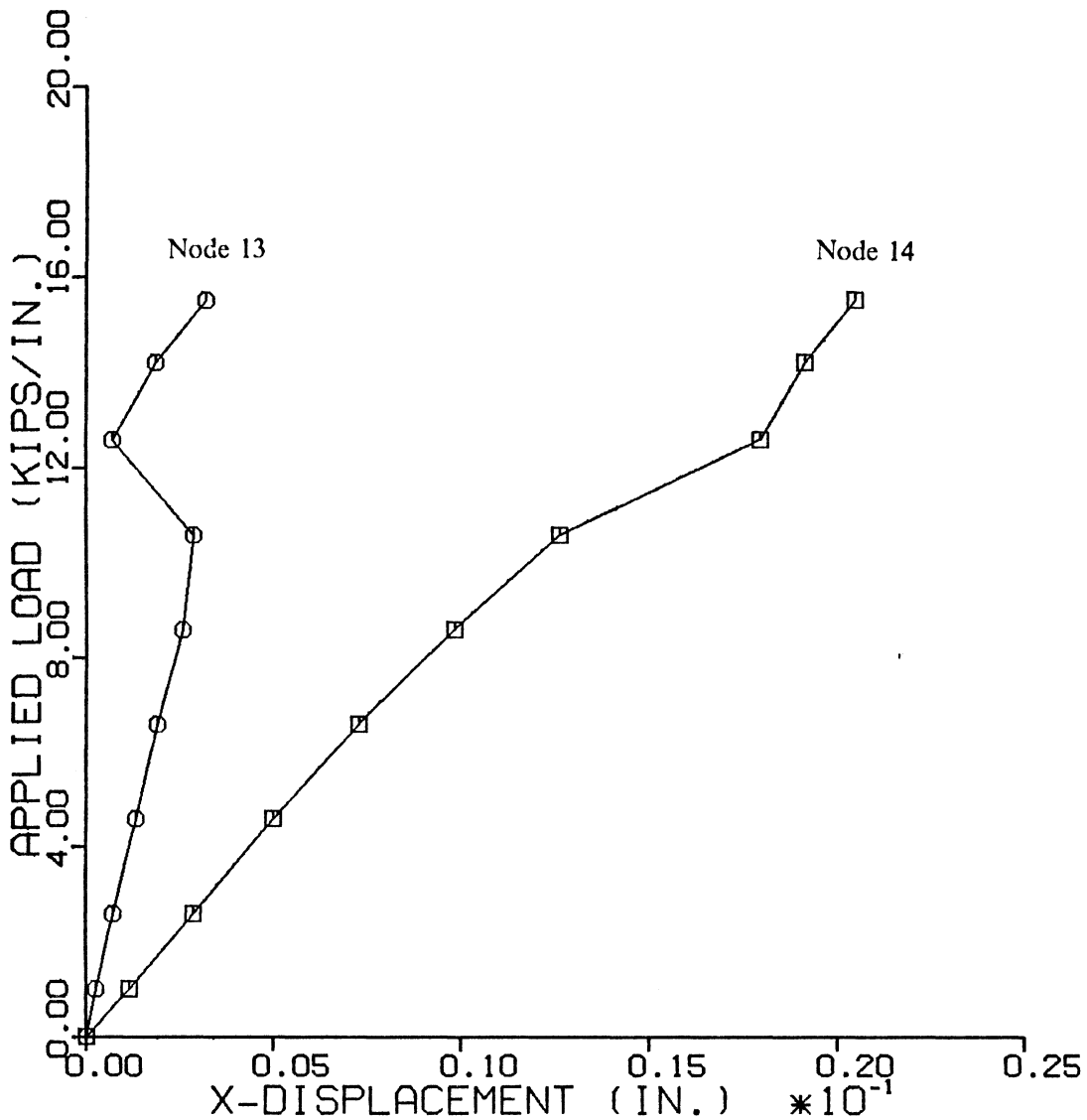

Figure 4.18. Longitudinal Displacement vs. Load for Contact Nodes 13, 14

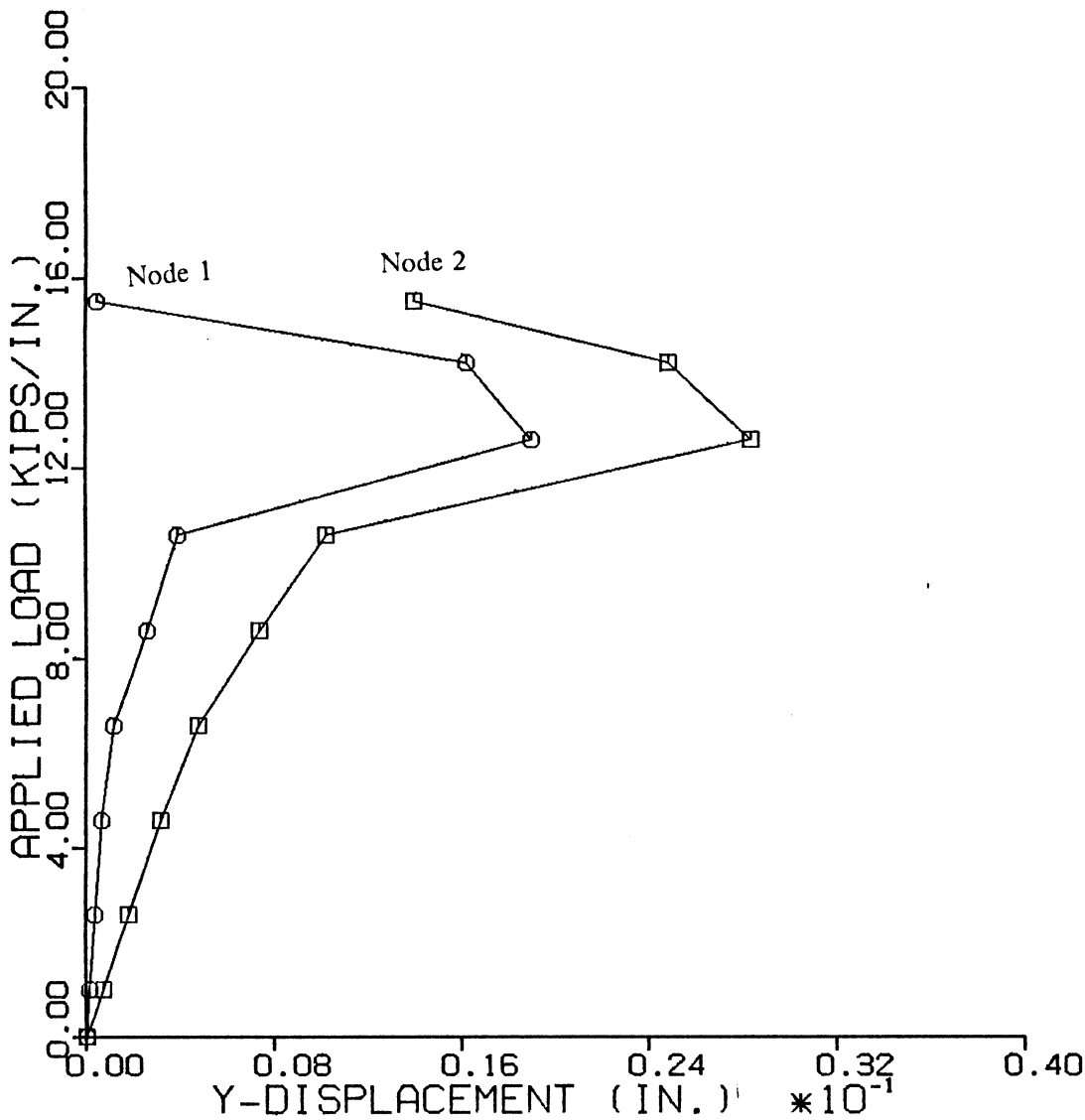

Figure 4.19. Lateral Displacement vs. Load for Contact Nodes 1, 2

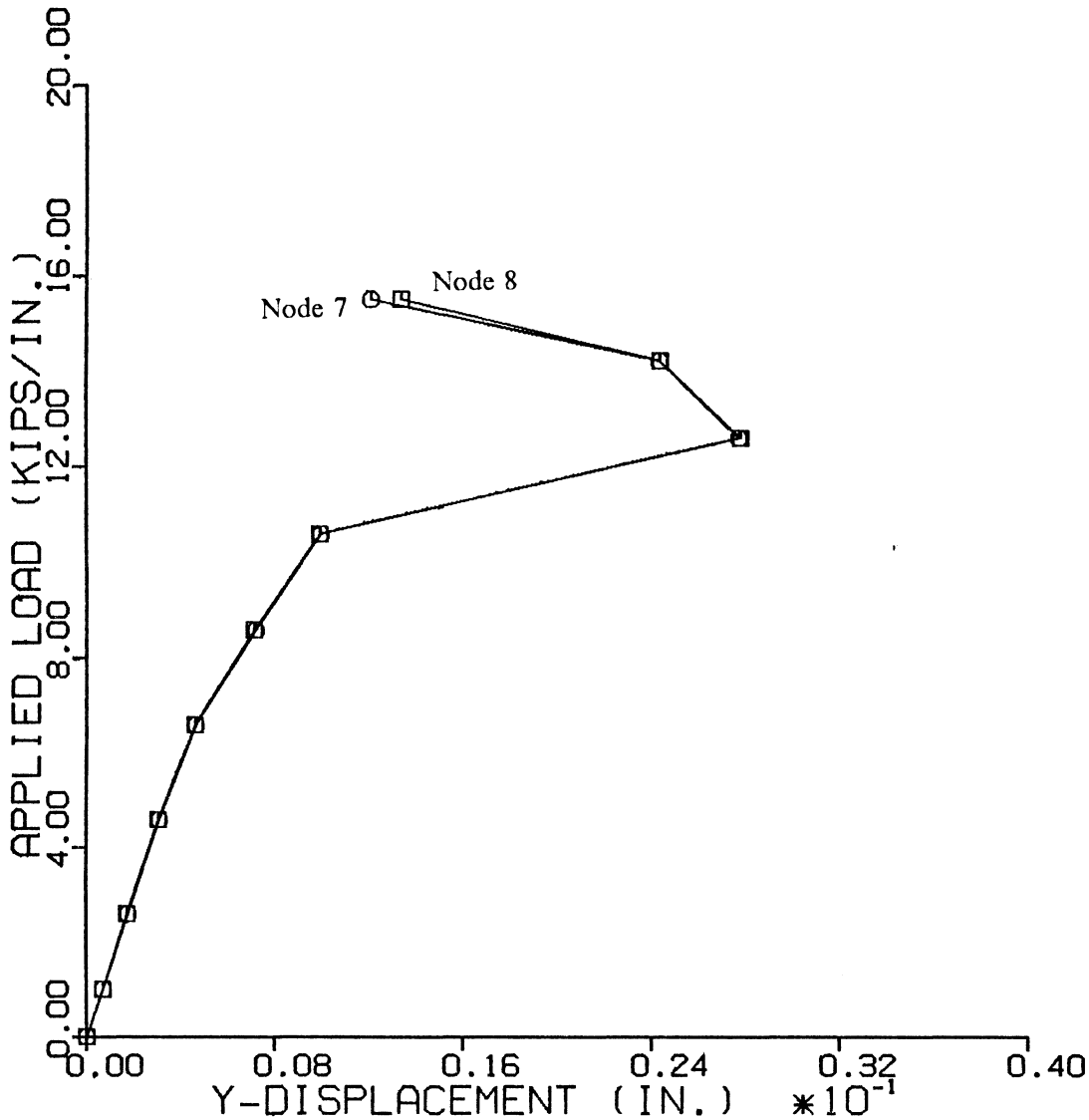

Figure 4.20. Lateral Displacement vs. Load for Contact Nodes 7, 8

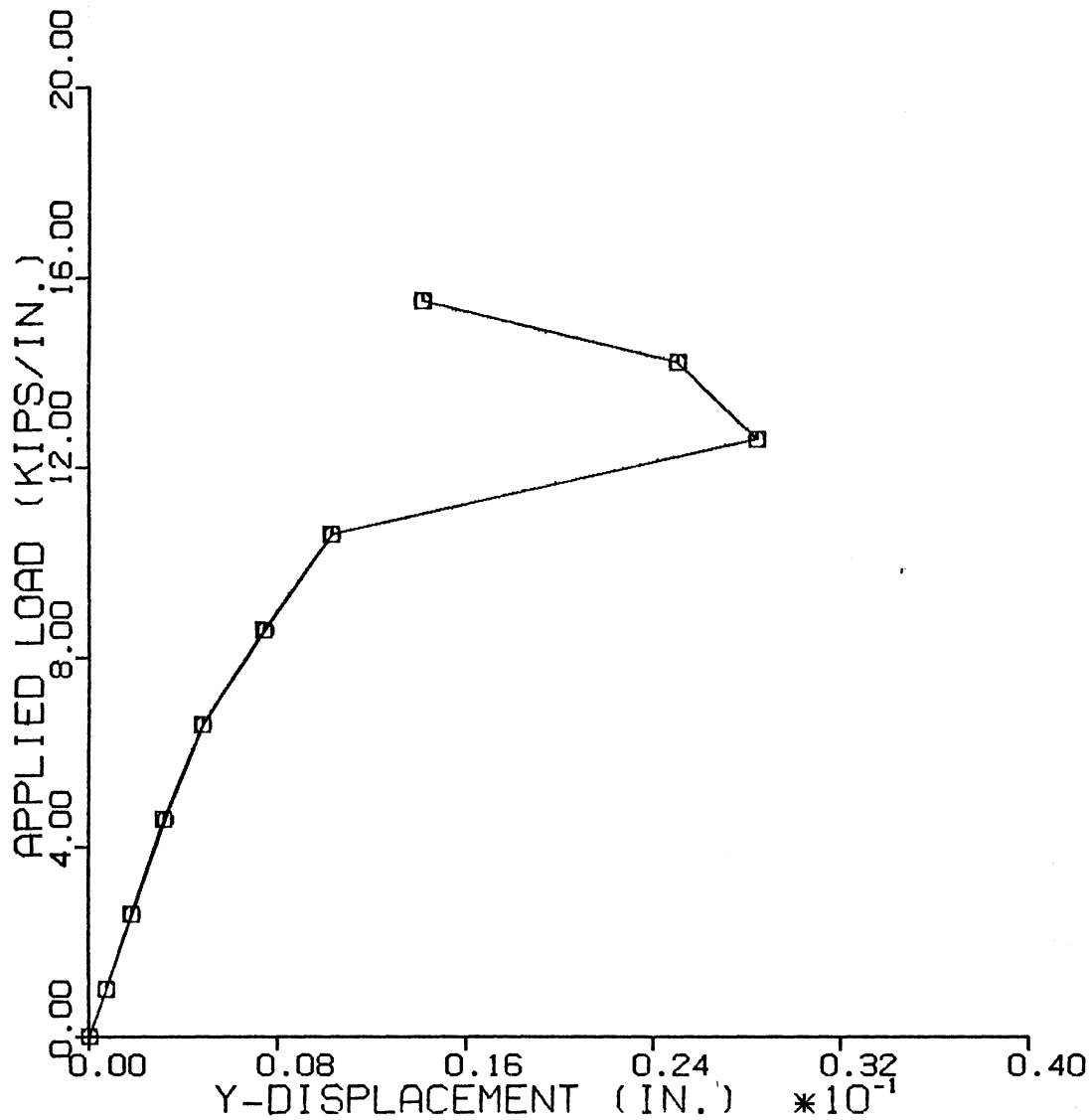

Figure 4.21. Lateral Displacement vs. Load for Contact Nodes 9, 10

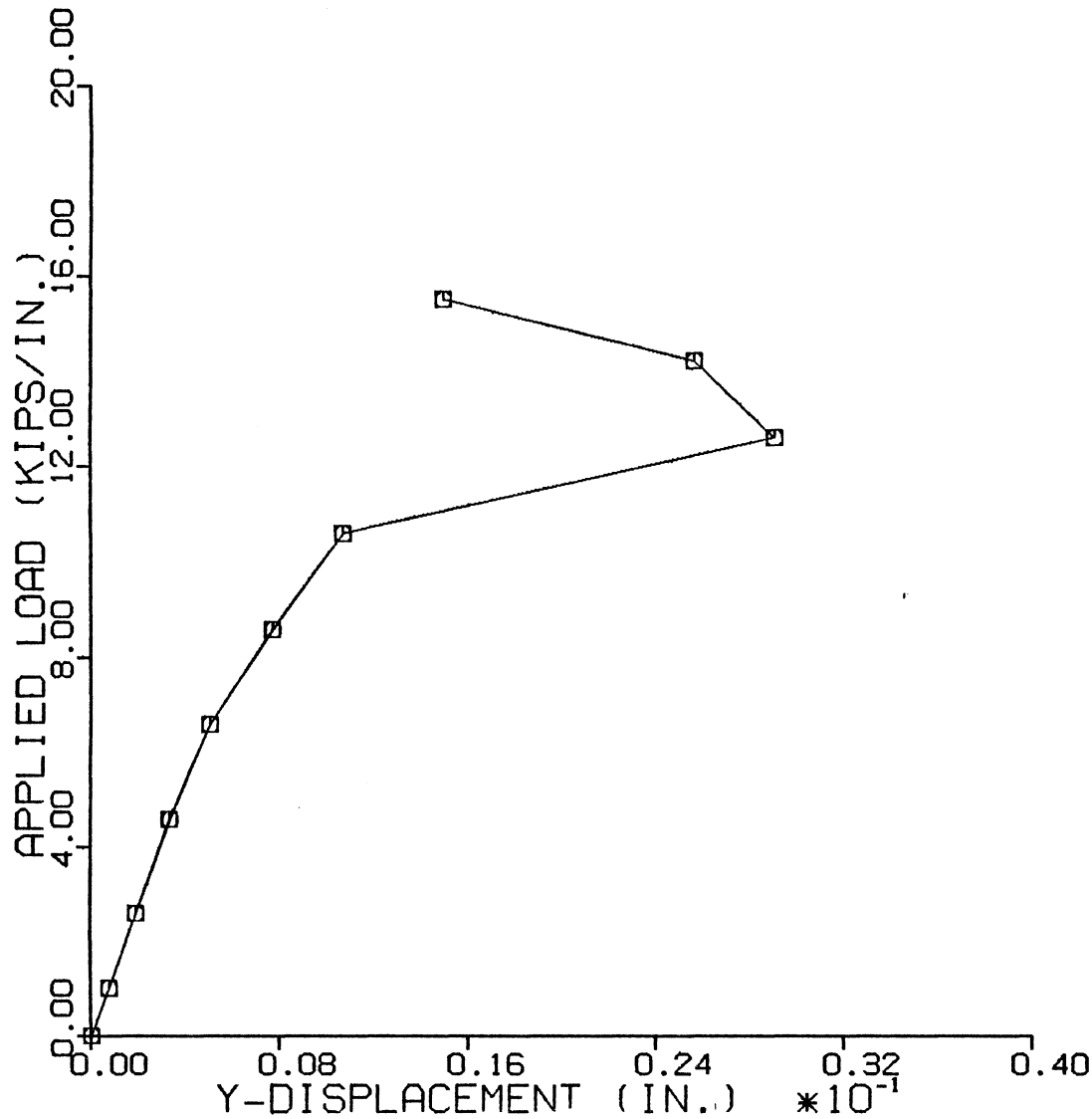

Figure 4.22. Lateral Displacement vs. Load for Contact Nodes 11, 12

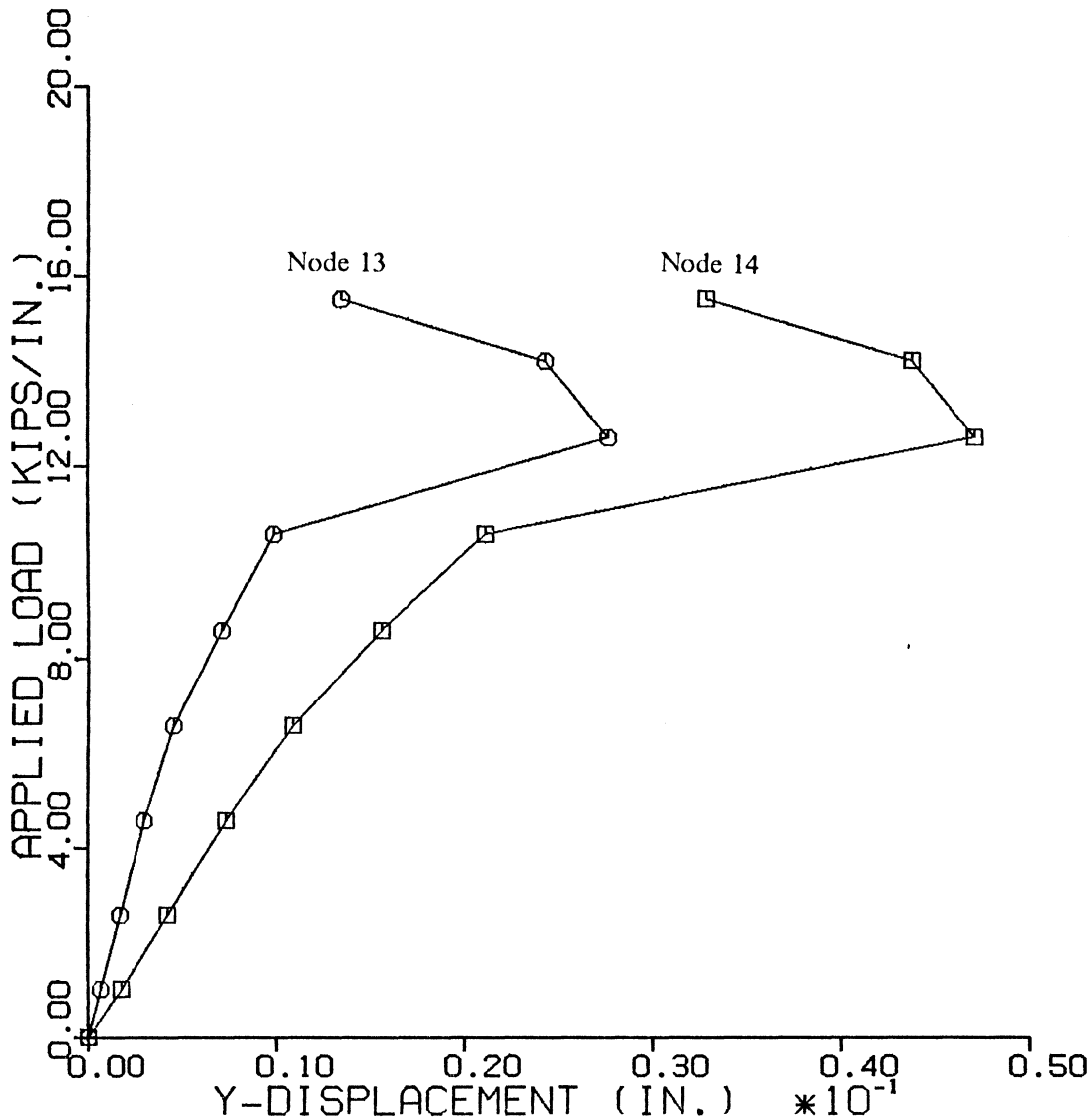

Figure 4.23. Lateral Displacement vs. Load for Contact Nodes 13, 14

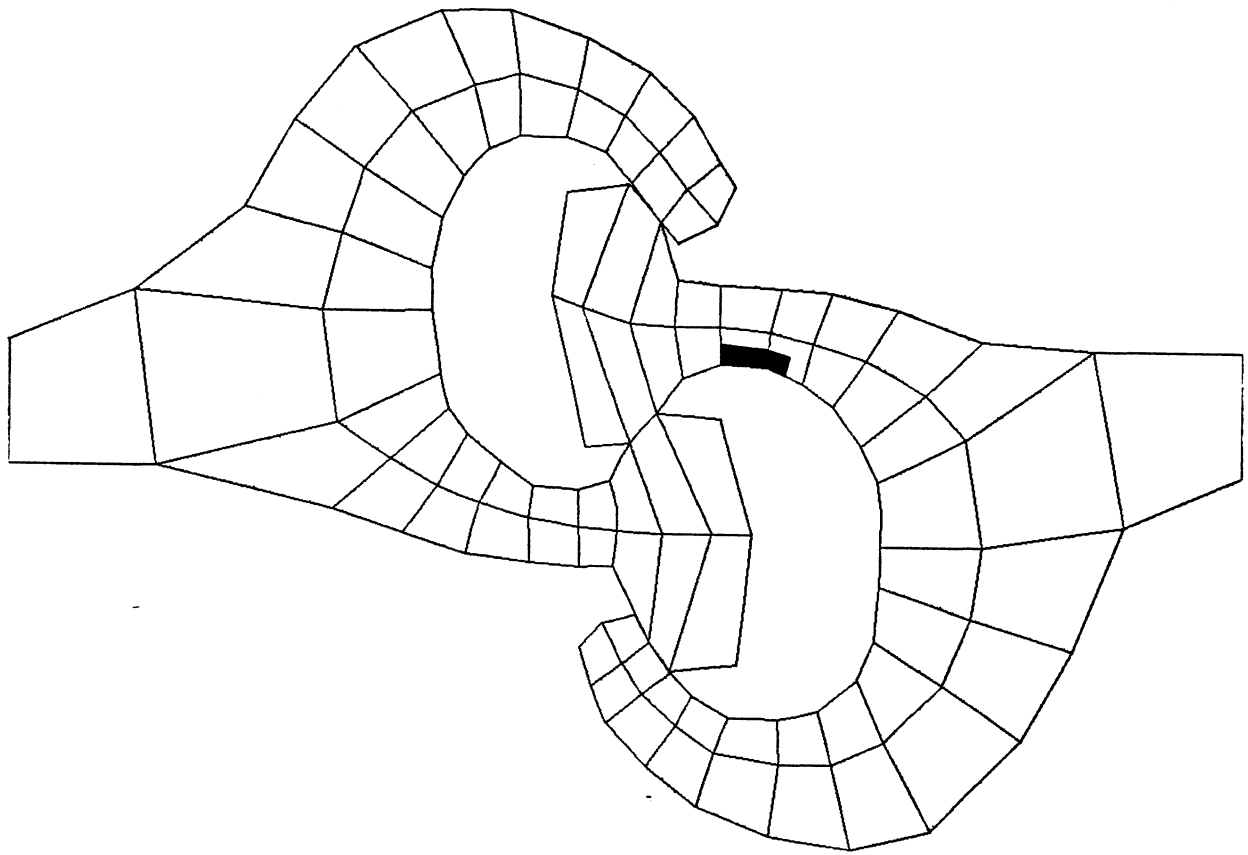

Figure 4.24. Plastic Zone in PS32 Sheet Pile at 6.58 kips/inch

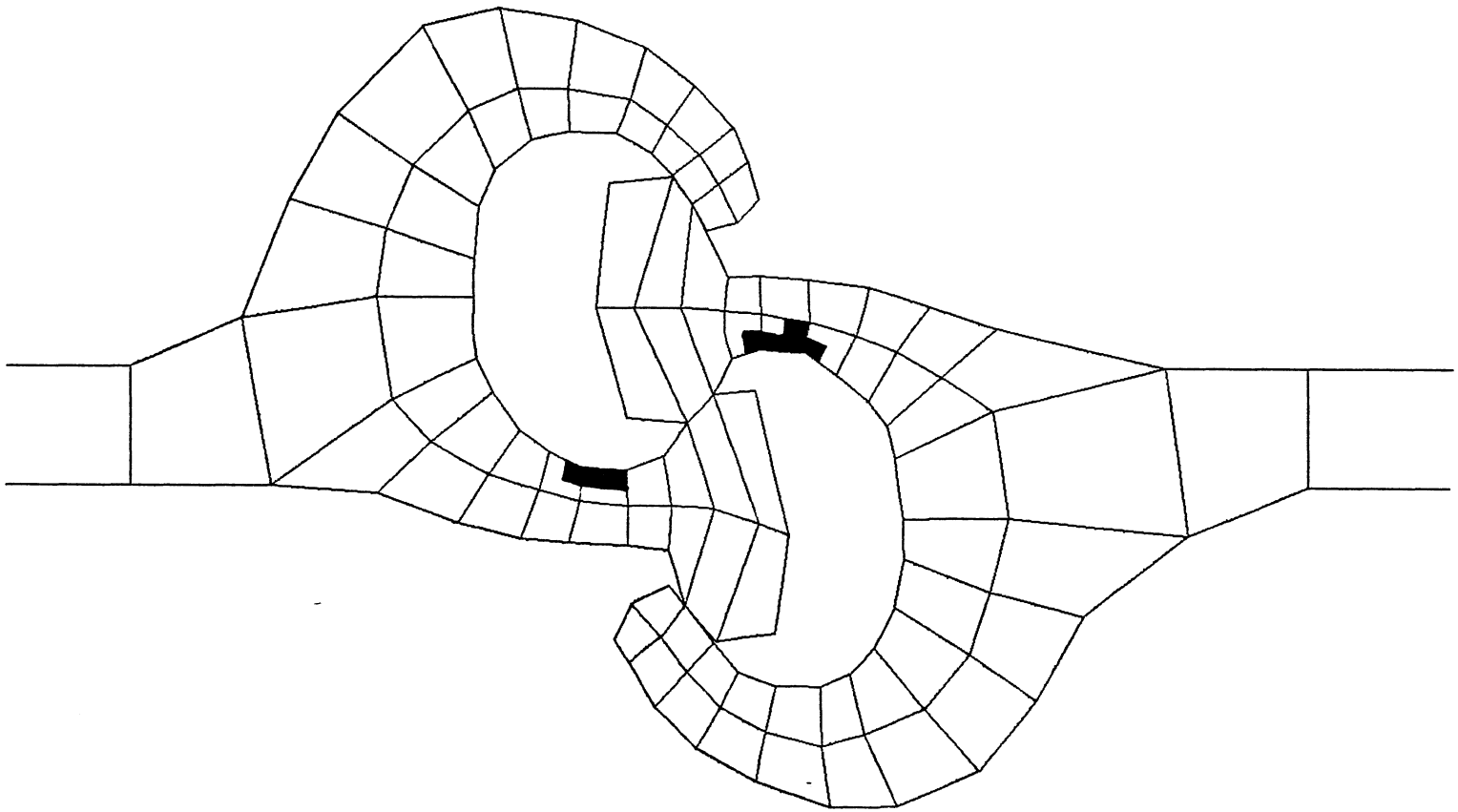

Figure 4.25. Plastic Zone in PS32 Sheet Pile at 8.58 kips/inch

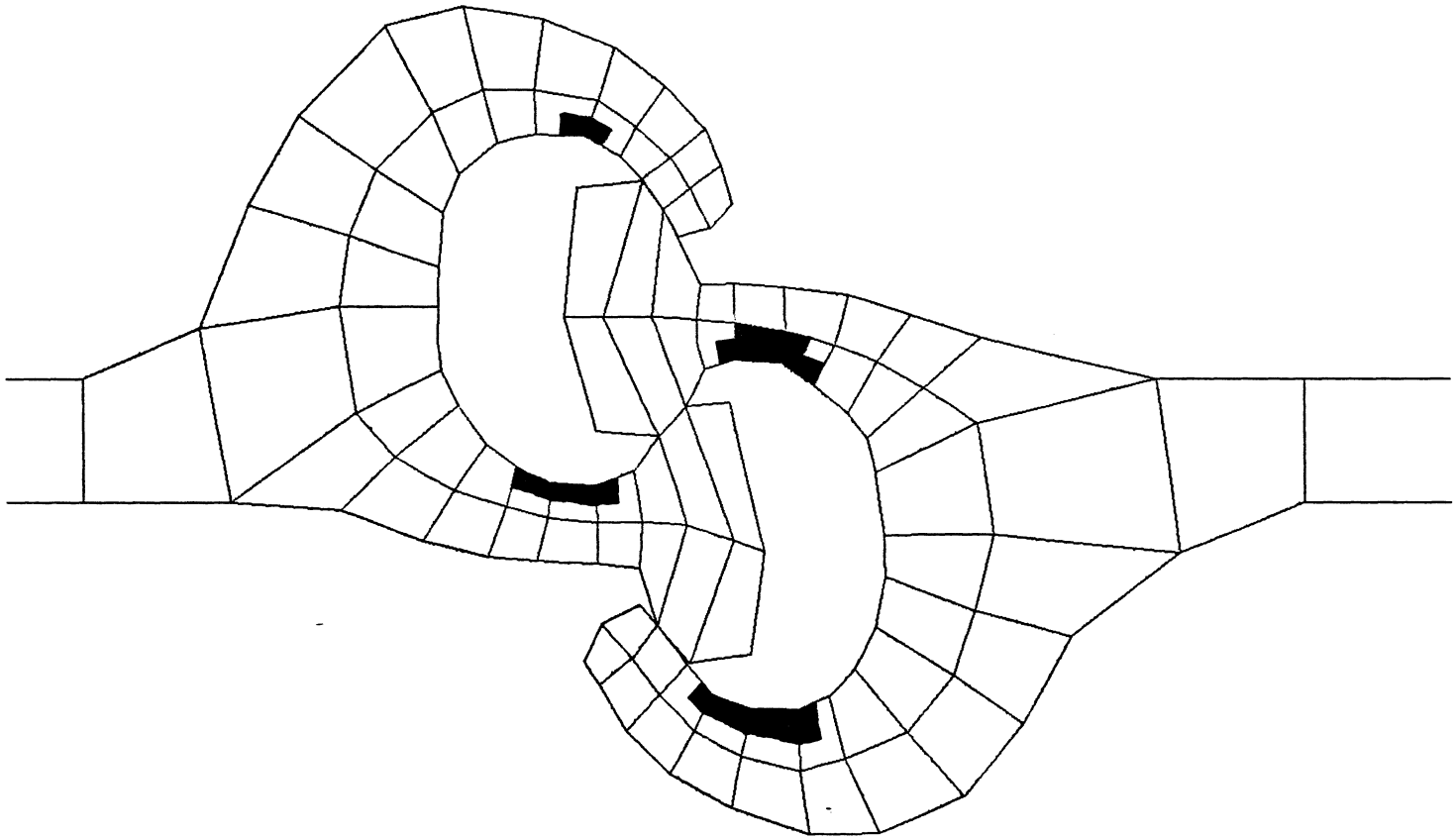

Figure 4.26. Plastic Zone in PS32 Sheet Pile at 10.58 kips/inch

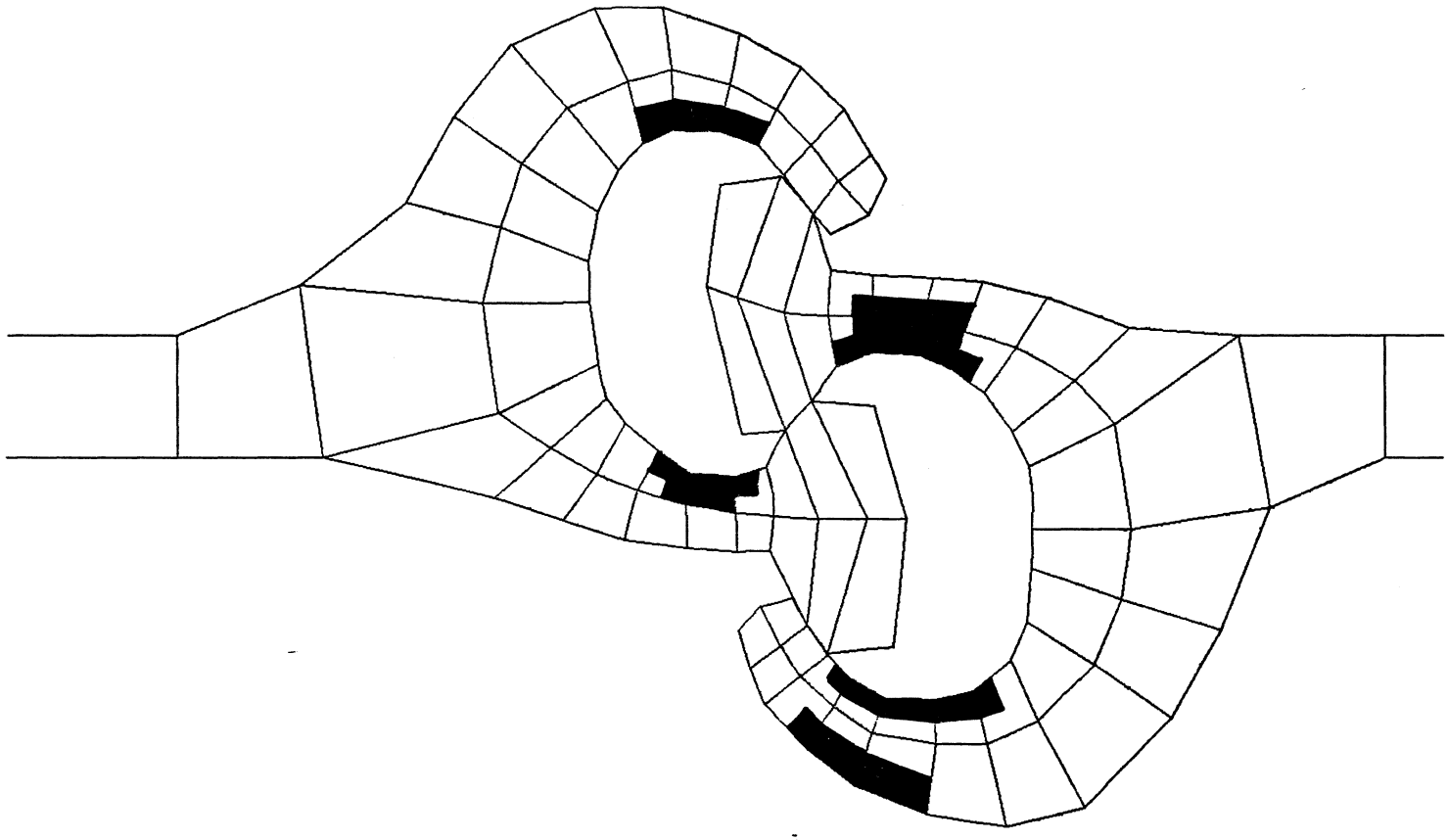

Figure 4.27. Plastic Zone in PS32 Sheet Pile at 12.58 kips/inch

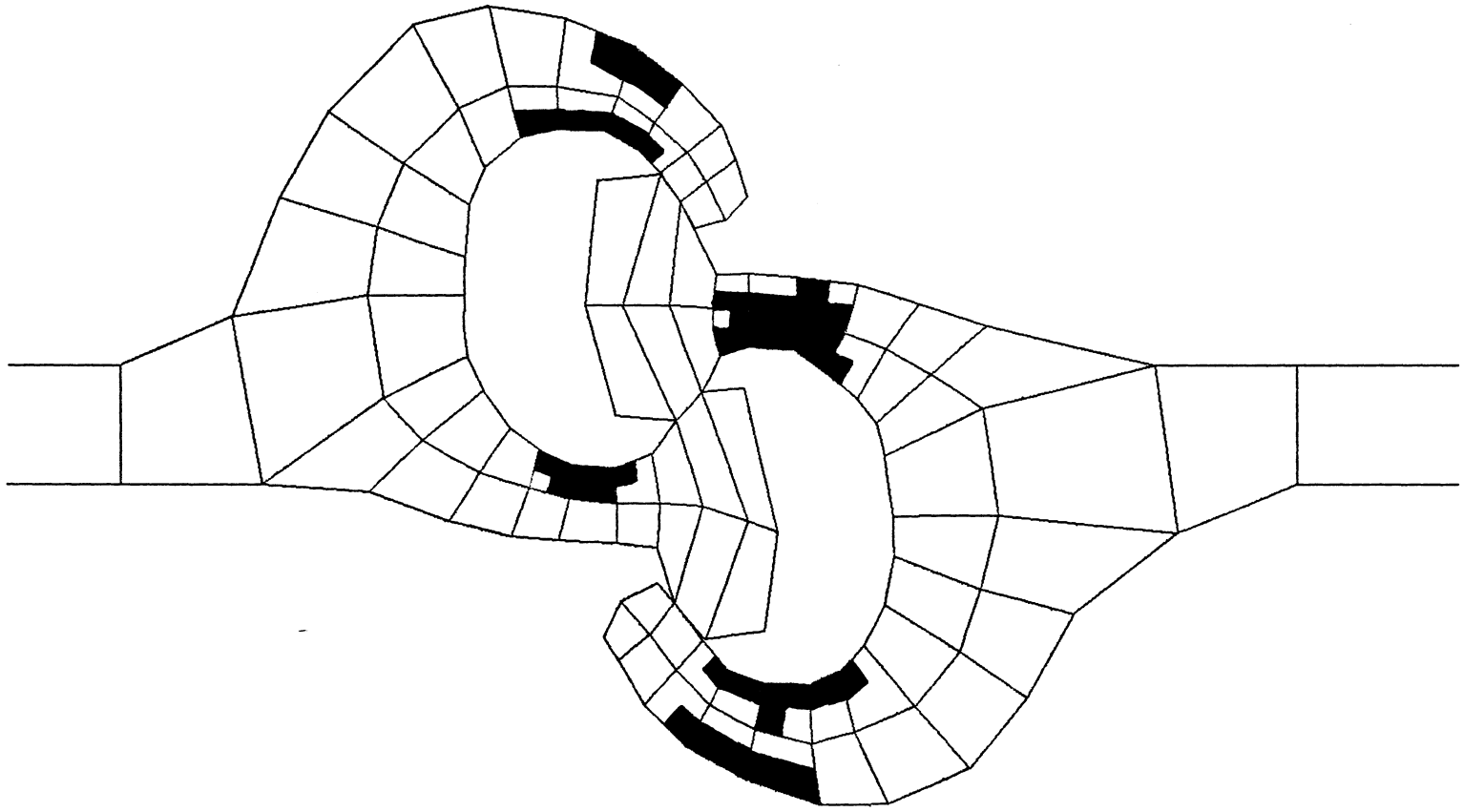

Figure 4.28. Plastic Zone in PS32 Sheet Pile at 14.21 kips/inch

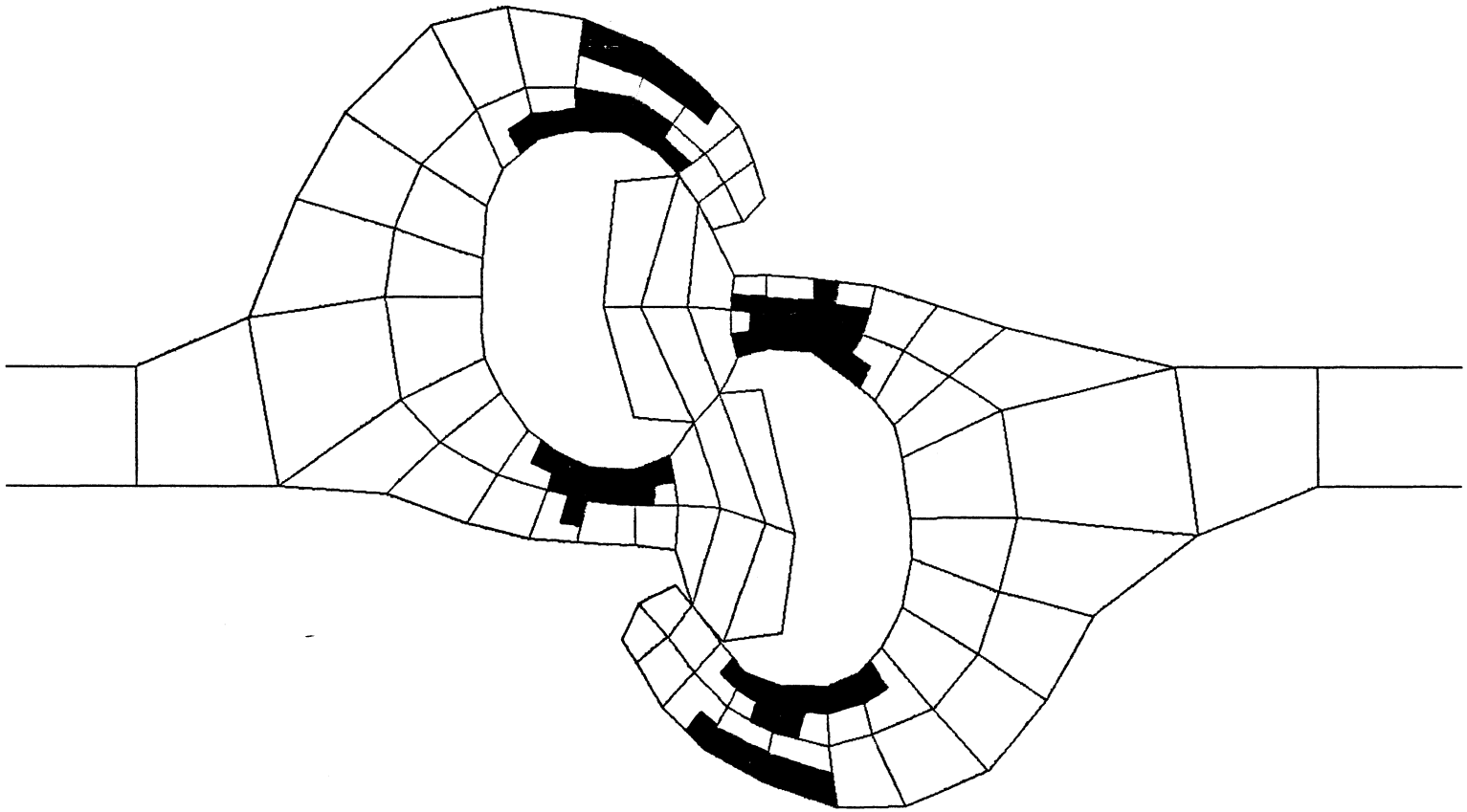

Figure 4.29. Plastic Zone in PS32 Sheet Pile at 15.5 kips/inch

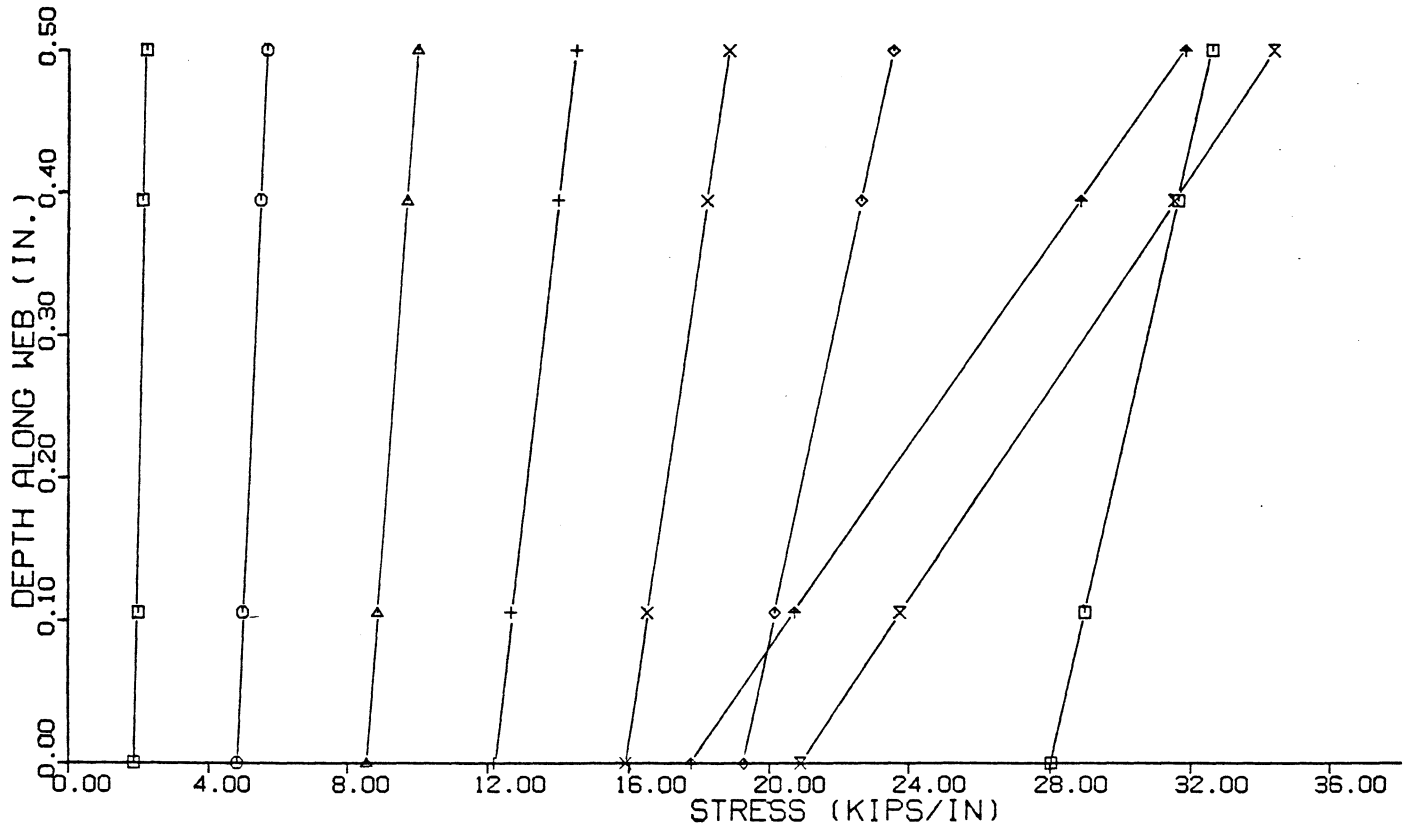

Figure 4.30. Stress Distribution along Web Section A-A at Different Load Steps

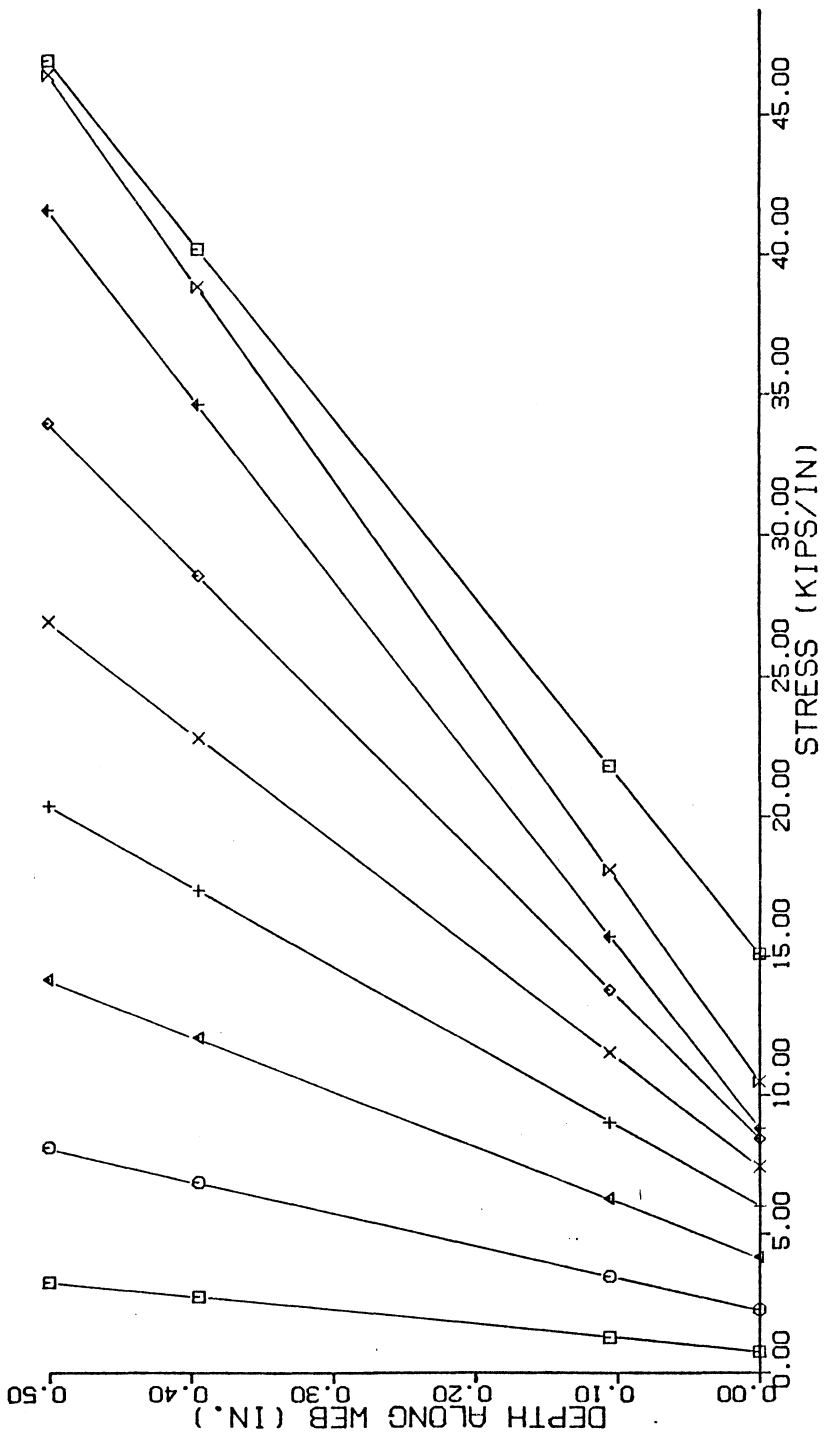

Figure 4.31. Stress Distribution along Web Section B-B at Different Load Steps

Chapter 5

Conclusions, Discussion, and Recommendations

5.1 Conclusions and Discussion

The modified Riks-Wempner method is successfully used in this study for solving a nonlinear moving contact problem with elastic-plastic material response and large displacements and rotations. Using this method, several observations were made from the implemented finite element analysis which are discussed below :

1. In the modified Riks-Wempner method, the arc length Δs is input from the data file and only used at the first load step. From then on, the arc length is updated and scaled by the square root of a value, which is the ratio of a prescribed number, $\hat{I}$, and current iteration number, I . After the new arc length is known, the first incremental load $\Delta\lambda^0$ can also be obtained. This is in contrast to the Newton-Raphson method where a lot of effort is spent on dividing the load steps, which is usually an effort of trial and error. When a small load increment is needed, the time and cost spent on data computation will be considerable.

Although the value of $\hat{I}$ varies from problem to problem and its selection depends on the user, it was found that the modified Riks-Wempner method is more efficient than the Newton-Raphson method used in previous work.

2. It has been found by other researchers that the simulation of a curved boundary by straight line elements and using irregular elements in the interior may cause the solutions in the direction normal to the boundary to converge to the wrong answer as the mesh is refined. This has been verified by analyzing the Hertz contact problem.

3. From the analysis of PS32 sheet pile interlocks, it was found that the failure of the interlocks is mainly caused by the bending of sheet piles and the shear force developing in the contact

regions. The simulated pull-out strength of the PS32 sheet piles is significantly increased by providing lateral restraint at the web midpoints.

4. Comparing the variation of maximum displacement versus applied load of the finite element analysis to that of experimental results, similar patterns of load-displacement curves were found except that the experimental results show more slip than the finite element analysis does. This is due to the initial slack between the interlocks. As indicated in a previous report, since the locations of the three contact regions in the interlock are assumed to be known a priori, the initial slack between the interlocks is not modeled, although this is more likely to be encountered during experimental work.

5.2 Recommendations for Future Studies

From the analysis, some recommendations were made to improve the computer program and to study in depth the behavior of sheet pile interlocks.

1. Develop new moving contact algorithm to model the initial slack between the interlocks.

2. Include the lateral pressure and study the behavior of the sheet pile interlocks under the combined effect of axial tensile load and lateral pressure to simulate the field condition of the sheet pile interlocks under hoop tension and earth pressure.

3. Perform the finite element analysis on a Wye pile connection and compare with the experimental results.

4. Extend the computer program capacity to include three-dimensional elements and study the frictional resistance of the sheet pile interlocks against tilting of the cell.

5. Implement mesh generation techniques in the current program. By using improved mesh smoothing algorithms and automatic mesh restructuring, shape optimization can be performed on the sheet pile interlocks.

6. Implement an interactive graphics procedure to display the sequential deformation process from the initial yielding of material to the final slipping of one interlock past another.

Appendix A.

REFERENCES

1. Argyris, J.H., "Continua and Discontinua", Proceedings of First Conference on Matrix Methods in Structural Mechanics , Wright-Patterson A. F. B., Ohio, 1965, pp. 11-189.

2. Babuska, I., "The Rate of Convergence for the Finite Element Method", SIAM Journal on Numerical Analysis , Vol. 8, No. 2, June, 1971, pp. 304-313.

3. Backlund, J., "On Isoparametric Elements", International Journal for Numerical Methods in Engineering , Vol. 12, 1978, pp. 731-732.

4. Barker, R., Lewis, C., Oliver, W., and Mould, K., "Sheet Pile Interlock Connection Testing Program", Report No. VPI/CE-ST-85/01 , Dept. of Civil Engrg. , Virginia Tech, Blacksburg, VA, May, 1985.

5. Bathe, K.J., Finite Element Procedures In Engineering Analysis , Prentice-Hall, Inc., Englewood Cliffs, New Jersey, 1982.

6. Bathe, K.J., and Chaudhary, A., "A Solution Method for Planar and Axisymmetric Contact Problems", International Journal for Numerical Methods in Engineering , Vol. 21, 1985, pp. 65-88.

7. Bathe, K.J., and Cimento, A.P., "Some Practical Procedures for the Solution of Nonlinear Finite Element Equations", Computer Methods in Applied Mechanics and Engineering , Vol. 27, 1980, pp. 59-85.

8. Bergan, P. G., "Solution Algorithms for Nonlinear Structural Problems", International Conference on Engineering Application of the Finite Element Method ,A. S. Computas, Hovik, Norway, 1979.

9. Birkhoff, G., "Piecewise Bicubic Interpolation and Approximation in Polygons", Approximation with Special Emphasis on Spline Functions , Academic Press, New York, 1969, pp. 185-221.

10. Butler, M.J., "A Comparison of Two Models for Geometrically Nonlinear Finite Element Analysis of Plane Frames", M.S. Thesis, Virginia Polytechnic Institute and State University, Blacksburg, VA, December, 1983.

11. Burns, J. Q., "An Analysis of Circular Cylindrical Shells Embedded in Elastic Media", Ph.D. Dissertation, University of Arizona, 1965.

12. Chan, M., and Barker, R., "Finite Element Studies of Sheet Pile Interlock Connection", Report No. VPI/CE-ST-85/02 , Dept. of Civil Engrg. , Virginia Tech, Blacksburg, VA, May, 1985.

13. Chan, M., and Barker, R., "Moving Contact Analysis of Sheet Pile Interlocks", Report No. VPI/CE-ST-85/03 , Dept. of Civil Engrg. , Virginia Tech, Blacksburg, VA, Nov., 1985.

14. Chan, S. K., and Tuba, I. S., "A Finite Element Method for Contact Problems of Solid Bodies", International Journal of Mechanical Sciences , Vol. 13, 1971, pp. 615-639.

15. Cook, R.D., Concepts and Applications of Finite Element Analysis , 2nd ed., John Wiley and Sons, New York, 1981.

16. Ergatoudis, I., Irons, B. M., and Ziewkiewicz, O. C., "Curved, Isoparametric, Quadrilateral Elements for Finite Element Analysis", International Journal of Solids and Structures , Vol. 4, 1968, pp. 31-42.

17. Francavilla, A., and Zienkiewicz, O. C., "A Note on Numerical Computation of Elastic Contact Problems", International Journal for Numerical Methods in Engineering , Vol. 9, 1975, pp. 913-924.

18. Gifford, L. N., "More on Distorted Isoparametric Elements" International Journal for Numerical Methods in Engineering , Vol. 14, 1979, pp. 290-291.

19. Hansen, M. C., "A Comparison of Two Solution Techniques for Snap- Through Instability of Trusses", M.S. Thesis, Virginia Polytechnic Institute and State University, Blacksburg, VA, March, 1981.

20. Hibbitt, Karlsson and Sorenson, Inc., ABAQUS Ver. 4.5: Theory Manual, September, 1984.

21. Holden, J. T., "On the Finite Deflections of Thin Beams", International Journal of Solids and Structures , Vol. 8, 1972, pp. 1051-1055.

22. Holzer, S.M., Computer Analysis of Structures, Matrix Structural Analysis, Structural Programming, , Elsevier, New York, 1985. 179-209.

23. Holzer, S.M., Watson, L.T., and Vu, P., "Stability Analysis of Lamella Domes", Proceedings of the ASCE Symposium on Long Span Roof Structures , St. Louis, Missouri, October, 1981, pp. 179-209.

24. Holzer, S. M., "Degree of Stability of Equilibrium", Journal of Structural Mechanics , Vol. 3, 1974, pp. 61-75.

25. Kamemura, K., and Lee, J. K., "Finite Element Approximations of Smooth Contact-Impact Problems", Proceeding of JSCE , 1981, pp. 119-128.

26. Katona, M. G., "A Simple Contact-Friction Interface Element with Applications to Buried Culverts", Journal of Numerical and Analytical Methods in Geomechanics , Vol. 7, 1983, pp. 371-384.

27. Kay, J. N., "Interlock Tension in Steel Piling", Journal of the Structural Division , Vol. 101, ST10, 1975, pp. 2093-2101.

28. Krauthammer, T., "Accuracy of the Finite Element Method Near a Curved Boundary", Computers and Structures , Vol. 10, 1979, pp. 921-929.

29. Lee, J. K., and Kamemura, K., "Analysis of Elastodynamics with Unilateral Supports", Proceedings of The Third Engineering Mechanics Division Speciality Conference , ASCE, 1979, pp. 777-780.

30. Lee, K., "Numerical Solution of Elastic Contact Problems", Ph.D. Dissertation, Ohio State University, 1985.

31. Lock, A.C., and Sabir, A. B., "Algorithm for Large Deflection Geometrically Nonlinear Plane and Curved Structures", Mathematics of Finite Elements and Applications , edited by Whiteman, J. R., , Academic Press, New York, 1973, PP. 483-494.

32. Macneal, R. H. and Harder, R. L., "A Proposed Standard Set of Problems to Test Finite Element Accuracy", Finite Elements in Analysis and Design , Vol. 1, 1985, pp. 3-20.

33. Nemat-Nasser, S., and Shatoff, H. D., "Numerical Analysis of Pre- and Postcritical Response of Elastic Continua at Finite Strains", Computers and Structures , Vol. 3, 1973, pp. 983-999.

34. Oden, J. T., and Pires, E. B., "Contact Problems in Elastostatics with Non-local Friction Laws", TICOM Report 81-12 , Austin, Texas, 1981.

35. Oden, J. T., and Pires, E. B., "Non-local and Nonlinear Friction Laws and Variational Principles for Contact Problems in Elasticity", TICOM Report 82-3 , Austin, Texas, 1982.

36. Oden, J. T., and Pires, E. B., "Numerical Analysis of Certain Contact Problems in Elasticity with Nonclassical Friction Laws", Computers and Structures , Vol. 16, 1983, pp. 481-485.

37. Okamoto, N., and Nakazawa, M., "Finite Element Incremental Contact Analysis with Various Frictional Conditions", International Journal for Numerical Methods in Engineering , Vol. 14, 1979, pp. 337-357.

38. Pian, T.H.H., and Tong, P., "Variational Formulation of Finite Displacement Analysis" IUTAM Symposium on High Speed Computing of Elastic Structures , Liege, 1970, pp. 43-63.

39. Ramm, E., "Strategies for Tracing Nonlinear Response Near Limit Points", Europe-U.S.-Workshop: Nonlinear Finite Element Analysis in Structural Mechanics , Bochum, G.F.R., July 28-31, 1980.

40. Rao, A. K. and Rajaiah, K., "Polygon Circle Paradox of Simply Supported Thin Plates under Uniform Pressure", AIAA Journal , Vol. 6, January, 1968, pp. 155-156.

41. Reddy, J. N., An Introduction to the Finite Element Method , McGraw-Hill, Inc., New York, 1984.

42. Sachdeva, T. D., and Ramakrishnan, C. V., "A Finite Element Solution for the Two Dimensional Elastic Contact Problem with Friction", International Journal for Numerical Methods in Engineering , Vol. 17, 1981, pp. 1257-1271.

43. Sachdeva, T. D., and Ramakishnan, C. V., "Determination of In-Plane Flexibilities of Dovetail Joints Using Finite Element Method", International Journal of Machine Tool Design , Vol. 21, 1981, pp. 153-161.

44. Schreyer, H. L., and Masur, E. F., "Buckling of Shallow Arches" Journal of the Engineering Mechanics Division , ASCE, Vol. 4, 1966, pp. 1-19.

45. Sharifi, P., and Popov, E. P., "Nonlinear Buckling Analysis of Sandwich Arches", Proceedings of the Engineering Mechanics Division , ASCE, Vol. 97, 1971, pp. 1397-1412.

46. Strang, G., and Fix, G. J., An Analysis of the Finite Element Method , Prentice-Hall, Englewood Cliffs, New Jersey, 1974.

47. Tang, S. C., Yeung, K. S., and Chon, C. T., "On the Tangent Stiffness Matrix in a Convected Coordinate System", Computers and Structures , Vol. 12, 1980, pp. 849-856.

48. Tillerson, J. R., Stricklin, J. A., and Hansen, M. C., "Numerical Methods for the Solution of Nonlinear Problems in Structural Analysis", in Numerical Solution of Nonlinear Structural Problems , ed. R. F. Hartung, ASME AMD-6, 1973, pp. 67-101.

49. Timoshenko, S. P., and Goodier, J. N., Theory of Elasticity , Second Edition, McGraw-Hill, New York, 1951.

50. Torstenfelt, B., "An Automatic Incrementation Technique for Contact Problems with Friction", Computers and Structures , Vol. 19, 1984, pp. 393-400.

51. Torstenfelt, B., "Contact Problems with Friction in General Purpose Finite Element Computer Programs", Computers and Structures , Vol. 16, 1983, pp. 487-493.

52. United States Steel, Steel Sheet Piling Handbook , May, 1983.

53. Vu, P.D., "Tracing Nonlinear Equilibrium Paths by the Modified Riks-Wempner Method", M.S. Thesis, Virginia Polytechnic Institute and State University, Blacksburg, VA, October, 1981.

54. Watson, L. T., "A Globally Convergent Algorithm for Computing Fixed Points of C Maps", Applied Mathematics and Computation , Vol. 5, 1979, pp. 297-311.

55. Wessels, M., "Das Statische und Dynamiche Durchschlagsproblem der Impertekten Flachen Kugelschale bei Elastischer Rotationssymmetrischer Verformung", Dissertation, TU Hannover, 1980.

56. Wright, E. W., and Gaylord, E. H., "Analysis of Unbraced Multistory Steel Rigid Frames", Journal of the Structural Division , ASCE, Vol. 94, 1968, pp. 1143-1163.

57. Zienkiewicz, O.C., The Finite Element Method , 3rd. ed., McGraw-Hill, New York, 1977

58. Zienkiewicz, O.C., "Incremental Displacement in Non-Linear Analysis", International Journal for Numerical Methods in Engineering , Vol. 3, 1971, pp. 587-588.

59. Zlamal, M.,"The Finite Element Method in Domains with Curved Boundaries" International Journal for Numerical Methods in Engineering , Vol. 5, 1973, pp. 367-373.

60. Zlamal, M.,"Curved Elements in Finite Element Method 1", SIAM Journal on Numerical Analysis , Vol. 10, 1973, pp. 229-240.

61. Zlamal, M.,"Curved Elements in Finite Element Method 2", SIAM Journal on Numerical Analysis , Vol. 11, 1974, pp. 347-362.

The vita has been removed from the scanned document